Nighttime magnetic perturbation events observed in Arctic Canada: 3. Occurrence and amplitude as functions of magnetic latitude, local time, and magnetic disturbances

Mark J. Engebretson[1,1], Vyacheslav A. Pilipenko[2,2], Erik S. Steinmetz[3,3], Mark B. Moldwin[4,4], Martin Connors[5,5], David H Boteler[6,6], Howard J. Singer[7,7], Hermann J. Opgenoorth[8,8], Audrey Schillings[9,9], Ohtani Shin[10,10], Jesper W. Gjerloev[11,11], and Christopher T. Russell[12,12]

[1]Department of Physics, Augsburg University
[2]Space Research Institute
[3]Department of Computer Science, Augsburg University
[4]University of Michigan-Ann Arbor
[5]Athabasca University
[6]Natural Resources Canada
[7]National Oceanic and Atmospheric Administration (NOAA)
[8]Umeå University
[9]Swedish Institute of Space Physics
[10]Applied Physics Lab
[11]APL-JHU
[12]University of California Los Angeles

November 30, 2022

Abstract

Rapid changes of magnetic fields associated with nighttime magnetic perturbation events (MPEs) with amplitudes |ΔB| of hundreds of nT and 5-10 min periods can induce geomagnetically-induced currents (GICs) that can harm technological systems. In this study we compare the occurrence and amplitude of nighttime MPEs with |dB/dt| [?] 6 nT/s observed during 2015 and 2017 at five stations in Arctic Canada ranging from 75.2° to 64.7° in corrected geomagnetic latitude (MLAT) as functions of magnetic local time (MLT), the SME and SYM/H magnetic indices, and time delay after substorm onsets. Although most MPEs occurred within 30 minutes after a substorm onset, ˜10% of those observed at the four lower latitude stations occurred over two hours after the most recent onset. A broad distribution in local time appeared at all 5 stations between 1700 and 0100 MLT, and a narrower distribution appeared at the lower latitude stations between 0200 and 0700 MLT. There was little or no correlation between MPE amplitude and the SYM/H index; most MPEs at all stations occurred for SYM/H values between -40 and 0 nT. SME index values for MPEs observed more than 1 hour after the most recent substorm onset fell in the lower half of the range of SME values for events during substorms, and dipolarizations in synchronous orbit at GOES 13 during these events were weaker or more often nonexistent. These observations suggest that substorms are neither necessary nor sufficient to cause MPEs, and hence predictions of GICs cannot focus solely on substorms.

Nighttime magnetic perturbation events observed in Arctic Canada: 3. Occurrence and amplitude as functions of magnetic latitude, local time, and magnetic disturbances

Mark J. Engebretson[1], Viacheslav A. Pilipenko[1,2], Erik S. Steinmetz[1], Mark B. Moldwin[3], Martin G. Connors[4], David H. Boteler[5], Howard J. Singer[6], Hermann Opgenoorth[7], Audrey Schilling[7], Shin Ohtani[8], Jesper Gjerloev[8], and Christopher T. Russell[9]

[1] Augsburg University, Minneapolis, MN
[2] Institute of Physics of the Earth, Moscow, Russia
[3] University of Michigan, Ann Arbor, MI
[4] Athabasca University, Athabasca, AB, Canada
[5] Natural Resources Canada, Ottawa, ON, Canada
[6] NOAA Space Weather Prediction Center, Boulder, CO
[7] Umeå University, Umeå, Sweden
[8] JHU/APL, Laurel, MD
[9] UCLA Department of Earth Planetary and Space Sciences, Los Angeles, CA

submitted to Space Weather
April 23, 2020

Key Words: geomagnetically-induced currents, magnetic perturbation events, substorms, magnetic storms, omega bands

Key Points:

We present 2 years of observations of ≥ 6 nT/s magnetic perturbation events (MPEs) from 5 Arctic stations between 65° and 75° magnetic latitude.

Most MPEs occurred within 30 min of a substorm onset, but substorms were neither necessary nor sufficient to cause MPEs.

Pre-midnight and post-midnight MPEs had different temporal relations to substorms and occurred at slightly different latitudes.

Abstract

Rapid changes of magnetic fields associated with nighttime magnetic perturbation events (MPEs) with amplitudes |ΔB| of hundreds of nT and 5-10 min periods can induce geomagnetically-induced currents (GICs) that can harm technological systems. In this study we compare the occurrence and amplitude of nighttime MPEs with |dB/dt| ≥ 6 nT/s observed during 2015 and 2017 at five stations in Arctic Canada ranging from 75.2° to 64.7° in corrected geomagnetic latitude (MLAT) as functions of magnetic local time (MLT), the SME and SYM/H magnetic indices, and time delay after substorm onsets. Although most MPEs occurred within 30 minutes after a substorm onset, ~10% of those observed at the four lower latitude stations occurred over two hours after the most recent onset. A broad distribution in local time appeared at all 5 stations between 1700 and 0100 MLT, and a narrower distribution appeared at the lower latitude stations between 0200 and 0700 MLT. There was little or no correlation between MPE amplitude and the SYM/H index; most MPEs at all stations occurred for SYM/H values between -40 and 0 nT. SME index values for MPEs observed more than 1 hour after the most recent substorm onset fell in the lower half of the range of SME values for events during substorms, and dipolarizations in synchronous orbit at GOES 13 during these events were weaker or more often nonexistent. These observations suggest that substorms are neither necessary nor sufficient to cause MPEs, and hence predictions of GICs cannot focus solely on substorms.

1. Introduction

Although early studies of nighttime magnetic perturbation events (MPEs) that induce large geoelectric fields and geomagnetically-induced currents (GICs) noted the small-scale character of these events (e.g., Viljanen, 1997), many efforts to predict GICs have continued to focus on global processes (geomagnetic storms and substorms). Recent observational studies by Belakhovsky et al. (2019), Dimmock et al. (2019), Engebretson et al. (2019a,b), and Apatenkov et al. (2020) have provided new evidence of the localized nature of the magnetospheric and/or ionospheric processes associated with these impulsive magnetic perturbations. This includes evidence of ionospheric current vortices, close association with poleward boundary intensifications and overhead auroral streamers, and the spatial scale size of individual events. Individual events also displayed no close or consistent temporal correlation with substorm onsets.

Here we present additional analyses of a large number of nighttime MPEs that document lack of any close correlation between their occurrence and levels of the SME index, the SYM/H index, or of near-tail dipolarizations, and show that a substantial fraction of these events are not temporally associated with substorms. MPEs occurring in the post-midnight sector showed a different dependence on both latitude and prior substorm activity than did the more numerous pre-midnight MPEs.

2. Data Set and Event Identification Technique

Vector magnetometer data used in this study were recorded during 2015 and 2017 by stations in the MACCS (Engebretson et al., 1995), CANMOS (Nikitina et al., 2016), and AUTUMNX (Connors et al., 2016) arrays in Arctic Canada, as detailed in Table 1 and Figure 1 (red circles). MACCS station CDR and the highest and lowest latitude stations in the AUTUMNX array, SALU and KJPK, form a latitudinal chain. MACCS station RBY extends this chain to the north and west, and CANMOS station IQA extends it to the east. Data from 2016 was not included because of significant station down time at RBY and CDR during that year. Also shown in Figure 1 (yellow circle) is the northern magnetic footpoint of the geosynchronous GOES 13 spacecraft (Singer et al., 1996), which provides magnetospheric context for the ground observations.

The semi-automated procedure used to identify and quantify MPEs in these data sets is detailed in Engebretson et al. (2019a), and is summarized here. Routinely produced daily magnetograms (24-hour plots of magnetic fields in local geomagnetic coordinates) were displayed on a computer screen. Once a < 10 minute duration magnetic perturbation with amplitude ≥ 200 nT in any component was identified, the IDL cursor function was used to visually select times before and after a region of interest containing the MPE. The times and values of extrema in this interval were recorded for each component, and after application of a 10-point smoothing to reduce noise and eliminate isolated bad data points, the data were numerically differentiated. Plots of the time series of data and derivatives were produced and saved, and the maximum and minimum derivative values were automatically determined and recorded. Figure 3 of Engebretson et al. (2019a) shows the amplitude vs. MLT distributions of MPEs at SALU during 2015 for both ΔBx and |dBx/dt| that were identified using this technique. This figure shows that MPEs with ΔBx amplitude ≥ 200 nT or derivative amplitude ≥ 6 nT/s were almost exclusively confined to nighttime hours.

We then compared the time of each MPE identified during full years 2015 and 2017 at each station to the times of substorm onsets listed in the SuperMAG substorm list for that year. We identified and recorded the time of all prior substorm onsets within a 2-hour window, and if none were found, to the time of the closest prior onset, which in some cases was several days prior to the MPE. The procedure used to identify substorm onsets included in the SuperMAG substorm lists is described in Newell and Gjerloev (2011a,b): substorm onsets are defined by a drop in SML (the SuperMAG version of the AL index) that was sharp (45 nT in 3 min) and that was sustained (-100 nT average for 25 min starting 5 min after onset). We note here that onsets are relatively easy to identify if preceded by quiet periods, but subsequent onsets (which may be called intensifications) are far more difficult to identify using either ground-based magnetometer data or auroral images. Table 2 shows the number of nighttime (1700 to 0700 MLT) MPEs with derivative amplitude ≥ 6 nT/s at each of these stations. Events are grouped into 3 categories of time delay Δt after the most recent prior substorm onset: Δt ≤ 30 min, 30 < Δt < 60 min, and Δt ≥ 60 min. In this study we define events with Δt ≤ 30 min as most likely to be associated with substorm processes, while those with Δt ≥ 60 min (and up to several days) are not. The fractions of events that occurred in these three different delay ranges remained roughly constant at all stations. Note, too, that the number of events peaked at SALU (70.7° MLAT), and was lowest at the two latitude extremes: RBY (75.2° MLAT) and KJPK (64.7° MLAT).

3. MPE Amplitudes as a function of Time Delay After Substorm Onset

Figure 2 shows the amplitude of the maximum |dB/dt| value in any nighttime MPE component observed at each station as a function of its delay (between 0 and 120 min) after the most recent substorm onset. The strongest events (≥20 nT/s) most often occurred for Δt < 60 min, but only at the highest latitude station (Repulse Bay) did these strongest events occur within 5 min of substorm onset. Most events were below 12 nT/s for all delay times.

MPEs occurred over a continuum of times from 0 to well beyond the 120 minute delay time range shown in this figure. The number and percentage of events occurring with delay times > 120 min are indicated in the inset box in each panel. Although most MPEs at each station occurred within 30 minutes after a substorm onset, from 13 to 20 % of the MPEs at each station occurred later than 1 hour after the most recent substorm onset, and from 6 to 12 % later than 2 hours. The number of events > 10 nT/s with time delays over two hours was 0 at RBY and CDR, 1 at IQA, 5 at SALU, and 3 at KJPK (not shown).

4. MPE Occurrences as a Function of Derivative Amplitude

Figure 3 shows the distribution of occurrences of MPEs as a function of derivative amplitude at all five stations and in all three time delay categories. Different symbols are used to designate events based on the time of MPE occurrence after the closest prior substorm onset: blue circles for Δt ≤ 30 min, green squares for Δt between 30 and 60 min, and red triangles for Δt ≥ 60 min. The number of MPEs in each 1 nT/s bin fell off roughly monotonically in each category from the lowest amplitude to higher values with a long tail, with no clear latitudinal trend. At each station, several events that occurred within 30 min of substorm onset had amplitudes exceeding 20 nT/s (up to 34 nT/s); only at CDR and IQA did > 20 nT/s MPEs occur after delays > 30 min.

5. Latitudinal Distributions of Occurrences and Amplitudes vs. MLT, SYM/H, and SME

For each of the five stations we sorted the MPE events as functions of several variables: magnetic local time (MLT), the SYM/H index, the SME index (the SuperMAG version of the AE index, described in Newell and Gjerloev, 2011a), and derivative amplitude.

Over the range of magnetic latitudes covered in this study (from 75° to 65° MLAT) all ≥ 6 nT/s perturbation events fell into the local time range from 17 to 07 MLT. Figure 4a shows the number of occurrences of these MPEs at each station grouped in 1-hour MLT bins and sorted by magnetic latitude. Different symbols are used to designate events based on the time of MPE occurrence after the closest prior substorm onset: plus signs for $\Delta t \leq 30$ min, open squares for Δt between 30 and 60 min, and open triangles for $\Delta t \geq 60$ min. Two populations are evident in this figure: a broad distribution extending from dusk to shortly after midnight (17 to 1 MLT) that appears at all latitudes shown, and a distribution in the midnight to dawn sector (2 to 7 MLT) that is prominent only at the lower latitude stations. This difference in latitudinal distribution, which is consistent with observations of large ionospheric equivalent current perturbations by Juusola et al. (2015), appears to reflect the latitudinal dependence of the auroral electrojet, which is located at higher latitudes pre-midnight and lower latitudes post-midnight. As will be shown in later parts of this study, the properties of these two populations also differed somewhat in their association with different geomagnetic conditions.

Consistent with the distribution of occurrences shown in Table 2 and Figure 2, Figure 4a shows that the MPEs that occurred within 30 minutes of the most recent substorm onset (shown with a plus sign) were the dominant category in nearly all MLT bins at each station. The local time trends for MPEs shown with squares and triangles were similar to those for MPEs shown with plus signs for the four most poleward stations, with a broad distribution gradually rising from ~17-18 h MLT to a broad pre-midnight peak before gradually falling to ~1-2 h MLT, and with very few events occurring at later MLT. At KJPK, the pre-midnight distribution of events shown with plus signs was somewhat narrower in time and shifted toward slightly later MLT, and a second post-midnight peak (with similar peak occurrences) appeared between 2-3 and 6 h MLT. In contrast, the distributions for events shown with squares and triangles were flat across the entire MLT range shown (but with fewer occurrences).

Figure 4b shows that the largest-amplitude MPEs occurred at all 5 stations between 1800 and 2300 h MLT, but derivatives with amplitude at or above 15 nT/s also appeared after 0300 h MLT at both SALU and KJPK. Table 3 shows an analysis of the distribution of these events as a function of time delay when separated into pre- and post-midnight occurrences. In order to clearly separate these categories, pre-midnight events were chosen to include those observed between 1700 and 0100 MLT, and post-midnight event those between 0200 and 0700 MLT. The time delay distributions were similar for pre- and post-midnight events at all 5 stations, but on average over all 5 stations, post-midnight events were slightly more likely to occur within 30 min after substorm onsets than pre-midnight events (70% vs. 66%), and less likely to occur more than 60 minutes after onset (12% vs. 17%). These differences, however, were not statistically significant.

Figure 5 shows plots similar to those in Figure 4 as a function of the SYM/H index, which ranged from ~-150 to +30 nT during these events. At all five stations the occurrence distributions (Figure 5a) peaked near SYM/H ~ -20 nT, and at all but the lowest latitude station nearly all events occurred when SYM/H was between -60 and +10 nT. The tail of the distribution at more negative SYM/H values increased at the lowest latitude station, KJPK. This most likely reflects the equatorward expansion of the auroral oval during geomagnetic storms. The occurrence distributions for the 3 time delay categories were roughly similar to each other at each station. In contrast to Figure 4, where the distribution of local times during which observations were available was essentially uniform, it is important to note that in Figures 5 and 6 the overall occurrences of SYM/H and SME values were strongly biased toward quiet conditions. The occurrences shown in Figures 5 and 6 are thus not normalized.

Figure 5b shows that the SYM/H range corresponding to the largest derivative amplitudes occurred for values between -40 and -20 nT at RBY and expanded toward lower SYM/H values at CDR and IQA. There was essentially no correlation between largest derivative amplitudes and SYM/H values at either SALU or KJPK; storm-time MPEs were no more likely to have extreme derivative values than MPEs during non-storm conditions, even near 65° MLAT.

At all five stations > 6 nT/s perturbation events occurred over a wide range of SME values, as shown in Figure 6a, but very few events occurred at any station for SME < 200 nT. At the four highest latitude stations a large majority of events in each of the 3 time delay categories occurred for SME values between 200 and 900 nT. This SME range also held at the lowest latitude station (KJPK) for the $\Delta t > 60$ min category, but most of the events in the $\Delta t \leq 30$ min category were associated with SME values > 800 nT. However, fewer events occurred for high SME at KJPK (64.7° MLAT) than at SALU (70.7° MLAT) – note the differing vertical scales.

Figure 6b shows that there was a modest correlation between the amplitude of the largest derivatives and the SME index only over the SME range between 200 and 600 nT at all 5 stations; the distribution of amplitudes was nearly flat for SME > 600 nT at all stations. Most events at all SME values and all 3 time ranges were below 12 nT/s. Only 7 of the 842 total events occurred when SME exceeded 2000 nT.

6. Event Occurrence in Relation to Substorms and Magnetotail Dipolarizations

In this section we address three questions: 1) What percentages of substorms are associated with a large nighttime MPE?, 2) How important are multiple-onset substorms for large-amplitude MPEs?, and 3) to what extent are nighttime MPEs associated or not with dipolarizations observed at geosynchronous orbit?

6.1 Percentages of substorms associated with large nighttime MPEs

Figure 2 and Table 2 have shown the numbers and percentages of MPEs that are associated with substorm onsets within given ranges of time delays. We now address the reverse association: in what percentage of substorm onsets does an MPE occur within one hour?

In order to address this question, we compared the number of observed MPEs to the number of substorm onsets listed in the SuperMAG onset data base for 2015 and 2017. Roughly 80% of the MPE events at the four northernmost stations occurred between 1900 and 0100 MLT (Figure 4), and most (~60%) of the MPEs observed at all five stations occurred from 0 to 30 minutes after the most recent substorm onset (Figure 2). We thus wish to determine the number of substorm onsets that might correspond to MPE events between 1830 and 0100 MLT. Figure 7 shows the distribution of substorm onsets in the MLT range from 17 to 07 h, the same MLT range as shown in Figure 4, for both 2015 and 2017. Although both substorm distributions peaked near or shortly before midnight, the peak of the onset distribution is clearly shifted ~1-2 hours later in MLT than the peak of the MPE distribution at all stations other than KJPK. The later rise and longer tail of the substorm onset distribution may reflect the occurrence of post-midnight onsets at lower MLATs, as suggested by the MLT distribution at KJPK. The percentage of onsets in the MLT range from 1830 to 0100 h was 50% for 2015, and 55% for 2017. Although this offset makes it clear that there was only an approximate correspondence between the peaks of the MLT distributions of MPEs and substorm onsets, a comparison may still provide helpful information.

At the CDR and SALU stations, located in magnetic longitude near the center of the 5 stations, the 1830 to 0100 MLT range corresponds to a time window from 2325 to 0555 UT. The SuperMAG substorm onset data base indicated that during 2015 and 2017 combined, 932 of a total of 4031 onsets occurred during this UT time window.

Columns 2-4 of Table 4 show the number of MPE events at each station that occurred within this UT time window as a function of their time delays (0-30, 30-60, and 0-60 min) after the most recent substorm onset. Columns 5-7 show the estimated percentage of events following a documented substorm onset within these time delays, calculated by dividing the number of events in columns 2-4 by 932. Column 7 shows that the percentage of MPEs per substorm onset that occurred within 60 min after an identified substorm varied from 8.0 to 25.1%. Column 8 shows the reverse occurrence: the estimated percentage of substorm onsets after which no MPE occurred within 60 minutes after onset. The percentages in this column ranged from 75 to 92%, indicating that most substorms were not associated with large amplitude MPEs. The percentages at CDR, IQA, and SALU were near the lower end of this range, and those at RBY and KJPK at the higher end. We note the roughly inverse correlation between these percentages and the number of MPE events observed at each station (Table 2). This suggests that the modest differences in magnetic longitude between the five stations were a smaller factor in determining the dependence of MPEs on substorm onsets than the magnetic latitude. This dependence on MLAT may reflect the limited spatial extent of large MPEs, such that a station farther away from the statistical auroral oval is more likely to detect an MPE with lower amplitude, and thus in many cases one below our selection threshold of 6 nT/s.

6.2 The importance of multiple prior substorm onsets for large nighttime MPEs

We also considered the effect of multiple prior substorm onsets separately for MPEs in the two populations shown in Figure 4a: the "pre-midnight" population observed between 1700 and 0100 MLT, and the "post-midnight" population observed between 0200 and 0700 MLT. Table 5 shows the number of > 6 nT/s MPEs observed during 2015 and 2017 at the three lowest latitude stations as a function of the number of substorm onsets that occurred within 2 hours prior to the MPE, and Figure 8 shows this same information in percentage form. Both Table 5 and

Figure 8 show that in the 1700-0100 MLT sector the distribution at each station peaked within 2 hours after 1 substorm onset and fell off rapidly after 2 substorm onsets. The much smaller number of MPEs that occurred at each station in the 0200-0700 MLT sector exhibited a broad maximum following 2-h intervals of between 1 and 4 onsets.

Comparison of the median |dB/dt| amplitude of MPEs as a function of prior substorm onsets (not shown) indicated a relatively flat distribution near 8 nT/s from 0 through 4 prior onsets in the pre-midnight sector, but a ~50% increase in median amplitude (~7 to ~11 nT/s) from 1 to 4 onsets in the post-midnight sector. These distributions were again very similar at all 3 stations.

Table 6 shows the results of applying Pearson's Chi-squared test to the data in Table 5, after reducing the number of prior substorm categories to 3: after 0, 1, and ≥ 2 onsets within 2 hours, respectively. The p values of $<< 0.05$ confirm that the difference between pre-midnight and post-midnight events is statistically significant at all 3 stations. Taken together, these differences indicate a much stronger relation between multiple substorms and subsequent MPEs in the post-midnight sector than in the pre-midnight sector.

Table 7 provides additional information on the relation between MPE onset and the level of magnetic disturbance (as represented by the SME index) following multiple substorms. This table shows for both pre-midnight and post-midnight time sectors and for IQA, SALU, and KJPK a) the total number of MPEs observed as a function of the number of substorm onsets during the 2 hours prior to the MPE, b) the number of MPEs simultaneous with very intense magnetic disturbances (SME ≥ 1000 nT), and c) the percentage of these MPEs compared to the total number of MPEs observed in each onset bin. At all 3 stations and for both pre-midnight and post-midnight events, 1) no MPEs occurred in the first bin (following a 2-h period after 0 substorms) and very few in the second bin (following 1 substorm), 2) most MPEs simultaneous with SME values ≥ 1000 nT occurred after two-hour intervals containing from 2 to 4 substorm onsets, and 3) because of the large difference in total MPE occurrence in each bin between pre-midnight and post-midnight MPEs, the percentage distribution of pre-midnight MPEs simultaneous with SME values ≥ 1000 nT increased greatly as the number of prior substorm onsets increased from 1 to 4, but was more nearly flat for post-midnight events. The overall fractions of pre-midnight MPEs associated with SME values ≥ 1000 nT were 9.2% at IQA, 8.5

% at SALU, and 19.4% at KJPK. The corresponding post-midnight fractions were much larger: 70%, 44%, and 52%, respectively.

The SME index is well correlated with auroral power (Newell and Gjerloev, 2011a). In general, the relationship among discrete precipitation, ionospheric conductance, and upward FAC density is instantaneous. In contrast, diffuse precipitation has a certain time lag; particles are injected and then later forced to precipitate into the ionosphere. The associated enhancement of ionospheric conductance lasts longer, which is favorable for more tail current to short-circuit through the ionosphere at subsequent substorms. As a result, SME may increase following multiple particle injections closely spaced in time more than it would without continuing activity, independently of the intensity of any individual substorm.

These differing patterns again indicate that intervals of large SME (or AE) index values are poorly correlated with intense pre-midnight dB/dt values but are better correlated for post-midnight events.

6.3 Relation of large nighttime MPEs to dipolarizations at synchronous orbit

In each of the three case studies of MPEs presented by Engebretson et al. (2019b), which occurred within 30 min of a substorm onset, rapid increases of from 15 to 30 nT in the Bz component of the magnetic field (dipolarizations) at GOES 13 coincided with an MPE to within a few minutes. Figure 9 presents a comparison of the Bz perturbations observed at GOES 13 within 45 minutes prior to each of the MPEs observed at RBY and KJPK during 2015 and 2017, grouped in two categories: MPEs with time delays $\geq$ 60 min and $\leq$ 30 min after the most recent substorm onset. GOES data were available for 13 (all) and 52 (all but one) of the MPEs at RBY and for 25 (all) and 79 (all) of the MPEs at KJPK, respectively. At RBY 2 of 13 and 4 of 52 GOES 13 perturbations, respectively, were negative and are not shown in Figure 9; the corresponding numbers at KJPK were 0 of 25 and 3 of 79, respectively. Figure 9 shows that at both stations the amplitude distribution of the perturbations did not extend to as large values for the Δt $\geq$ 60 min MPE population as for the $\leq$ 30 min MPE population.

Some of the smaller GOES 13 Bz perturbations, and especially those in the Δt $\geq$ 60 min category, were associated with brief (few min) transient pulses rather than step functions (dipolarizations). It is difficult to discern whether such pulses arise from spatial or temporal effects. If spatial, GOES 13 may have been rather distant in MLT from the center of a more large-scale dipolarization. If temporal, the perturbation may have been associated with a bursty bulk flow, dipolarization front, and/or pseudobreakup (e.g., Palin et al., 2015). Further analysis of the features of the GOES 13 dataset during these MPE events is certainly warranted, but is beyond the scope of this paper.

7. Summary of Observations

This study has described the distributions of nighttime MPEs as functions of several physical parameters and geomagnetic indices, and has identified two different populations on the basis of differences in both MLT and dependence on magnetic activity levels. The first two of the MPE characteristics below confirm and extend the observations in previous reports, but others appear to provide new information.

1: Distributions of MPEs as functions of the time delay after a substorm onset were presented by Viljanen et al. (2006), using data from Longyearbyen, Sodankylä, and Nurmijarvi and by Engebretson et al. (2019a), using data from Repulse Bay. Both studies found that these distributions had long tails. This study confirms and quantifies the occurrence of these long tails: Although many of the most intense MPEs at each station occurred within 30 min of a substorm onset, from 13 to 20 % of the MPEs at each station occurred later than 1 hour after the most recent substorm onset, and from 6 to 12 % later than 2 h. The strongest MPEs at all 5 stations most often occurred within 60 min of a substorm onset, but the amplitudes of most events were below 12 nT/s at all delay times.

2. A broad distribution of nighttime MPEs appeared at all 5 stations between 1700 and 0100 MLT, and a narrower distribution appeared at the lower latitude stations between 0200 and 0700 MLT. This is consistent with earlier studies by Viljanen et al. (2001), Viljanen and Tanskanen (2011), Juusola et al. (2015), and most recently by Vorobev et al. (2019) that showed both pre-midnight and post-midnight occurrence peaks. Our study has shown that 1) MPEs occurring within 30 min of a substorm onset dominated in nearly all MLT bins at each station.

3. The number of MPEs decreased roughly linearly with amplitude at all 5 stations and in all 3 time delay categories, with no clear latitudinal trend.

4. MPE occurrences at all 5 stations peaked during quiet conditions (near SYM/H ~ -20 nT), and at all but the lowest latitude station nearly all MPEs occurred for SYM/H values

between -60 and +10 nT. The tail of the SYM/H distribution at more negative values increased at the lowest magnetic latitude station, reflecting the equatorward expansion of the auroral oval during geomagnetic storms. We would thus expect that stations at subauroral latitudes would observe even more MPEs at times corresponding to more negative SYM/H values.

The SYM/H range corresponding to the largest MPE amplitudes was between -40 and -20 nT at RBY and expanded toward lower SYM/H values with lower latitudes, but there was little or no correlation between the largest MPE amplitudes and SYM/H values at the two lowest latitude stations (SALU and KJPK). Storm-time MPEs were no more likely to have extreme derivative values than MPEs during non-storm conditions, even near 65° MLAT (KJPK).

5. MPE occurrences at all 5 stations were spread over a wide range of SME values above ~200 nT. At the 4 highest latitude stations a large majority of MPEs in each of the 3 time delay categories occurred for SME values between 200 and 900 nT. Only at KJPK was the distribution dominated by events with SME > 800 nT, and that only for events within 30 min of substorm onset. There was a modest correlation between the amplitude of the largest MPEs and the SME index over the SME range from ~200 to ~600 nT at all 5 stations, but the distribution of amplitudes was nearly flat for SME > 600 nT. The amplitude of most MPEs at all SME values and in all 3 time categories was below 12 nT/s.

6. We compared the peak range of the distributions of substorm onsets and MPE onsets during 2015 and 2017 in order to estimate the percentages of substorm onsets after which no MPE occurred within 60 minutes. These ranged from 75 to 92% at the 5 stations, indicating that most substorms were not associated with ≥ 6 nT/s MPEs.

7. The importance of multiple prior substorm onsets (within 2 h) for MPE occurrence was different for pre- and post-midnight MPEs. In the 1700-0100 MLT sector the distribution of MPEs peaked in the 1 prior substorm onset bin and fell off rapidly above 2; in the 0200-0700 MLT sector the distribution of MPEs exhibited a broad maximum between 1 and 4 prior onset bins. Pre-midnight MPEs exhibited a relatively flat distribution of median MPE amplitudes across all prior onset bins, while post-midnight MPEs exhibited a ~50 % increase in median amplitudes from 1 to 4 prior onsets. The percentage of pre-midnight MPEs associated with highly disturbed geomagnetic conditions (SME ≥ 1000 nT) varied inversely with the number of MPEs in each bin, whereas the percentage of post-midnight MPEs associated with SME ≥ 1000 nT was largest in the same bins as the number of MPEs. The overall fractions of MPEs

associated with SME ≥ 1000 nT conditions ranged from 9.2 to 19.4% pre-midnight and 44 to 70% post-midnight.

8. At both RBY and KJPK the amplitude of dipolarizations of the magnetic field at geosynchronous orbit observed by GOES 13 did not extend to as large values for the Δt ≥ 60 min MPE events as for the ≤ 30 min events. Many of the smaller dipolarizations at GOES 13 were associated with short-lived pulses rather than step functions.

8. Discussion and Conclusions

Much of the literature on GICs has focused on magnetic storms. This is reasonable because many of the regions most threatened by GICs are located at magnetic latitudes equatorward of the nominal auroral oval, and only during major magnetic storms does the auroral oval expand significantly toward the equator. However, the extreme magnetic perturbations that cause nighttime GICs occur much more often at high latitudes, so that a study of MPEs at these latitudes provides a larger data base to characterize their occurrence and amplitude distributions, as well as to provide more information on their location in latitude and local time relative to auroral features, their temporal relation to substorms and nightside dipolarizations, and their occurrence and amplitude relative to indices of magnetic storm and substorm activity.

This study has shown that at the stations studied here, MPEs most often occurred during magnetically quiet periods, with SYM/H > - 40 nT, and that there was little or no correlation between the occurrence of the largest MPEs and disturbed conditions (as parameterized by more negative SYM/H values) at any of these stations. This result confirms that large MPEs are not restricted to times when SYM/H is large and negative; it simply means that they occur at higher latitudes at these times.

We have also found that only 60 - 67% of the ≥ 6 nT/s MPEs we observed occurred within 30 minutes of the most recent substorm onset. A recent study by Freeman et al. (2019) found a similar result. They noted that in data from 3 stations in the UK over two solar cycles (only) 54–56% of all extreme rate of change values occurred during substorm expansion or recovery phases.

The separation of nighttime MPEs into two populations in MLT, a pre-midnight one that appeared at all 5 stations and a post-midnight one that was prominent only at the two lowest latitude stations, has been noted by other recent observers. This study has shown that the post-midnight MPE population occurred more often in conjunction with large SME values and after multiple substorm onsets than the pre-midnight MPEs.

Engebretson et al. (2019b) presented 3 cases of multi-station magnetometer observations of MPEs that occurred within the 17-01 h MLT range as well as simultaneous auroral images and satellite observations, and reviewed several studies linking these phenomena to westward traveling surges, polar boundary intensifications, auroral streamers, and small-scale nighttime magnetospheric phenomena such as BBFs (Angelopoulos et al., 1992) and their associated dipolarization fronts (Runov et al., 2009, 2011; Palin et al., 2015) and dipolarizing flux bundles (Gabrielse et al., 2014; Liu et al., 2015).

The local time range of the 02 – 07 h MLT distribution matches that of omega bands (Syrjäsuo and Donovan, 2004), which were identified along with other auroral phenomena by Akasofu and Kimball (1964) and Akasofu (1974). Omega bands have been associated with substorms, and especially their recovery phase (e.g., Opgenoorth et al., 1983; 1994), but they can also occur during extended intervals of steady magnetospheric convection (SMC) when no substorm signatures are present (Solovyev et al., 1999). They have also been closely associated with long period irregular Pi3 or Ps6 magnetic pulsations with periods of 5 – 15 min (e.g., Kawasaki and Rostoker, 1979; Andre and Baumjohann, 1982; Solovyev et al., 1999; Henderson et al., 2002, Connors et al., 2003; and Wild et al., 2011).

Several of the above studies and many others, including those of Lühr and Schlegel (1994), Henderson et al. (2002), Sergeev et al. (2003), Amm et al. (2005), Henderson et al. (2012), Weygand et al. (2015), Henderson (2016), and Partamies et al. (2017), have also looked at ionospheric and magnetospheric phenomena associated with these bands and pulsations. Opgenoorth et al. (1983) used magnetometer, radar, riometer, and all-sky imager data to develop a model current system for omega bands consisting of a meandering ionospheric Hall current composed of a westward background electrojet and circular Hall current vortices around the locations of eastward-moving localized field-aligned currents. Lühr and Schlegel (1994) similarly proposed that omega bands are driven by a pair of counterrotating source-free ionospheric current vortices driven by field-aligned currents, an upward current centered in the luminous part of the Ω band and a downward current in the dark part with its center about 400 km west of the upward current. Opgenoorth et al. (1994) also characterized these events as incorporating both large scale and small scale instabilities, leading to omega bands and pulsations, respectively.

Weygand et al. (2015), using both ground- and space-based data sets, concluded that the most probable mechanism driving omega bands involved azimuthally localized high speed flows in the magnetotail that distorted magnetic shells when they reach the inner magnetosphere. Similarly, Henderson (2016) provided evidence that magnetotail flow bursts penetrated close to the Earth and produced omega bands between substorm onsets, and Partamies et al. (2017) found that the occurrence distribution of omega bands in their large statistical study was in very good agreement with the distribution of fast earthward flows in the plasma sheet during expansion and recovery phases reported by Juusola et al. (2011).

Most recently, Apatenkov et al. (2020) provided detailed observations in northern Scandinavia and northwest Russia of a very large GIC that was associated with an interval of omega bands. As a result of pointing out that the magnetic field created by ionospheric and magnetospheric currents may vary due to both temporal changes of current amplitudes and to motion of the current structures, they modeled this event using the sum of two basic current systems: a 1D linear current (mimicking the auroral electrojet) and a 2D vortex that passed eastward over the field of view of the ground magnetometers. Based on this model, they suggested that propagating nonexplosive and relatively long-lived structures might be responsible for large rapid magnetic field variations if their propagation speeds were sufficiently large.

The main implications of this study are 1) that neither a magnetic storm nor a fully developed substorm is a necessary or sufficient condition for the occurrence of the extreme nighttime magnetic perturbation events that can cause GICs, and 2) that the pre-midnight and post-midnight populations of ≥ 6 nT/s MPEs and their consequent GICs differ not only in their occurrence in local time and latitude but also in their dependence on prior substorm activity and magnetospheric disturbance level. Both this study and the several studies cited above thus point to localized processes in the nightside magnetosphere, several of which often occur during substorms but can also occur at other times and may take different configurations before and after midnight, as being responsible for generating these events. This underlines the importance of further studies of the associations between MPEs and these processes in order to fully understand their role in generating MPEs and the resulting GICs.

Acknowledgments

This work was supported by NSF grants AGS-1651263 to Augsburg University, AGS-1654044 to the University of Michigan, and AGS-1502700 to JHU/APL, and at UCLA by the MMS project. MC thanks NSERC for research support and the Canadian Space Agency for support of AUTUMNX. HO and AS thank the National Swedish Space Agency (SNSA) for support. We thank Laura Simms for contributing statistical analyses.

MACCS magnetometer data are available at http://space.augsburg.edu/maccs/requestdatafile.jsp, AUTUMNX magnetometer data are available in IAGA 2002 ASCII format at http://autumn.athabascau.ca/autumnxquery.php?year=2015&mon=01&day=01, and CANMOS magnetometer data, provided by the Geological Survey of Canada, are available in IAGA 2002 ASCII format at http://geomag.nrcan.gc.ca/data-donnee/sd-en.php. GOES 13 magnetometer data are available at https://satdat.ngdc.noaa.gov/sem/goes/data/new_full/. SYM/H index data are available at the Goddard Space Flight Center Space Physics Data Facility at https://cdaweb.sci.gsfc.nasa.gov/index.html/. SME index data are available from SuperMAG (http://supermag.jhuapl.edu/indices/), Principal Investigator Jesper Gjerloev, derived from magnetometer data from INTERMAGNET, Alan Thomson; USGS, Jeffrey J. Love; CARISMA, PI Ian Mann; CANMOS, Geomagnetism Unit of the Geological Survey of Canada; The S-RAMP Database, PI K. Yumoto and Dr. K. Shiokawa; The SPIDR database; AARI, PI Oleg Troshichev; The MACCS program, PI M. Engebretson; GIMA; MEASURE, UCLA IGPP and Florida Institute of Technology; SAMBA, PI Eftyhia Zesta; 210 Chain, PI K. Yumoto; SAMNET, PI Farideh Honary; IMAGE, PI Liisa Juusola; Finnish Meteorological Institute, PI Liisa Juusola; Sodankylä Geophysical Observatory, PI Tero Raita; UiT the Arctic University of Norway, Tromsø Geophysical Observatory, PI Magnar G. Johnsen; GFZ German Research Centre For Geosciences, PI Jürgen Matzka; Institute of Geophysics, Polish Academy of Sciences, PI Anne Neska and Jan Reda; Polar Geophysical Institute, PI Alexander Yahnin and Yarolav Sakharov; Geological Survey of Sweden, PI Gerhard Schwarz; Swedish Institute of Space Physics, PI Masatoshi Yamauchi; AUTUMN, PI Martin Connors; DTU Space, PI Dr. Thom R. Edwards and Anna Willer; PENGUIn; South Pole and McMurdo Magnetometer, PIs Louis J. Lanzerotti and Allan T. Weatherwax; ICESTAR; RAPIDMAG; British Antarctic

Survey; McMAC, PI Dr. Peter Chi; BGS, PI Dr. Susan Macmillan; Pushkov Institute of Terrestrial Magnetism, Ionosphere and Radio Wave Propagation (IZMIRAN);; MFGI, PI B. Heilig; Institute of Geophysics, Polish Academy of Sciences, PI Anne Neska and Jan Reda; and University of L'Aquila, PI M. Vellante; BCMT, V. Lesur and A. Chambodut; Data obtained in cooperation with Geoscience Australia, PI Marina Costelloe; AALPIP, co-PIs Bob Clauer and Michael Hartinger; SuperMAG, Data obtained in cooperation with the Australian Bureau of Meteorology, PI Richard Marshall.

References

Akasofu, S.-I, and D. S. Kimball (1964), The dynamics of the aurora, 1, Instabilities of the aurora, *Journal of Atmospheric and Terrestrial Physics, 26,* 205-211, doi:10.1016/0021-9169(64)90147-3

Akasofu, S.-I. (1974), A study of auroral displays photographed from the DMSP-2 satellite and from the Alaska meridian chain of stations, *Space Science Reviews, 16,* 617-725, ISSN: 0038-6308

Amm, O., Aksnes, A., Stadsnes, J., Østgaard, N., Vondrak, R. R., Germany, G. A., et al. (2005), Mesoscale ionospheric electrodynamics of omega bands determined from ground-based electromagnetic and satellite optical observations, *Annales Geophysicae*, *23*, 325–342, doi:10.5194/angeo-23-325-2005

André, D., and W. Baumjohann (1982), Joint two-dimensional observations of ground magnetic and ionospheric electric fields associated with auroral currents. 5. Current system associated with eastward drifting omega bands, *Journal of Geophysics*, *50,* 194–201, https://journal.geophysicsjournal.com/JofG/article/view/201.

Angelopoulos, V., W. Baumjohann, C. F. Kennel, F. V. Coroniti, M. G. Kivelson, R. Pellat, R. J. Walker, H. Lühr, and G. Paschmann (1992), Bursty Bulk Flows in the inner central plasma sheet, *Journal of Geophysical Research*, *97*, 4027-4039, doi:10.1029/91JA02701

Apatenkov, S. V., Pilipenko, V. A., Gordeev, E. I., Viljanen, A., Juusola, L., Belakhovsky, V. B.,Sakharov, Ya. A., and Selivanov, V. N. (2020). Auroral omega bands are a significant cause of large geomagnetically induced currents, *Geophysical Research Letters*, *47*, e2019GL086677, doi:10.1029/2019GL086677

Belakhovsky, V. B. et al. (2018), Characteristics of the variability of a geomagnetic field for studying the impact of the magnetic storms and substorms on electrical energy systems, Izvestiya, *Physics of the Solid Earth*, *54*, 52–65, doi:10.1134/S1069351318010032

Belakhovsky, V., V. Pilipenko, M. Engebretson, Ya. Sakharov, and V. Selivanov (2019), Impulsive disturbances of the geomagnetic field as a cause of induced currents of electric power lines, *Journal of Space Weather and Space Climate, 9*, A18, doi:10.1051/swsc/2019015

Connors, M., G. Rostoker, G. Sofko, R. L. McPherron, and M. Henderson (2003), Ps 6 disturbances: Relation to substorms and the auroral oval, *Annales Geophysicae, 21,* 493-508, doi:10.5194/angeo-21-493-2003

Connors, M., Schofield, I., Reiter, K., Chi, P. J., Rowe, K. M., & Russell, C. T. (2016), The AUTUMNX magnetometer meridian chain in Québec, Canada, *Earth, Planets and Space*, *68,* doi:10.1186/s40623-015-0354-4

Dimmock, A. P. et al. (2019), The GIC and geomagnetic response over Fennoscandia to the 7-8 September 2017 geomagnetic storm, *Space Weather, 17,* 989 –1010, doi:10.1029/ 2018SW002132.

Engebretson, M. J., W. J. Hughes, J. L. Alford, E. Zesta, L. J. Cahill, Jr., R. L. Arnoldy, and G. D. Reeves (1995), Magnetometer array for cusp and cleft studies observations of the spatial extent of broadband ULF magnetic pulsations at cusp/cleft latitudes, *Journal of Geophysical Research, 100,* 19371-19386, doi:10.1029/95JA00768

Engebretson, M. J., Pilipenko, V. A., Ahmed, L. Y., Posch, J. L., Steinmetz, E. S., Moldwin, M. B., Connors, M. G., Weygand, J. M., Mann, I. R., Boteler, D. H., Russell, C. T., and Vorobev, A. V. (2019a), Nighttime magnetic perturbation events observed in Arctic Canada: 1. Survey and statistical analysis, *Journal of Geophysical Research: Space Physics, 124,* 7442–7458, doi: 10.1029/2019JA026794.

Engebretson, M. J., E. S. Steinmetz, J. L. Posch, V. A. Pilipenko, M. B. Moldwin, M. G. Connors, D. H. Boteler, I. R. Mann, M. D. Hartinger, J. M. Weygand, L. R. Lyons, Y. Nishimura , H. J. Singer, S. Ohtani, C. T. Russell, A. Fazakerley, and L. M. Kistler (2019b), Nighttime magnetic perturbation events observed in Arctic Canada: 2. Multiple-instrument observations, *Journal of Geophysical Research: Space Physics, 124,* 7459-7476, doi:10.1029/2019JA026797.

Freeman, M. P., C. Forsyth, and I. J. Rae (2019), The influence of substorms on extreme rates of change of the surface horizontal magnetic field in the United Kingdom, *Space Weather, 17,* 827 –844, doi:10.1029/2018SW002148.

Gabrielse, C., V. Angelopoulos, A. Runov, and D. L. Turner (2014), Statistical characteristics of particle injections throughout the equatorial magnetotail, *Journal of Geophysical Research: Space Physics, 119,* 2512–2535, doi:10.1002/2013JA019638

Henderson, M. G., Kepko, L., Spence, H. E., Connors, M., Sigwarth, J. B., Frank, L. A., Singer, H.,J., and Yumoto, K. (2002), The evolution of north-south aligned auroral forms into auroral torch structures: The generation of omega bands and Ps6 pulsations via flow bursts, in the *Proceedings of the Sixth International Conference on Substorms*, edited by R. M. Winglee, University of Washington, Seattle, WA, ISBN:0971174032 9780971174030

Henderson, M. G. (2012). Auroral substorms, poleward boundary activations, auroral streamers, omega bands, and onset precursor activity, In A. Keiling et al. (Eds.), *Auroral phenomenology and magnetospheric processes: Earth and other planets* (Vol. 197, pp. 39–54), Washington, DC: American Geophysical Union.

Henderson, M. G. (2016), Recurrent embedded substorms during the 19 October 1998 GEM storm, *Journal of Geophysical Research: Space Physics, 121*, 7847–7859, doi:10.1002/2015JA022014

Juusola, L., Østgaard, N., Tanskanen, E., Partamies, N., and Snekvik, K. (2011), Earthward plasma sheet flows during substorm phases, *Journal of Geophysical Research, 116,* A10228, https://doi.org/10.1029/2011JA016852

Juusola, L., A. Viljanen, M. van de Kamp, E. I. Tanskanen, H. Vanhamäki, N. Partamies, and K. Kauristie (2015), High-latitude ionospheric equivalent currents during strong space storms: Regional perspective, *Space Weather, 13*, 49–60, doi:10.1002/2014SW001139

Kawasaki, K., and Rostoker, G. (1979), Perturbation magnetic fields and current systems associated with eastward drifting auroral structures, *Journal of Geophysical Research*, *84*, 1464–1480, doi:10.1029/JA084iA04p01464

Liu, J., V. Angelopoulos, X. Chu, X.-Z. Zhou, and C. Yue (2015), Substorm Current Wedge Composition by Wedgelets, *Geophysical Research Letters, 42,* 1669–1676, doi:10.1002/2015GL063289.

Lühr, H., and K. Schlegel (1994), Combined measurements of EISCAT and the EISCAT magnetometer cross to study Ω bands, *Journal of Geophysical Research, 99,* 8951-8959, doi:10.1029/94JA00487

Newell, P. T., and Gjerloev, J. W. (2011a), Evaluation of SuperMAG auroral electrojet indices as indicators of substorms and auroral power, *Journal of Geophysical Research, 116,* A12211, doi:10.1029/2011JA016779.

Newell, P. T., and Gjerloev, J. W. (2011b), Substorm and magnetosphere characteristic scales inferred from the SuperMAG auroral electrojet indices, *Journal of Geophysical Research*,

116, A12232, doi:10.1029/2011JA016936
Nikitina, L., Trichtchenko, L., and Boteler, D. H. (2016), Assessment of extreme values in geomagnetic and geoelectric field variations for Canada. *Space Weather, 14,* 481–494, doi:10.1002/2016SW001386
Opgenoorth, H., Oksman, J., Kaila, K., Nielsen, E., & Baumjohann, W. (1983), Characteristics of eastward drifting omega bands in the morning sector of the auroral oval, *Journal of Geophysical Research*, *88*, 9171–9185, doi:10.1029/JA088iA11p09171
Opgenoorth, H. J., M. A. L. Persson, T. I. Pulkkinen, and R. J. Pellinen (1994), Recovery phase of magnetospheric substorms and its association with morning-sector aurora, *Journal of Geophysical Research*, *99*, 4115-4129, doi:10.1029/93JA01502
Palin, L., C. Jacquey, H. Opgenoorth, M. Connors, V. Sergeev, J.-A. Sauvaud, R. Nakamura, G. D. Reeves, H. J. Singer, V. Angelopoulos, and L. Turc (2015), Three-dimensional current systems and ionospheric effects associated with small dipolarization fronts, *Journal of Geophysical Research - Space Physics*, *120*, 3739–3757, doi:10.1002/2015JA021040
Partamies, N., Weygand, J. M., and Juusola, L. (2017), Statistical study of auroral omega bands, *Annales Geophysicae*, 35, 1069–1083, doi:10.5194/angeo-35-1069-2017
Runov, A., Angelopoulos, V., Sitnov, M. I., Sergeev, V. A., Bonnell, J., McFadden, J. P., et al. (2009), THEMIS observations of an earthward propagating dipolarization front, *Geophysical Research Letters*, *36*, L14106, doi:10.1029/2009GL038980
Runov, A., Angelopoulos, V., Zhou, X.-Z., Zhang, X.-J., Li, S., Plaschke, F., & Bonnell, J. (2011), A THEMIS multicase study of dipolarization fronts in the magnetotail plasma sheet, *Journal of Geophysical Research*, *116*, A05216, doi:10.1029/2010JA016316
Sergeev, V. A., Yahnin, D. A., Liou, K., Thomsen, M. F., and Reeves, G. D, (2003), Narrow plasma streams as a candidate to populate the inner magnetosphere, in *The Inner Magnetosphere*, edited by T. I. Pulkkinen, N. A. Tsyganenko, and R. H. W. Friedel, Geophysical Monograph Series, 55–60, Washington, D.C., American Geophysical Union, doi:10.1029/155GM07
Singer, H. J., Matheson, L., Grubb, R., Newman, A., & Bouwer, S. D. (1996). Monitoring space weather with the GOES magnetometers, in *SPIE Conference Proceedings, vol. 2812*, edited by E. R. Washwell, pp. 299–308, GOES-8 and Beyond, SPIE, Bellingham, Wash.

Solovyev, S. I., Baishev, D. G., Barkova, E. S., Engebretson, M. J., Posch, J. L., Hughes, W. J., Yumoto, K., and Pilipenko, V. A. (1999), Structure of disturbances in the dayside and nightside ionosphere during periods of negative interplanetary magnetic field Bz, *Journal of Geophysical Research*, *104*, 28,019–28,039, doi:10.1029/1999JA900286

Syrjäsuo, M. T., and Donovan, E. F. (2004), Diurnal auroral occurrence statistics obtained via machine vision, *Annales Geophysicae*, *22*, 1103–1113, doi:10.5194/angeo-22-1103-2004

Viljanen, A., Nevanlinna, H., Pajunpää, K., & Pulkkinen, A. (2001), Time derivative of the horizontal geomagnetic field as an activity indicator, *Annales Geophysicae*, *19*(9), 1107–1118, doi:10.5194/angeo-19-1107-2001

Viljanen, A., E. I. Tanskanen, and A. Pulkkinen (2006), Relation between substorm characteristics and rapid temporal variations of the ground magnetic field, *Annales Geophysicae*, *24*, 725-733, doi:10.5194/angeo-24-725-2006.

Viljanen, A., and Tanskanen, E. (2011), Climatology of rapid geomagnetic variations at high latitudes over two solar cycles. *Annales Geophysicae*, *29*, 1783–1792, doi:10.5194/angeo-29-1783-2011

Viljanen, A., (1997), The relation between geomagnetic variations and their time derivatives and implications for estimation of induction risks, *Geophysical Research Letters*, *2*4, 631–634, doi:10.1029/97GL00538

Vorobev, A., Pilipenko, V., Sakharov, Y.,and Selivanov, V. (2019), Statistical relationships between variations of the geomagnetic field, auroral electrojet, and geomagnetically induced currents, *Solar-Terrestrial Physics*, *5*, 35–42, doi:10.12737/stp-51201905

Weygand, J. M., Kivelson, M. G., Frey, H. U., Rodriguez, J. V., Angelopoulos, V., Redmon, R., Barker-Ream, J., Grocott, A., and Amm, O. (2015), An interpretation of spacecraft and ground based observations of multiple omega band events, *Journal of Atmospheric and Solar-Terrestrial Physics, 133,* 185–204, doi:10.1016/j.jastp.2015.08.014

Wild, J. A., Woodfield, E. E., Donovan, E., Fear, R. C., Grocott, A., Lester, M., Fazakerley, A. N., Lucek, E., Khotyaintsev, Y., Andre, M., Kadokura, A., Hosokawa, K., Carlson, C., McFadden, J. P., Glassmeier, K. H., Angelopoulos, V., and Björnsson, G. (2011), Midnight sector observations of auroral omega bands, *Journal of Geophysical Research,*

116, A00130, doi:10.1029/2010JA015874

Table 1. Locations of the magnetometer stations used in this study. Geographic and corrected geomagnetic (CGM) latitude and longitude are shown, as well as the universal time (UT) of local magnetic noon.

Array	Station	Code	Geog. lat.	Geog. lon.	CGM lat.	CGM lon.	UT of Mag Noon	Cadence, s
MACCS	Repulse Bay	RBY	66.5°	273.8°	75.2°	-12.8°	17:47	0.5
	Cape Dorset	CDR	64.2°	283.4°	72.7°	3.0°	16:58	0.5
CANMOS	Iqaluit	IQA	63.8°	291.5°	71.4°	15.1°	16:19	1.0
AUTUMNX	Salluit	SALU	62.2°	284.3°	70.7°	4.1°	16:54	0.5
	Kuujuarapik	KJPK	55.3°	282.2°	64.4°	0.2°	17.06	0.5

Note: CGM coordinates were calculated for epoch 2015, using http://sdnet.thayer.dartmouth.edu/aacgm/aacgm_calc.php#AACGM .

Table 2. Numbers of MPEs observed at each station with derivative amplitude $|dB/dt| \geq 6$ nT/s in any component, as a function of Δt.

Station	MLAT	$\Delta t \leq 30$ min		$30 < \Delta t < 60$ min		$\Delta t \geq 60$ min		All
		#	%	#	%	#	%	#
RBY	75.2°	53	60	22	25	13	15	88
CDR	72.7°	112	67	32	19	22	13	166
IQA	71.4°	119	66	29	16	32	18	180
SALU	70.7°	187	66	47	17	48	17	282
KJPK	64.4°	79	64	20	16	25	20	124

Table 3. Distribution of pre- and post-midnight ≥ 6 nT/s MPEs at each station as a function of time between the most recent substorm onset and event occurrence. Pre-midnight MPEs include those observed between 1700 and 0100 MLT, and post-midnight events those between 0200 and 0700 MLT.

Pre-midnight

Station	RBY		CDR		IQA		SALU		KJPK	
	#	%	#	%	#	%	#	%	#	%
$t \leq 30$ min	50	60	105	69	107	65	168	69	46	59
30-60 min	20	24	28	18	24	15	37	15	15	19
$t \geq 60$ min	13	16	20	13	34	21	39	16	17	22
Sum	83		153		165		244		78	

Combined: $t \leq 30$ min: 66%, 30-60 min: 17%, $t \geq 60$ min: 17%

Post-midnight

Station	RBY		CDR		IQA		SALU		KJPK	
	#	%	#	%	#	%	#	%	#	%
$t \leq 30$ min	3	75	5	71	7	70	17	61	30	75
30-60 min	1	25	1	14	3	30	5	18	6	15
$t \geq 60$ min	0	0	1	14	0	0	6	21	4	10
Sum	4		7		10		28		40	

Combined: $t \leq 30$ min: 70%, 30-60 min: 18%, $t \geq 60$ min: 12%

Table 4. The numbers of ≥ 6 nT/s MPEs observed at 5 stations during 2015 and 2017 between 2325 and 0555 UT as a function of their time delays (0-30, 30-60, and 0-60 min) after the most recent substorm onset (columns 2-4), these numbers as percentages of the estimated number of substorm onsets (columns 5-7), and the estimated percentages of substorm onsets after which no MPE occurred within 60 minutes after onset (column 8).

Station	Number of Events			% following a substorm onset			SS onset % not
	0- 30 min	30 - 60 min	0-60 min	0- 30 min	30 - 60 min	0-60 min	related to MPEs
RBY	53	22	75	5.7	2.4	8.0	92.0
CDR	112	32	144	12.0	3.4	15.5	84.5
IQA	119	29	148	12.8	3.1	15.9	84.1
SALU	187	47	234	20.1	5.0	25.1	74.9
KJPK	79	20	99	8.5	2.1	10.6	89.4

Table 5. The number of ≥ 6 nT/s MPEs observed during 2015 and 2017 at the three lowest latitude stations as a function of the number of substorm onsets that occurred within 2 hours prior to the MPE. Events are separated into two local time ranges: from 1700 to 0100 MLT and 0200-0700 MLT.

	Number of Onsets							
Station	0	1	2	3	4	5	6	Total
IQA								
1700-0100 MLT	20	102	43	15	4	0	0	184
0200-0700 MLT	0	2	2	4	2	0	0	10
SALU								
1700-0100 MLT	21	118	71	21	5	1	0	237
0200-0700 MLT	3	4	7	7	6	0	0	27
KJPK								
1700-0100 MLT	12	28	23	11	2	1	0	77
0200-0700 MLT	1	5	16	10	8	0	2	42

Table 6. Application of Pearson's Chi-squared test with 2 degrees of freedom to the number of pre-midnight and post-midnight MPE occurrences as a function of the number of prior substorm onsets with 2 hours.

MLT Range	17 - 1	2 - 7	17 - 1	2 - 7	17 - 1	2 – 7
Station	IQA		SALU		KJPK	
0 onsets	20	0	21	3	12	1
1 onset	102	2	118	4	28	5
≥ 2 onsets	62	8	98	20	37	36
X^2	8.94		12.36		16.48	
p-value	0.011		0.0021		0.00026	

Table 7. The normalized percentage of pre- and post-midnight ≥ 6 nT/s MPEs events with SME ≥ 1000 nT observed at IQA, SALU, and KJPK during 2015 and 2017, as a function of the number of substorm onsets that occurred within 2 hours prior to the MPE.

	Number of Onsets							
Station	0	1	2	3	4	5	6	7
1700-0100 MLT								
IQA								
Total MPEs	20	102	43	15	4	0	0	0
# SME ≥ 1000 nT	0	2	6	5	4			
% SME ≥ 1000 nT	0	2	14	33	100			
SALU								
Total MPEs	21	118	71	21	5	1	0	0
# SME ≥ 1000 nT	0	6	6	5	3	1		
% SME ≥ 1000 nT	0	5	8	24	60	100		
KJPK								
Total MPEs	12	28	23	11	2	1	0	0
# SME ≥ 1000 nT	0	2	6	5	2	0		
% SME ≥ 1000 nT	0	7	26	45	100	0		
0200-0700 MLT								
IQA								
Total MPEs	0	2	2	4	2	0	0	0
# SME ≥ 1000 nT	0	0	2	3	2			
% SME ≥ 1000 nT	0	0	100	75	100			
SALU								
Total MPEs	3	4	7	7	6	0	0	0
# SME ≥ 1000 nT	0	1	2	5	4			
% SME ≥ 1000 nT	0	25	29	71	67			
KJPK								
Total MPEs	1	5	16	10	8	0	1	1
# SME ≥ 1000 nT	0	1	9	6	4		1	1
% SME ≥ 1000 nT	0	20	56	60	50		100	100

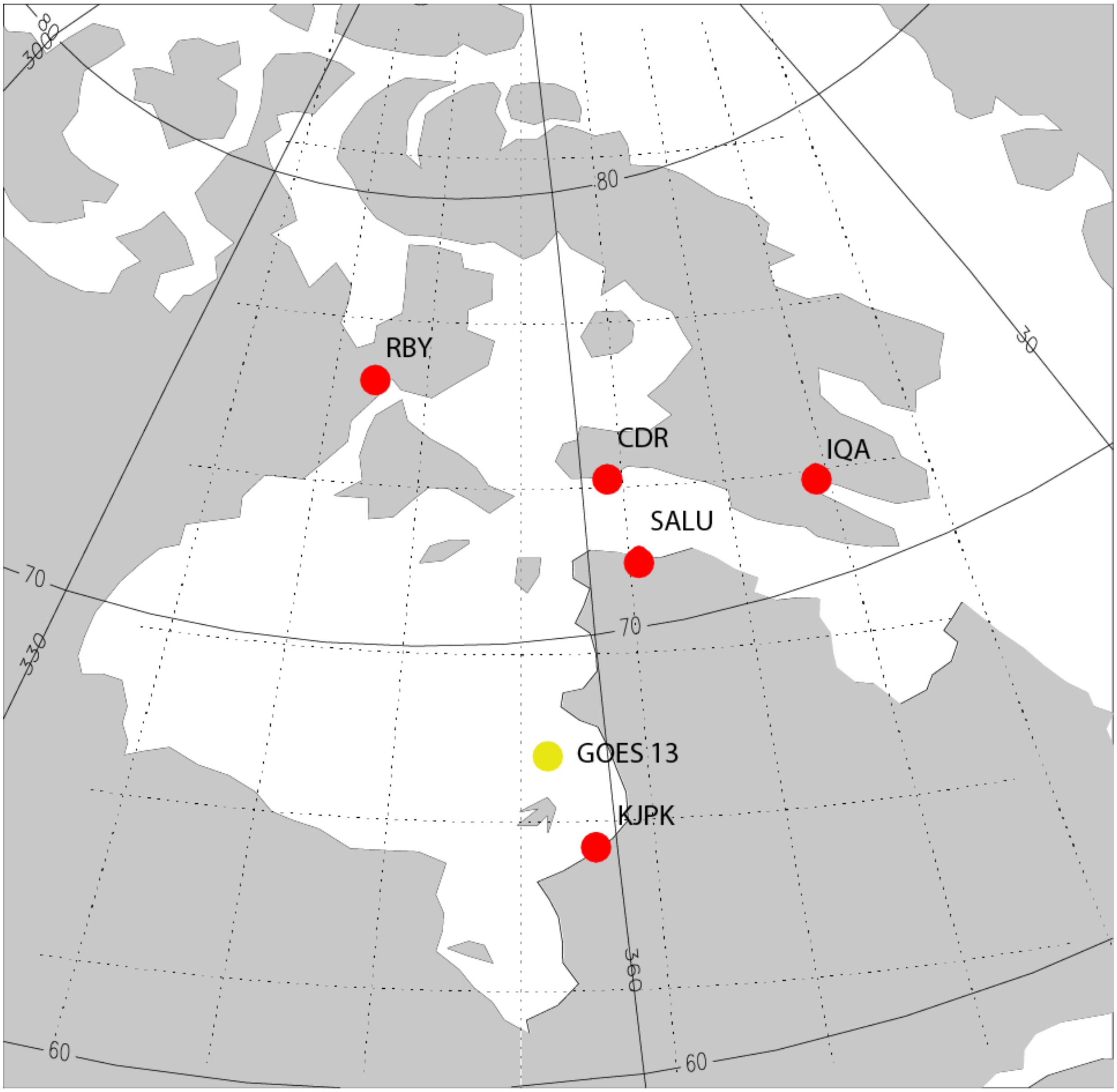

Figure 1. Map of Eastern Arctic Canada showing the location of the five ground magnetometers that provided data for this study. Also shown by the yellow circle is the approximate northern magnetic footpoint of the geosynchronous GOES-13 spacecraft. Solid lines show corrected geomagnetic coordinates.

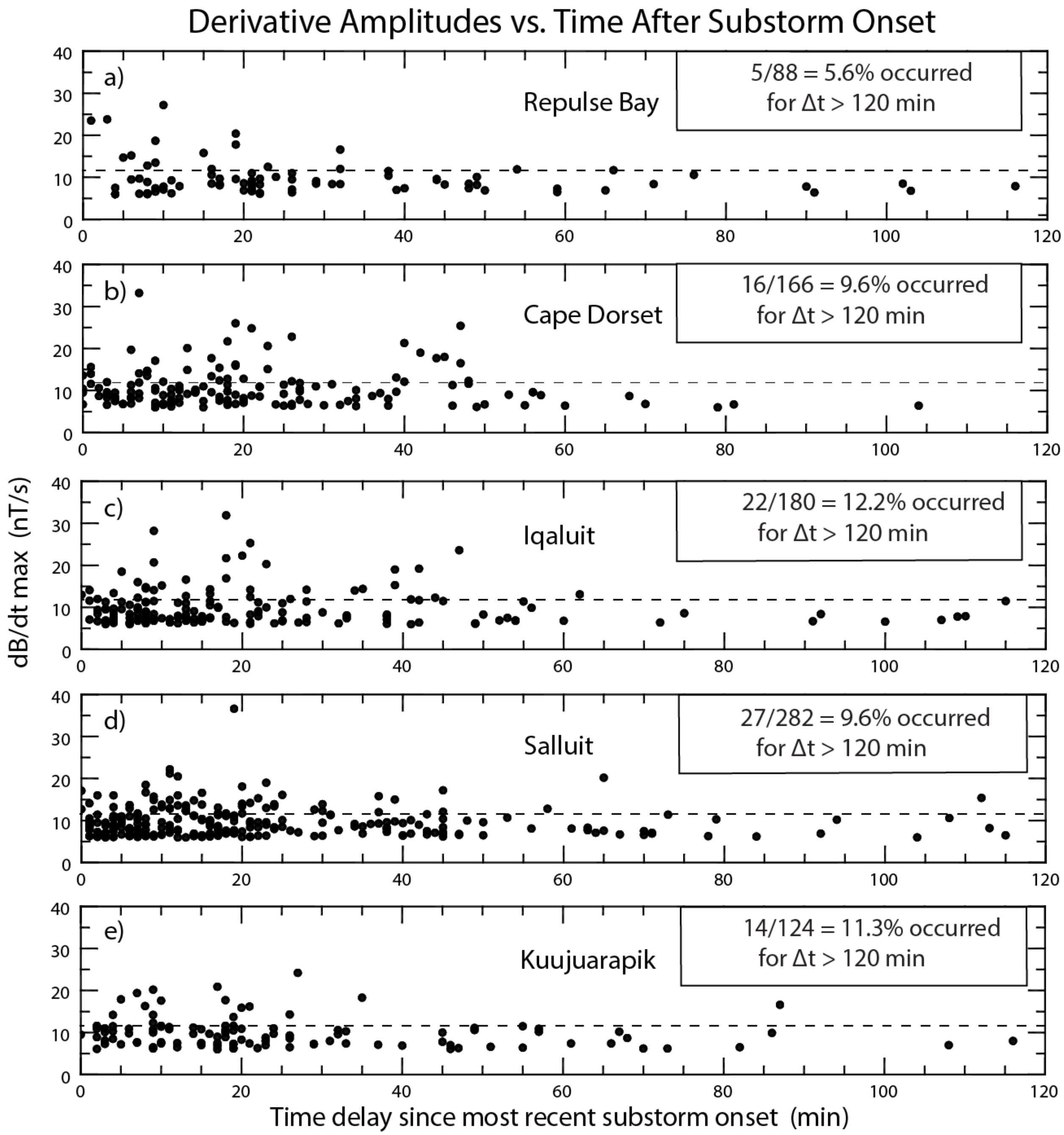

Figure 2. Plot of the amplitude of the maximum |dB/dt| value in any nighttime MPE component observed at each station as a function of its delay after the most recent substorm onset: a) Repulse Bay, b) Cape Dorset, c) Iqaluit, d) Salluit, and e) Kuujuarapik. Only events with maximum derivative amplitude ≥ 6 nT/s are shown. The horizontal dotted line indicates an amplitude of 12 nT/s.

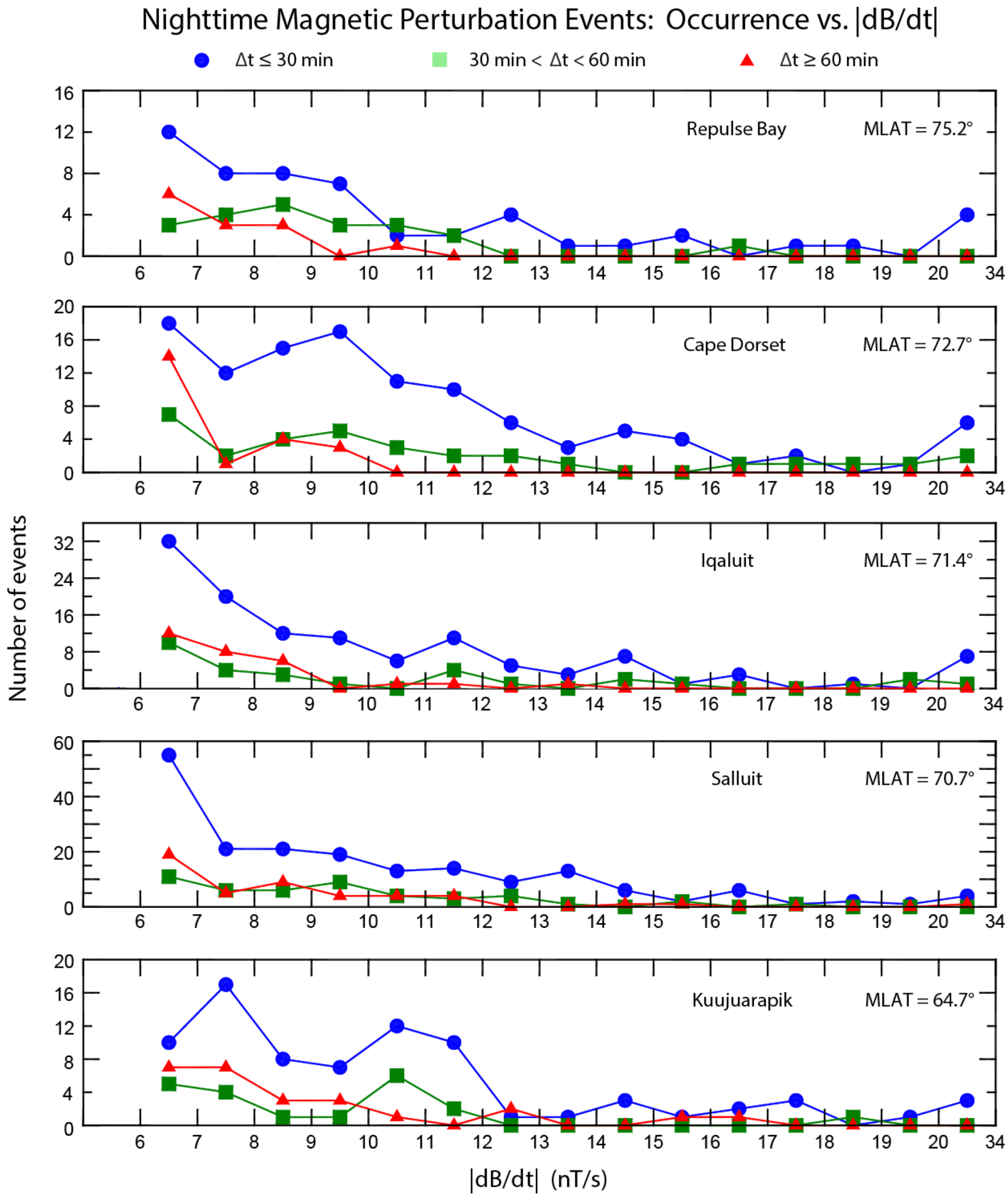

Figure 3. Plots of the number of occurrences of ≥ 6 nT/s nighttime MPEs observed at Repulse Bay, Cape Dorset, Iqaluit, Salluit, and Kuujuarapik as a function of the maximum derivative amplitude, sorted by each station's magnetic latitude. Events are color-coded based on time of occurrence after the closest prior substorm onset: $\Delta t \leq 30$ min (blue circles), $30 < \Delta t < 60$ min (green squares), and $\Delta t \geq 60$ min (red triangles). The last interval at the right includes all events with amplitude > 20 nT/s. Note that the vertical scales are different in each panel.

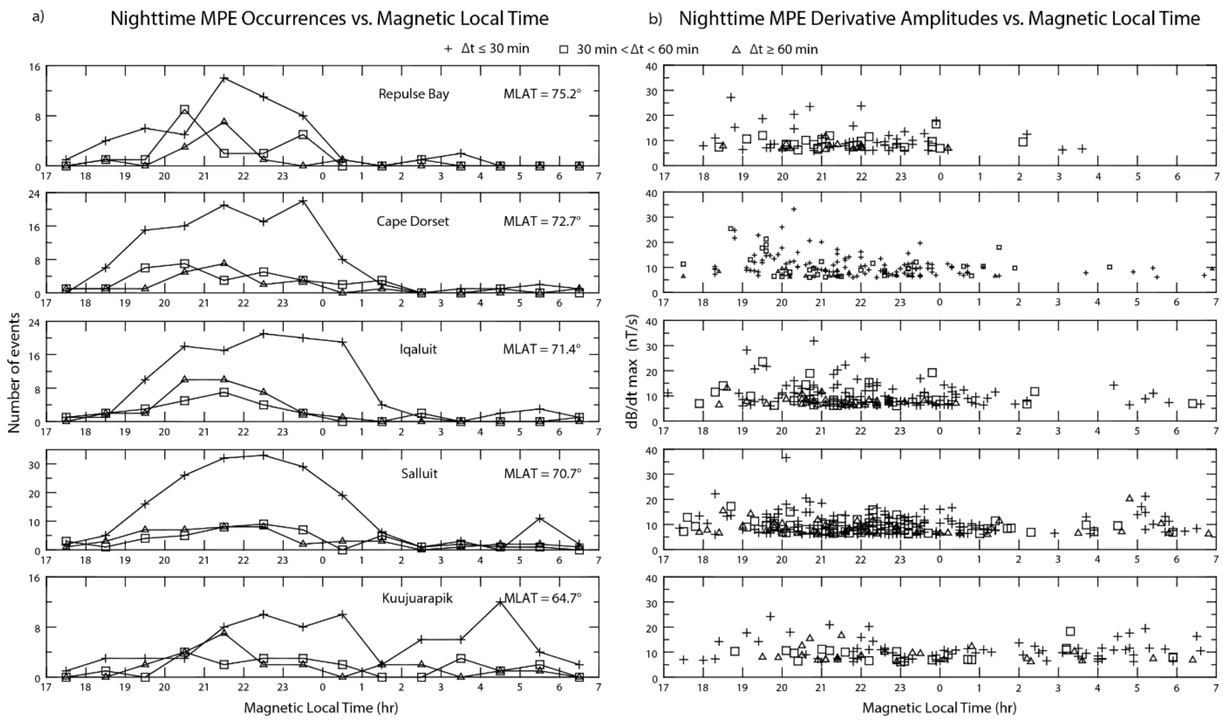

Figure 4. Panel a shows the number of occurrences of ≥ 6 nT/s nighttime MPEs observed at Repulse Bay, Cape Dorset, Iqaluit, Salluit, and Kuujuarapik in 1-hour bins of magnetic local time (MLT) from 17 h to 07 h, sorted by each station's magnetic latitude. Panel b shows the distribution of MPE derivative amplitude at these same stations. Different symbols are used to designate events based on the time of MPE occurrence after the closest prior substorm onset: plus signs for Δt ≤ 30 min, open squares for Δt between 30 and 60 min, and open triangles for Δt ≥ 60 min.

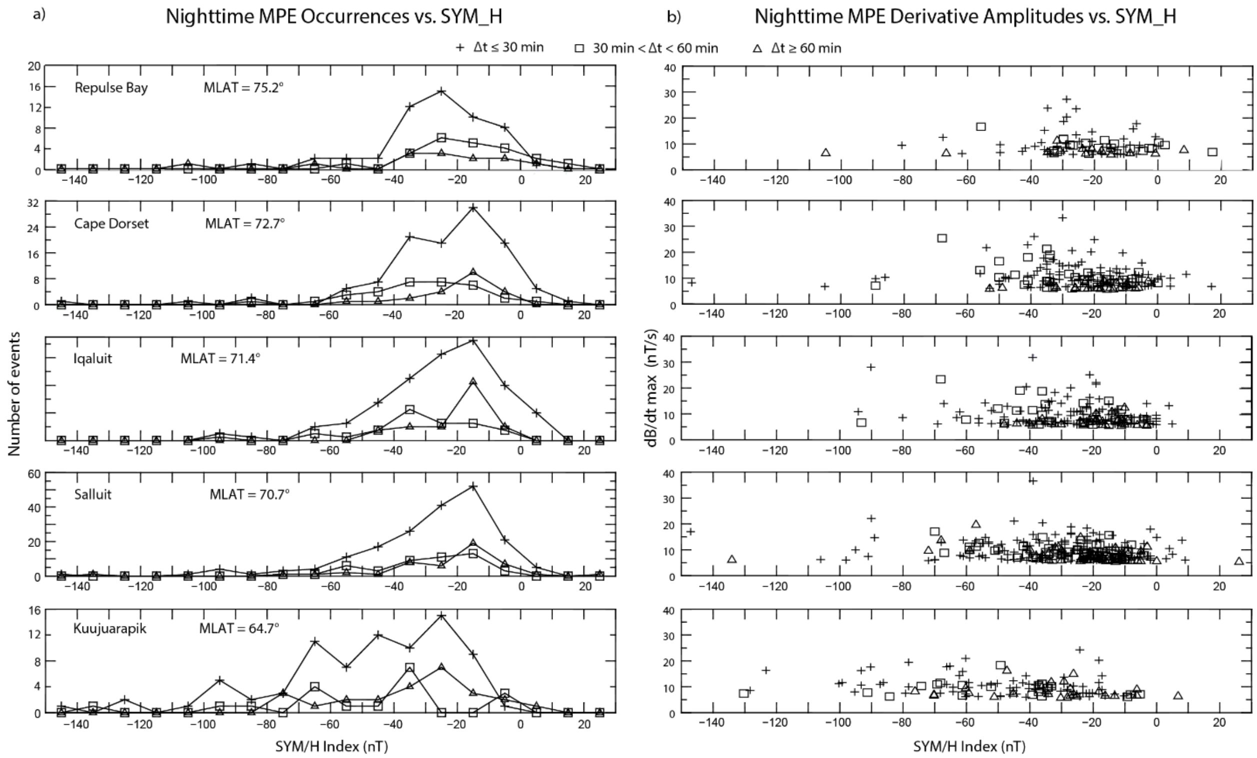

Figure 5. Plot of ≥ 6 nT/s nighttime MPE occurrences and amplitudes as in Figure 4, but as a function of the SYM/H index.

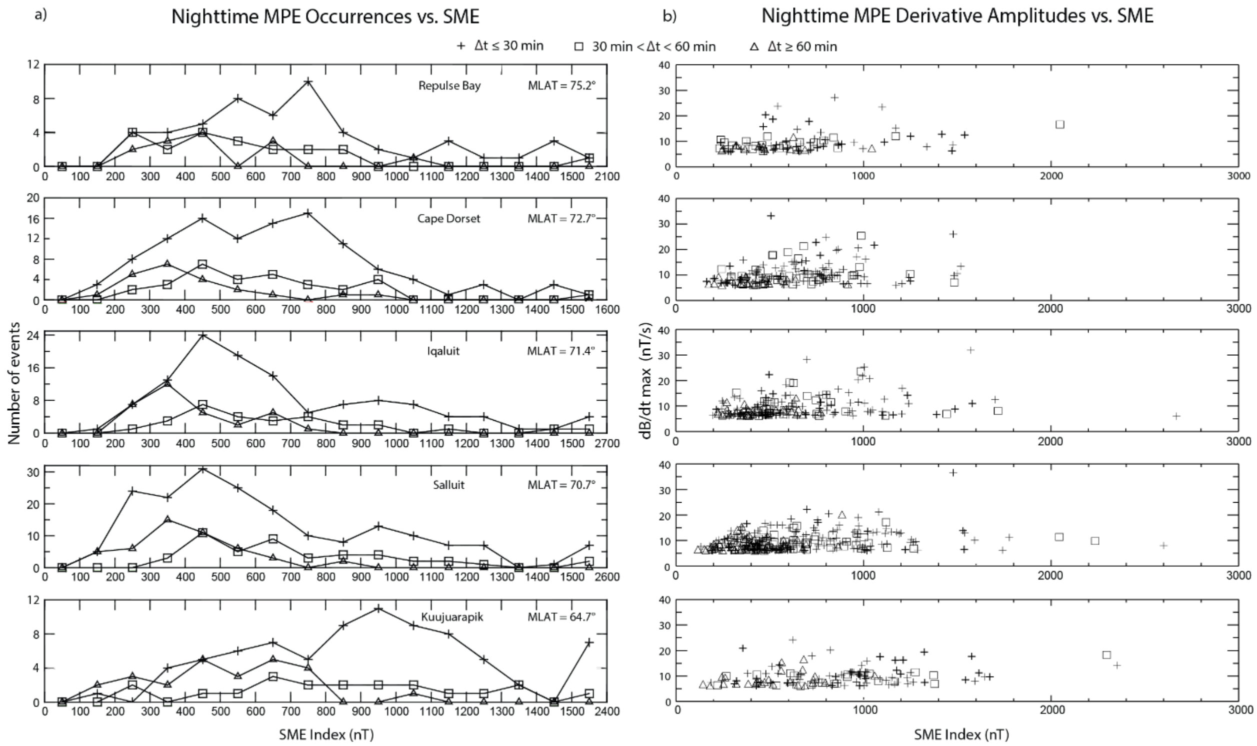

Figure 6. Plot of ≥ 6 nT/s nighttime MPE occurrences and amplitudes as in Figure 4, but as a function of the SME index. In panel a) the events at each station are binned in steps of 100 nT, except for the rightmost bin, which includes all events with SME between 1500 and the maximum value shown in the horizontal legend for each station.

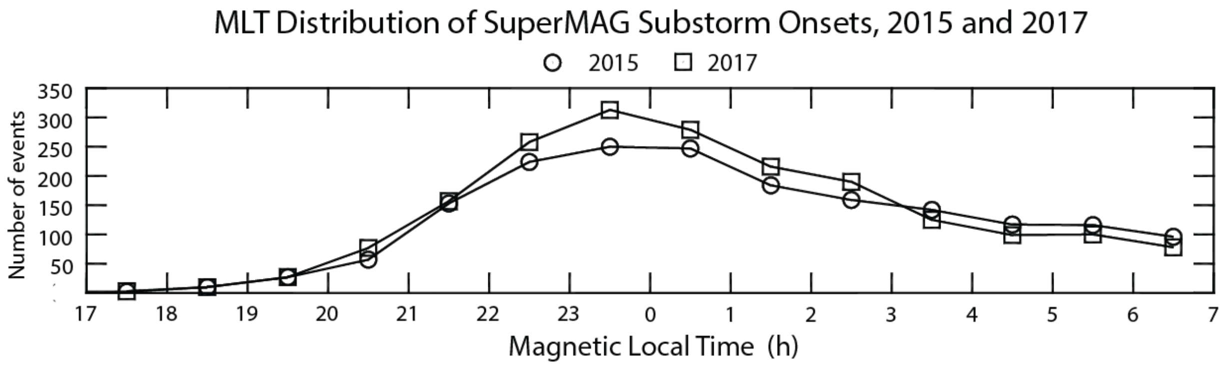

Figure 7. Plot of the number of substorm onsets during 2015 (circles) and 2017 (squares) in 1-h bins between 17 and 07 MLT, based on the SuperMAG substorm onset data base.

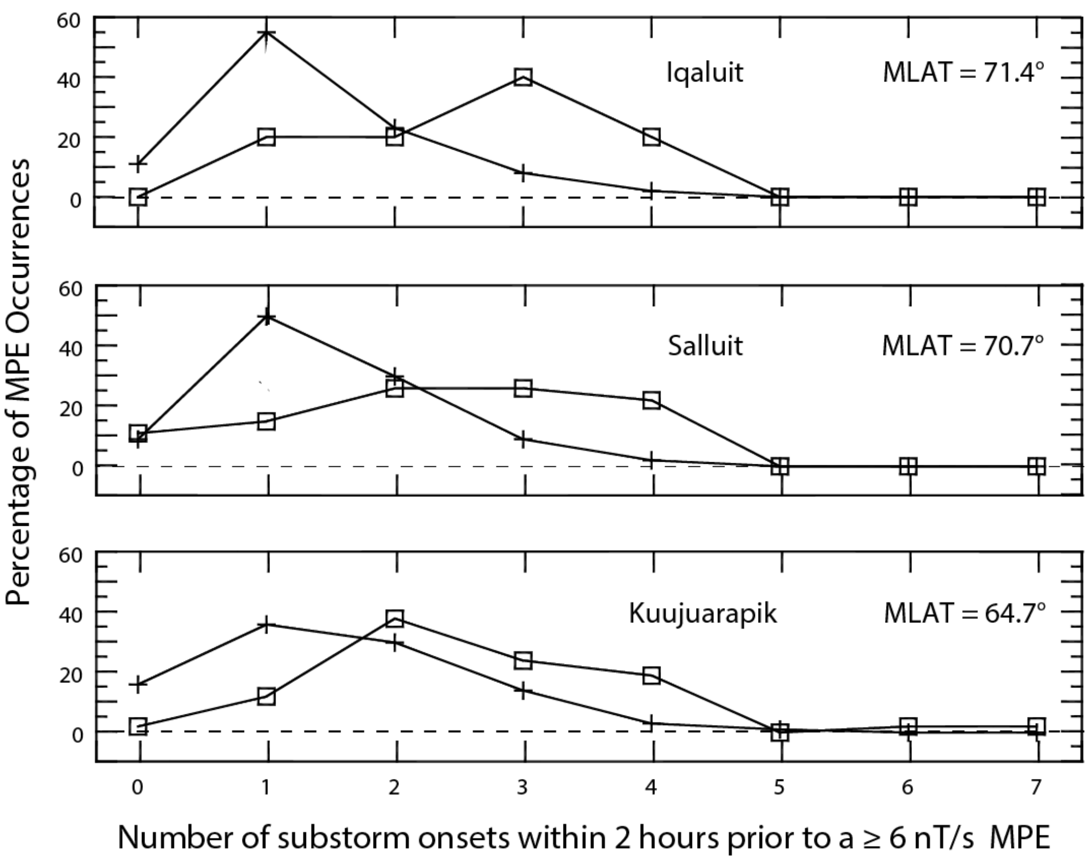

Figure 8. Plot of the percentage of MPEs observed during 2015 and 2017 as a function of the number of substorm onsets that occurred within 2 hours prior to the MPE, at IQA, SALU, and KJPK. Plus signs and open squares indicate pre-midnight and post-midnight events, respectively.

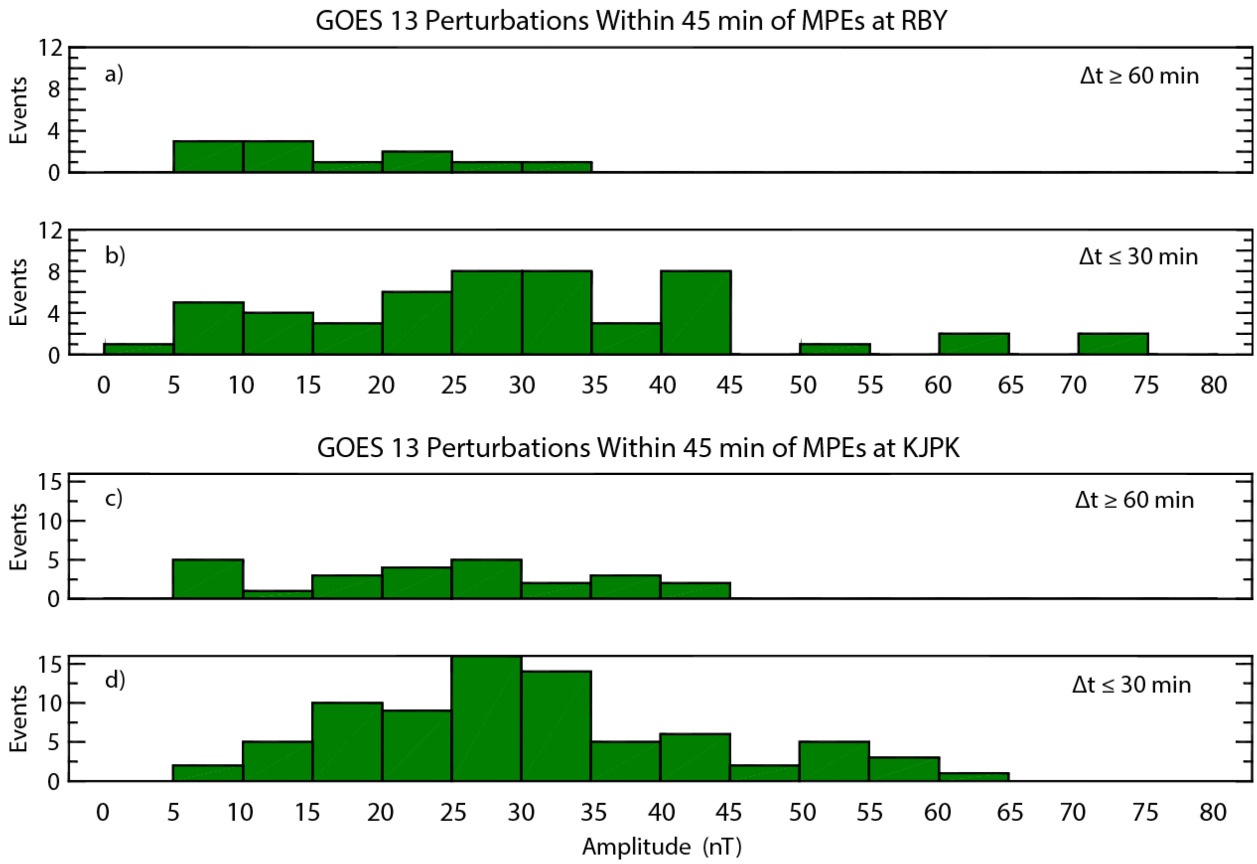

Figure 9. Plots of the number of GOES 13 perturbations occurring within 45 minutes prior to MPEs observed at RBY and KJPK, as a function of amplitude. Panels a) and c) show the distribution of amplitudes for MPEs occurring ≥ 60 min after the most recent substorm onset, and panels b) and d) show the distribution for MPEs occurring ≤ 30 min after the most recent substorm onset.

Figure 1.

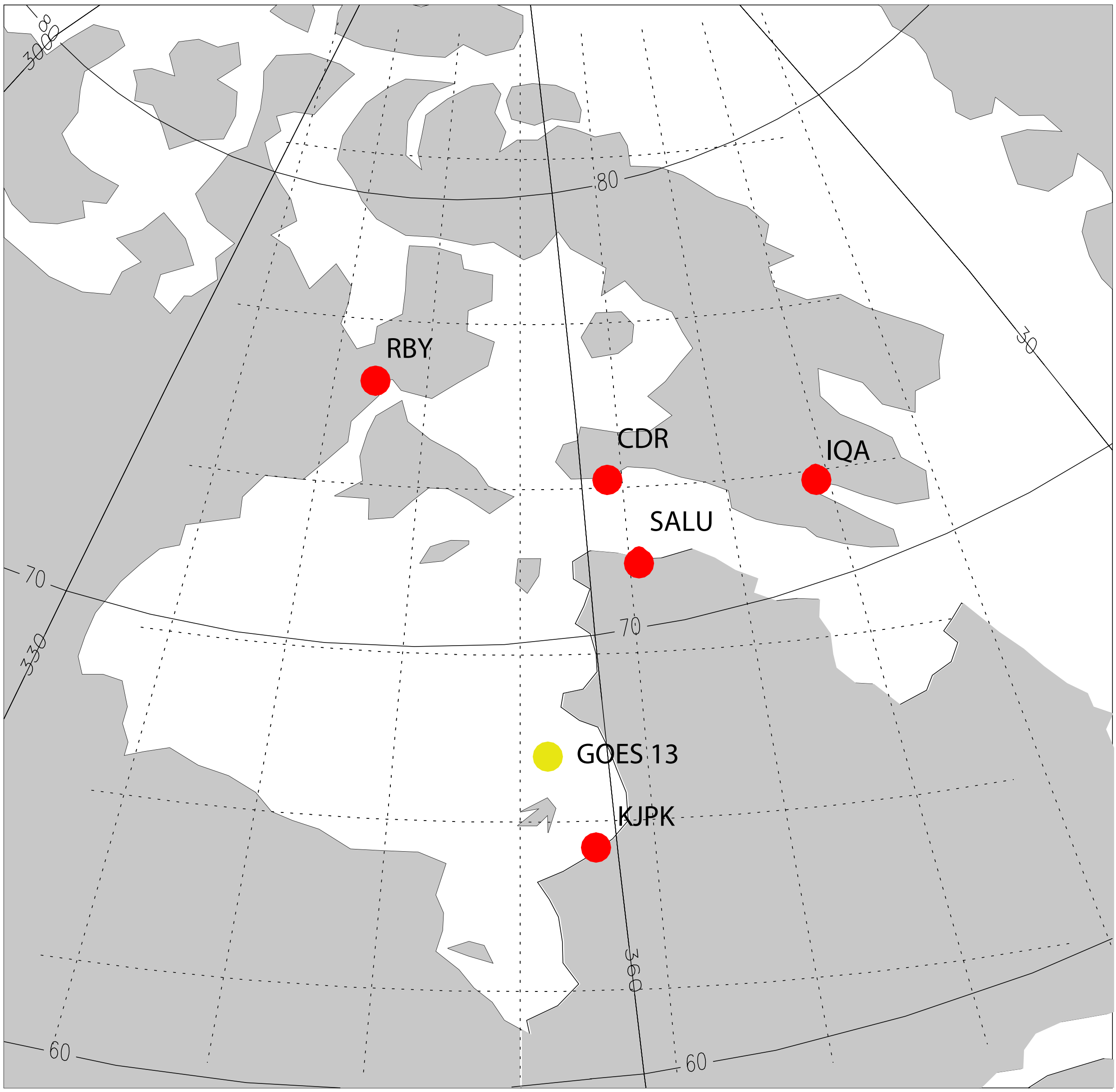
RBY
CDR
IQA
SALU
GOES 13
KJPK
80
70
60
30
330
360
300

Figure 2.

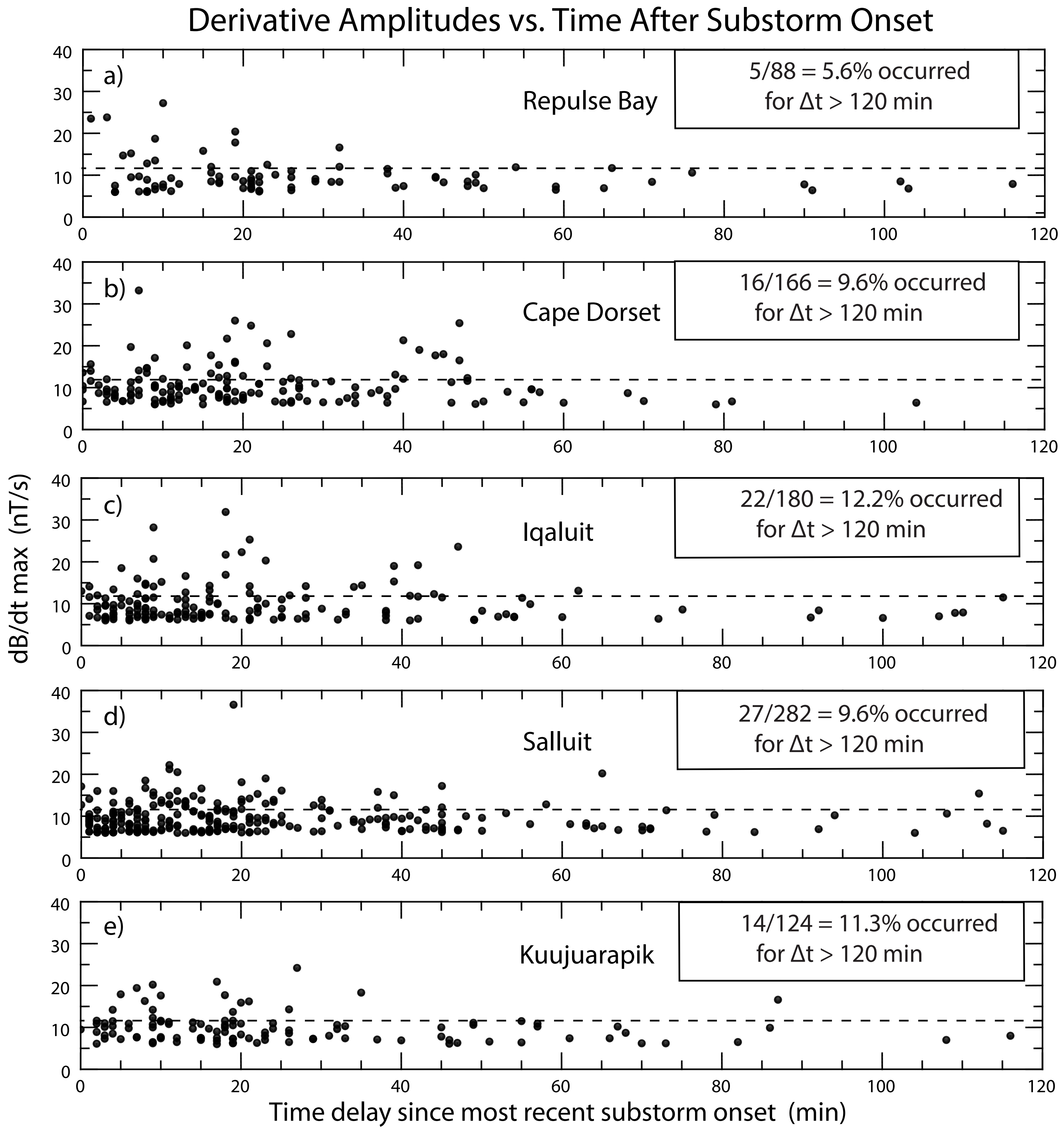
Derivative Amplitudes vs. Time After Substorm Onset
a)
Repulse Bay
5/88 = 5.6% occurred for Δt > 120 min
b)
Cape Dorset
16/166 = 9.6% occurred for Δt > 120 min
c)
Iqaluit
22/180 = 12.2% occurred for Δt > 120 min
d)
Salluit
27/282 = 9.6% occurred for Δt > 120 min
e)
Kuujuarapik
14/124 = 11.3% occurred for Δt > 120 min
dB/dt max (nT/s)
Time delay since most recent substorm onset (min)
0
10
20
30
40
0
20
40
60
80
100
120

Figure 3.

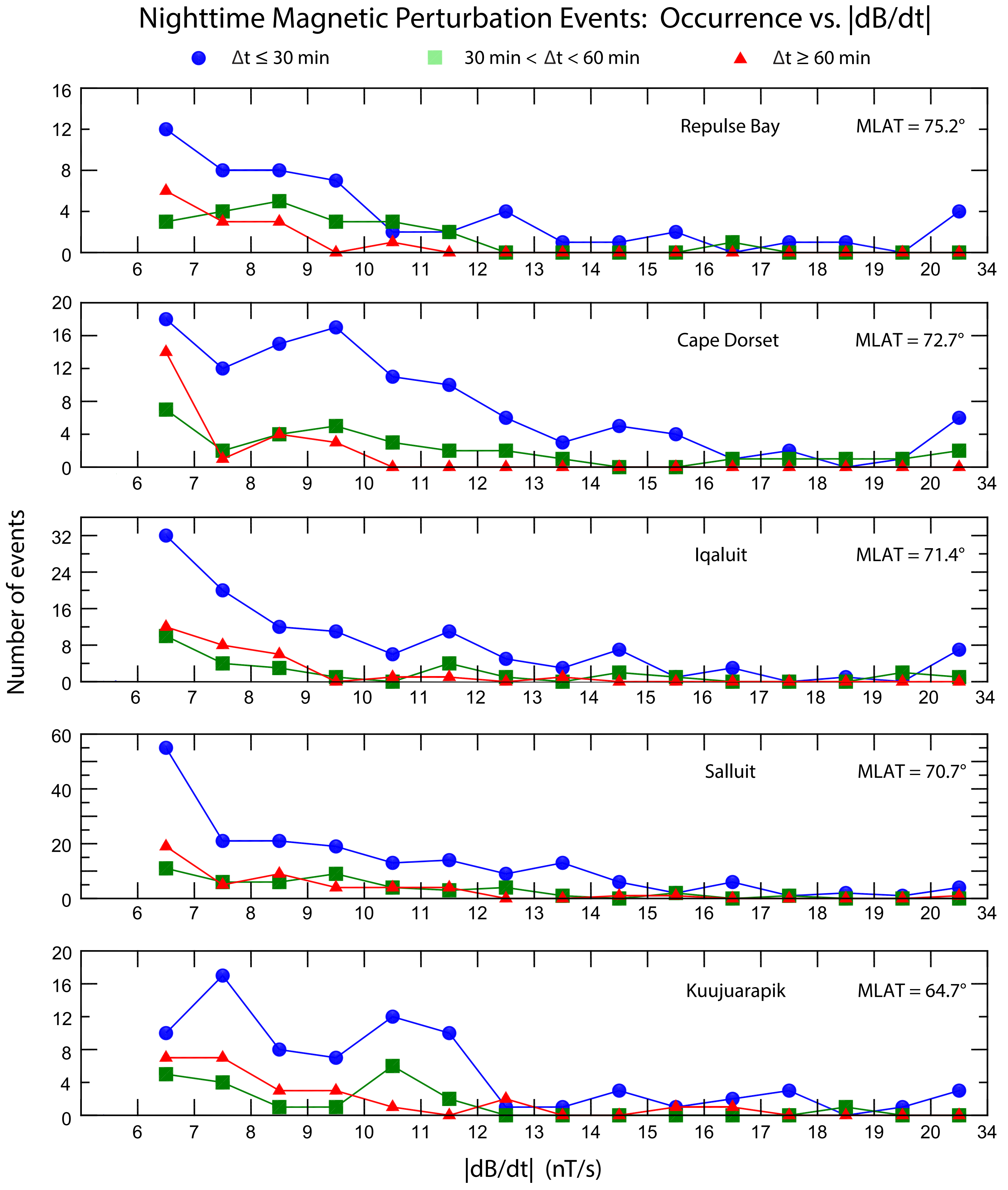
Nighttime Magnetic Perturbation Events: Occurrence vs. |dB/dt|
Δt ≤ 30 min
30 min < Δt < 60 min
Δt ≥ 60 min
Repulse Bay
MLAT = 75.2°
Cape Dorset
MLAT = 72.7°
Iqaluit
MLAT = 71.4°
Salluit
MLAT = 70.7°
Kuujuarapik
MLAT = 64.7°
Number of events
|dB/dt| (nT/s)

Figure 4.

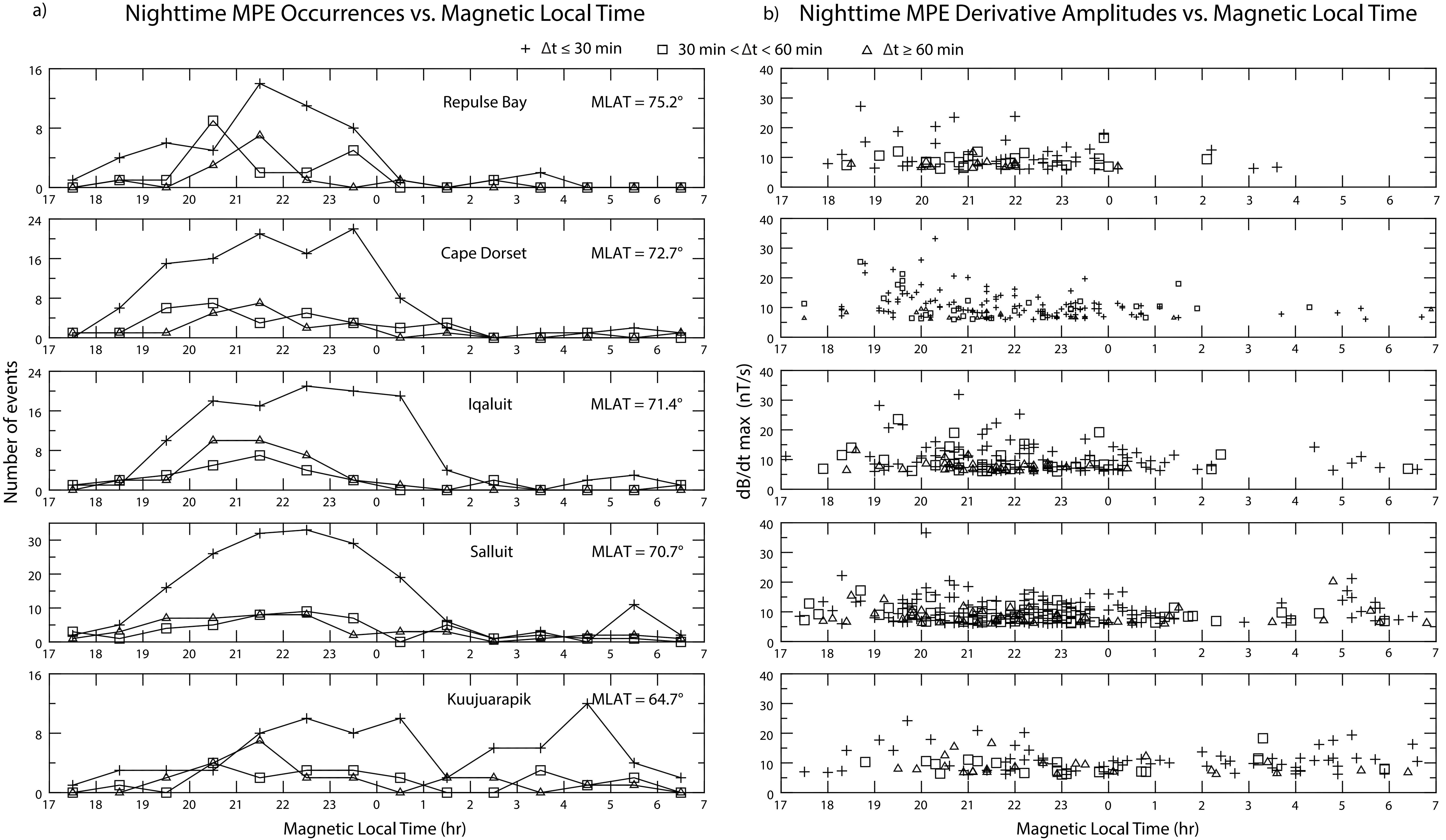
a)
Nighttime MPE Occurrences vs. Magnetic Local Time
b)
Nighttime MPE Derivative Amplitudes vs. Magnetic Local Time
+ Δt ≤ 30 min
□ 30 min < Δt < 60 min
△ Δt ≥ 60 min
Repulse Bay
MLAT = 75.2°
Cape Dorset
MLAT = 72.7°
Iqaluit
MLAT = 71.4°
Salluit
MLAT = 70.7°
Kuujuarapik
MLAT = 64.7°
Number of events
dB/dt max (nT/s)
Magnetic Local Time (hr)
Magnetic Local Time (hr)

Figure 5.

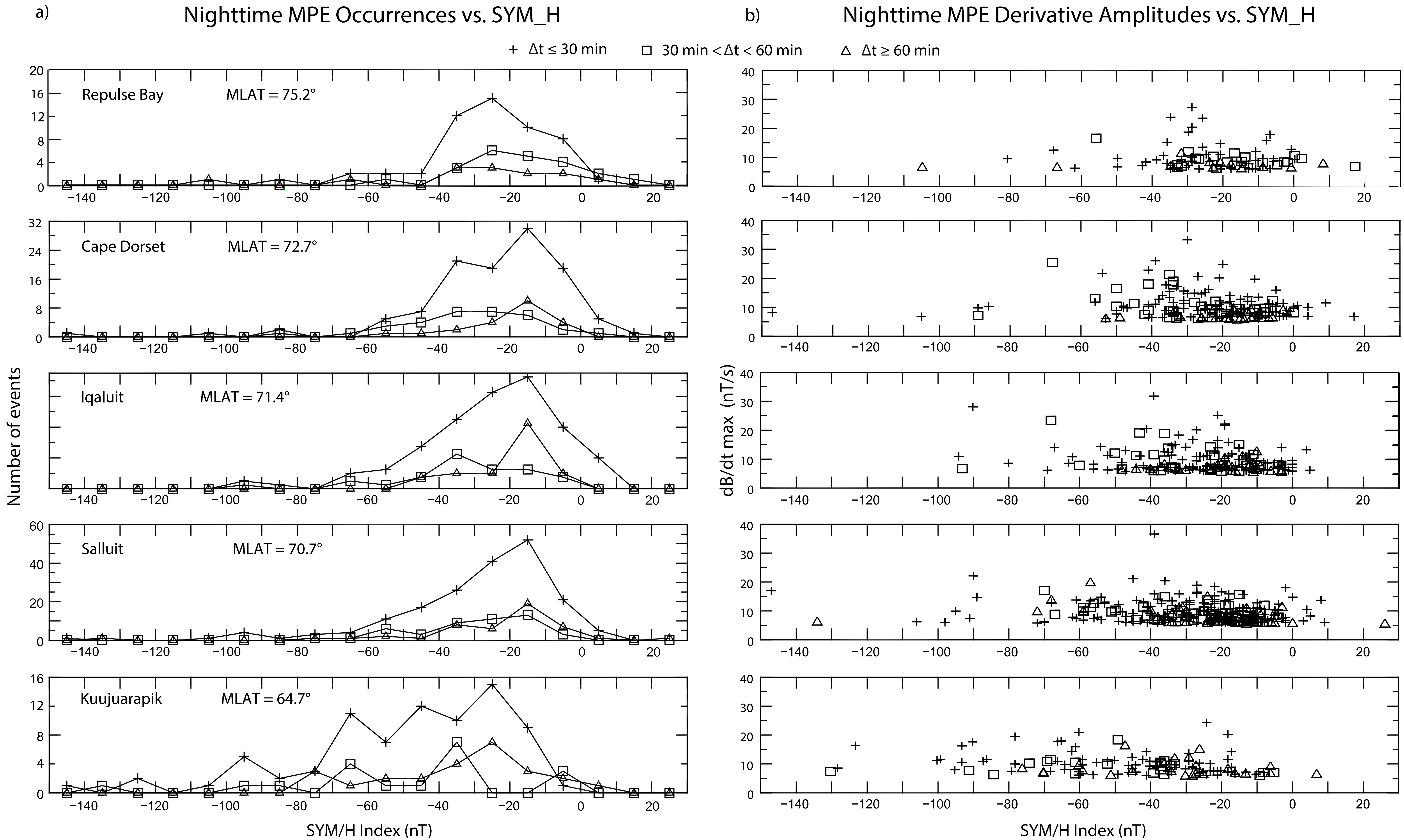

a)
Nighttime MPE Occurrences vs. SYM_H
b)
Nighttime MPE Derivative Amplitudes vs. SYM_H
+ Δt ≤ 30 min
□ 30 min < Δt < 60 min
△ Δt ≥ 60 min
Repulse Bay
MLAT = 75.2°
Cape Dorset
MLAT = 72.7°
Iqaluit
MLAT = 71.4°
Salluit
MLAT = 70.7°
Kuujjuarapik
MLAT = 64.7°
Number of events
dB/dt max (nT/s)
SYM/H Index (nT)
SYM/H Index (nT)

Figure 6.

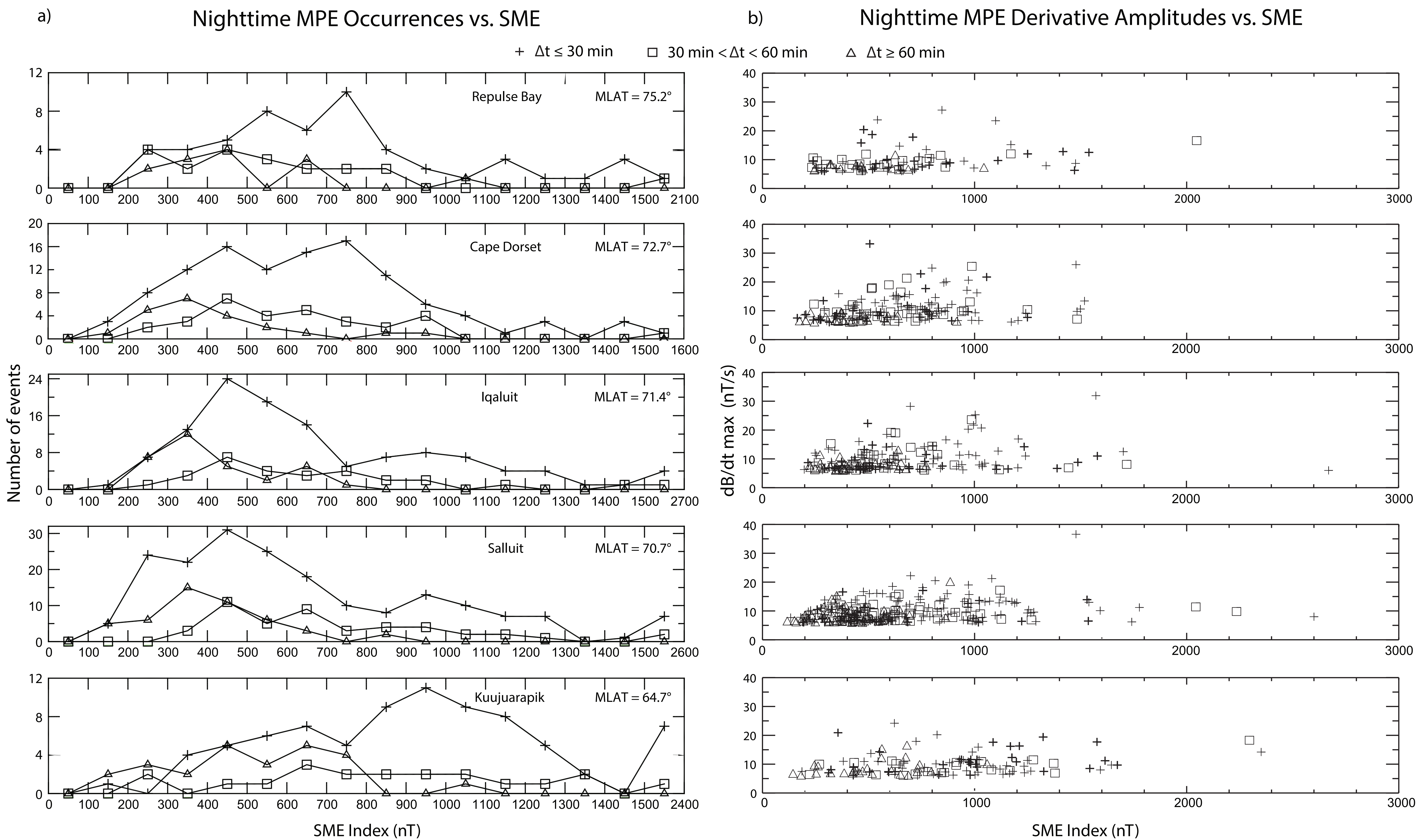

a)
Nighttime MPE Occurrences vs. SME
b)
Nighttime MPE Derivative Amplitudes vs. SME
+ Δt ≤ 30 min
□ 30 min < Δt < 60 min
△ Δt ≥ 60 min
Repulse Bay
MLAT = 75.2°
Cape Dorset
MLAT = 72.7°
Iqaluit
MLAT = 71.4°
Salluit
MLAT = 70.7°
Kuujuarapik
MLAT = 64.7°
Number of events
SME Index (nT)
dB/dt max (nT/s)
SME Index (nT)

Figure 7.

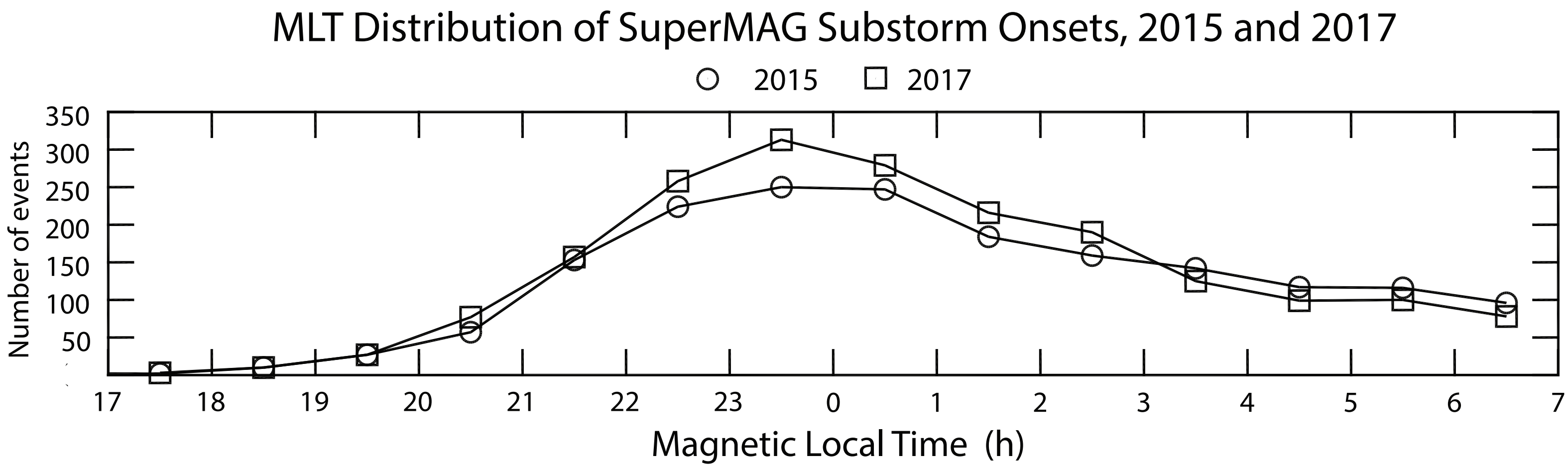
MLT Distribution of SuperMAG Substorm Onsets, 2015 and 2017
2015
2017
Number of events
350
300
250
200
150
100
50
17
18
19
20
21
22
23
0
1
2
3
4
5
6
7
Magnetic Local Time (h)

Figure 8.

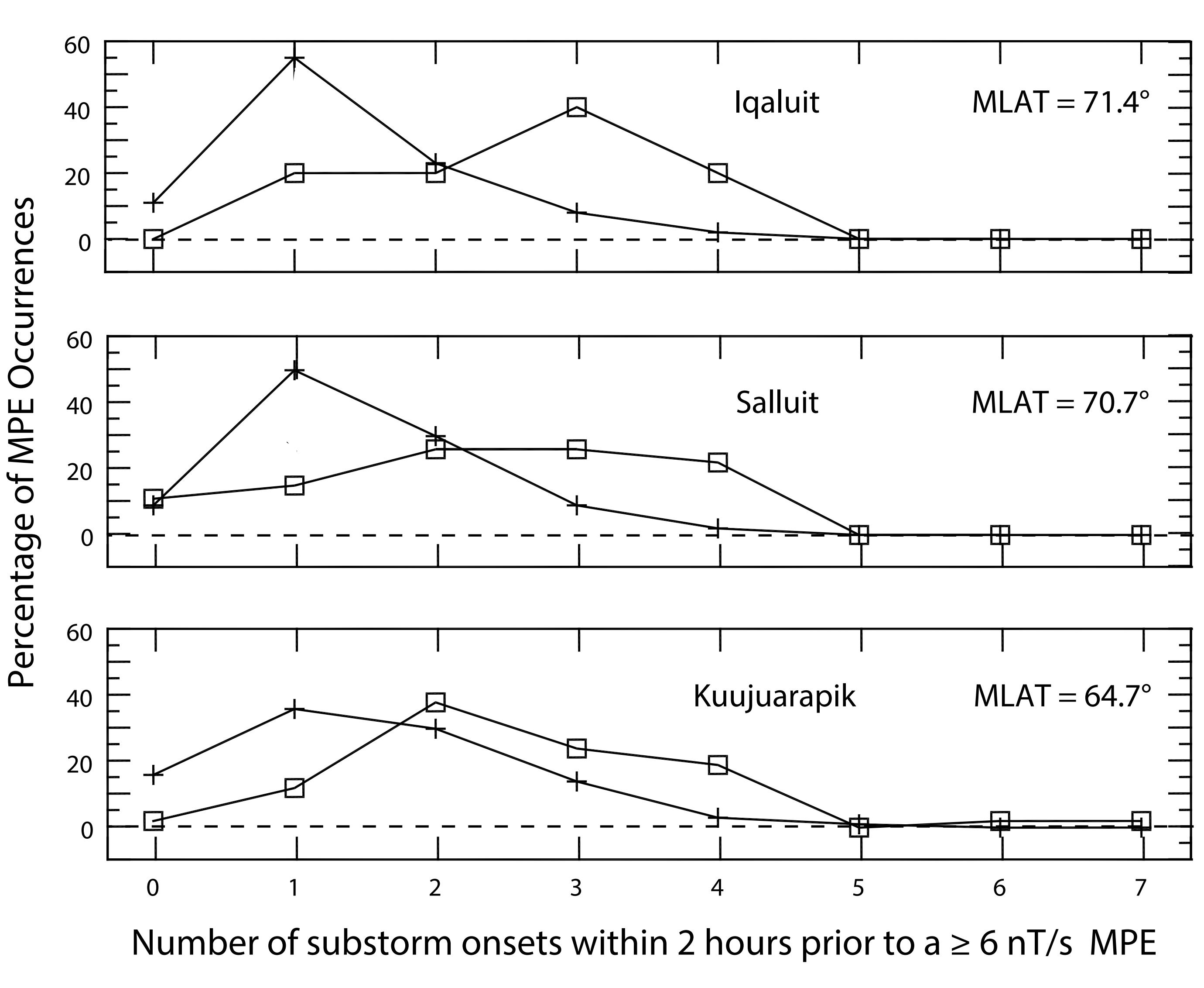

Iqaluit
MLAT = 71.4°
Salluit
MLAT = 70.7°
Kuujuarapik
MLAT = 64.7°
Percentage of MPE Occurrences
60
40
20
0
0
1
2
3
4
5
6
7
Number of substorm onsets within 2 hours prior to a ≥ 6 nT/s MPE

Figure 9.

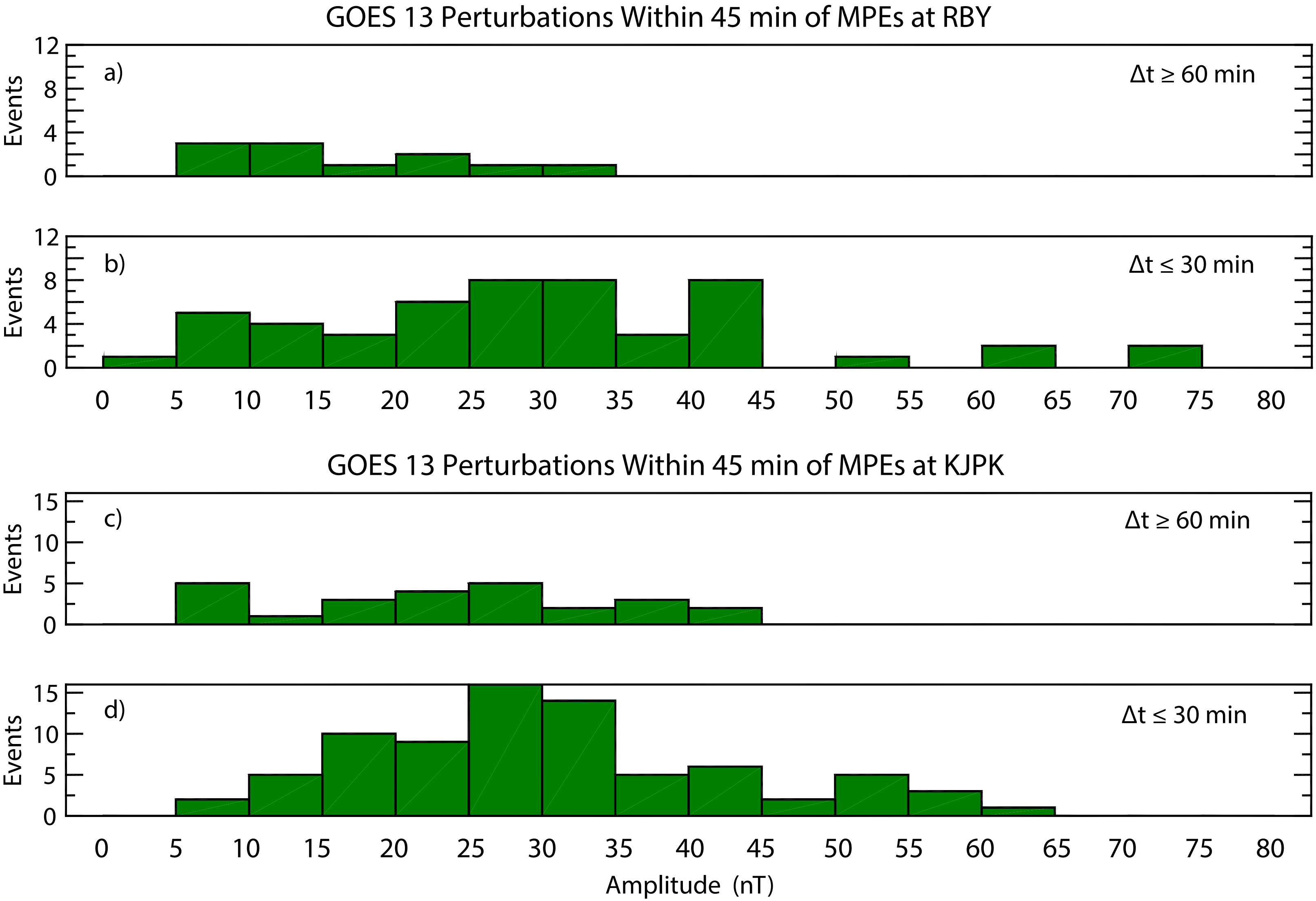
GOES 13 Perturbations Within 45 min of MPEs at RBY
a)
Δt ≥ 60 min
b)
Δt ≤ 30 min
GOES 13 Perturbations Within 45 min of MPEs at KJPK
c)
Δt ≥ 60 min
d)
Δt ≤ 30 min
Events
Amplitude (nT)
0 5 10 15 20 25 30 35 40 45 50 55 60 65 70 75 80

Nighttime magnetic perturbation events observed in Arctic Canada: 3. Occurrence and amplitude as functions of magnetic latitude, local time, and magnetic disturbances

Mark J. Engebretson[1], Viacheslav A. Pilipenko[1,2], Erik S. Steinmetz[1], Mark B. Moldwin[3], Martin G. Connors[4], David H. Boteler[5], Howard J. Singer[6], Hermann Opgenoorth[7], Audrey Schilling[7], Shin Ohtani[8], Jesper Gjerloev[8], and Christopher T. Russell[9]

[1] Augsburg University, Minneapolis, MN
[2] Institute of Physics of the Earth, Moscow, Russia
[3] University of Michigan, Ann Arbor, MI
[4] Athabasca University, Athabasca, AB, Canada
[5] Natural Resources Canada, Ottawa, ON, Canada
[6] NOAA Space Weather Prediction Center, Boulder, CO
[7] Umeå University, Umeå, Sweden
[8] JHU/APL, Laurel, MD
[9] UCLA Department of Earth Planetary and Space Sciences, Los Angeles, CA

submitted to Space Weather

April 23, 2020

Key Words: geomagnetically-induced currents, magnetic perturbation events, substorms, magnetic storms, omega bands

Key Points:

We present 2 years of observations of ≥ 6 nT/s magnetic perturbation events (MPEs) from 5 high latitude Arctic stations.

Most MPEs occurred within 30 min of a substorm onset, but substorms were neither necessary nor sufficient to cause MPEs.

Pre-midnight and post-midnight MPEs had different temporal relations to substorms and occurred at slightly different latitudes.

Abstract

Rapid changes of magnetic fields associated with nighttime magnetic perturbation events (MPEs) with amplitudes |ΔB| of hundreds of nT and 5-10 min periods can induce geomagnetically-induced currents (GICs) that can harm technological systems. In this study we compare the occurrence and amplitude of nighttime MPEs with |dB/dt| ≥ 6 nT/s observed during 2015 and 2017 at five stations in Arctic Canada ranging from 75.2° to 64.7° in corrected geomagnetic latitude (MLAT) as functions of magnetic local time (MLT), the SME and SYM/H magnetic indices, and time delay after substorm onsets. Although most MPEs occurred within 30 minutes after a substorm onset, ~10% of those observed at the four lower latitude stations occurred over two hours after the most recent onset. A broad distribution in local time appeared at all 5 stations between 1700 and 0100 MLT, and a narrower distribution appeared at the lower latitude stations between 0200 and 0700 MLT. There was little or no correlation between MPE amplitude and the SYM/H index; most MPEs at all stations occurred for SYM/H values between -40 and 0 nT. SME index values for MPEs observed more than 1 hour after the most recent substorm onset fell in the lower half of the range of SME values for events during substorms, and dipolarizations in synchronous orbit at GOES 13 during these events were weaker or more often nonexistent. These observations suggest that substorms are neither necessary nor sufficient to cause MPEs, and hence predictions of GICs cannot focus solely on substorms.

1. Introduction

Although early studies of nighttime magnetic perturbation events (MPEs) that induce large geoelectric fields and geomagnetically-induced currents (GICs) noted the small-scale character of these events (e.g., Viljanen, 1997), many efforts to predict GICs have continued to focus on global processes (geomagnetic storms and substorms). Recent observational studies by Belakhovsky et al. (2019), Dimmock et al. (2019), Engebretson et al. (2019a,b), and Apatenkov et al. (2020) have provided new evidence of the localized nature of the magnetospheric and/or ionospheric processes associated with these impulsive magnetic perturbations. This includes evidence of ionospheric current vortices, close association with poleward boundary intensifications and overhead auroral streamers, and the spatial scale size of individual events. Individual events also displayed no close or consistent temporal correlation with substorm onsets.

Here we present additional analyses of a large number of nighttime MPEs that document lack of any close correlation between their occurrence and levels of the SME index, the SYM/H index, or of near-tail dipolarizations, and show that a substantial fraction of these events are not temporally associated with substorms. MPEs occurring in the post-midnight sector showed a different dependence on both latitude and prior substorm activity than did the more numerous pre-midnight MPEs.

2. Data Set and Event Identification Technique

Vector magnetometer data used in this study were recorded during 2015 and 2017 by stations in the MACCS (Engebretson et al., 1995), CANMOS (Nikitina et al., 2016), and AUTUMNX (Connors et al., 2016) arrays in Arctic Canada, as detailed in Table 1 and Figure 1 (red circles). MACCS station CDR and the highest and lowest latitude stations in the AUTUMNX array, SALU and KJPK, form a latitudinal chain. MACCS station RBY extends this chain to the north and west, and CANMOS station IQA extends it to the east. Data from 2016 was not included because of significant station down time at RBY and CDR during that year. Also shown in Figure 1 (yellow circle) is the northern magnetic footpoint of the geosynchronous GOES 13 spacecraft (Singer et al., 1996), which provides magnetospheric context for the ground observations.

The semi-automated procedure used to identify and quantify MPEs in these data sets is detailed in Engebretson et al. (2019a), and is summarized here. Routinely produced daily magnetograms (24-hour plots of magnetic fields in local geomagnetic coordinates) were displayed on a computer screen. Once a < 10 minute duration magnetic perturbation with amplitude ≥ 200 nT in any component was identified, the IDL cursor function was used to visually select times before and after a region of interest containing the MPE. The times and values of extrema in this interval were recorded for each component, and after application of a 10-point smoothing to reduce noise and eliminate isolated bad data points, the data were numerically differentiated. Plots of the time series of data and derivatives were produced and saved, and the maximum and minimum derivative values were automatically determined and recorded. Figure 3 of Engebretson et al. (2019a) shows the amplitude vs. MLT distributions of MPEs at SALU during 2015 for both ΔBx and |dBx/dt| that were identified using this technique. This figure shows that MPEs with ΔBx amplitude ≥ 200 nT or derivative amplitude ≥ 6 nT/s were almost exclusively confined to nighttime hours.

We then compared the time of each MPE identified during full years 2015 and 2017 at each station to the times of substorm onsets listed in the SuperMAG substorm list for that year. We identified and recorded the time of all prior substorm onsets within a 2-hour window, and if none were found, to the time of the closest prior onset, which in some cases was several days prior to the MPE. The procedure used to identify substorm onsets included in the SuperMAG substorm lists is described in Newell and Gjerloev (2011a,b): substorm onsets are defined by a drop in SML (the SuperMAG version of the AL index) that was sharp (45 nT in 3 min) and that was sustained (-100 nT average for 25 min starting 5 min after onset). We note here that onsets are relatively easy to identify if preceded by quiet periods, but subsequent onsets (which may be called intensifications) are far more difficult to identify using either ground-based magnetometer data or auroral images. Table 2 shows the number of nighttime (1700 to 0700 MLT) MPEs with derivative amplitude ≥ 6 nT/s at each of these stations. Events are grouped into 3 categories of time delay Δt after the most recent prior substorm onset: Δt ≤ 30 min, 30 < Δt < 60 min, and Δt ≥ 60 min. In this study we define events with Δt ≤ 30 min as most likely to be associated with substorm processes, while those with Δt ≥ 60 min (and up to several days) are not. The fractions of events that occurred in these three different delay ranges remained roughly constant at all stations. Note, too, that the number of events peaked at SALU (70.7° MLAT), and was lowest at the two latitude extremes: RBY (75.2° MLAT) and KJPK (64.7° MLAT).

3. MPE Amplitudes as a function of Time Delay After Substorm Onset

Figure 2 shows the amplitude of the maximum |dB/dt| value in any nighttime MPE component observed at each station as a function of its delay (between 0 and 120 min) after the most recent substorm onset. The strongest events ($\geq$20 nT/s) most often occurred for $\Delta t < 60$ min, but only at the highest latitude station (Repulse Bay) did these strongest events occur within 5 min of substorm onset. Most events were below 12 nT/s for all delay times.

MPEs occurred over a continuum of times from 0 to well beyond the 120 minute delay time range shown in this figure. The number and percentage of events occurring with delay times > 120 min are indicated in the inset box in each panel. Although most MPEs at each station occurred within 30 minutes after a substorm onset, from 13 to 20 % of the MPEs at each station occurred later than 1 hour after the most recent substorm onset, and from 6 to 12 % later than 2 hours. The number of events > 10 nT/s with time delays over two hours was 0 at RBY and CDR, 1 at IQA, 5 at SALU, and 3 at KJPK (not shown).

4. MPE Occurrences as a Function of Derivative Amplitude

Figure 3 shows the distribution of occurrences of MPEs as a function of derivative amplitude at all five stations and in all three time delay categories. Different symbols are used to designate events based on the time of MPE occurrence after the closest prior substorm onset: blue circles for $\Delta t \leq 30$ min, green squares for Δt between 30 and 60 min, and red triangles for $\Delta t \geq 60$ min. The number of MPEs in each 1 nT/s bin fell off roughly monotonically in each category from the lowest amplitude to higher values with a long tail, with no clear latitudinal trend. At each station, several events that occurred within 30 min of substorm onset had amplitudes exceeding 20 nT/s (up to 34 nT/s); only at CDR and IQA did > 20 nT/s MPEs occur after delays > 30 min.

5. Latitudinal Distributions of Occurrences and Amplitudes vs. MLT, SYM/H, and SME

For each of the five stations we sorted the MPE events as functions of several variables: magnetic local time (MLT), the SYM/H index, the SME index (the SuperMAG version of the AE index, described in Newell and Gjerloev, 2011a), and derivative amplitude.

Over the range of magnetic latitudes covered in this study (from 75° to 65° MLAT) all ≥ 6 nT/s perturbation events fell into the local time range from 17 to 07 MLT. Figure 4a shows the number of occurrences of these MPEs at each station grouped in 1-hour MLT bins and sorted by magnetic latitude. Different symbols are used to designate events based on the time of MPE occurrence after the closest prior substorm onset: plus signs for $\Delta t \leq 30$ min, open squares for Δt between 30 and 60 min, and open triangles for $\Delta t \geq 60$ min. Two populations are evident in this figure: a broad distribution extending from dusk to shortly after midnight (17 to 1 MLT) that appears at all latitudes shown, and a distribution in the midnight to dawn sector (2 to 7 MLT) that is prominent only at the lower latitude stations. This difference in latitudinal distribution, which is consistent with observations of large ionospheric equivalent current perturbations by Juusola et al. (2015), appears to reflect the latitudinal dependence of the auroral electrojet, which is located at higher latitudes pre-midnight and lower latitudes post-midnight. As will be shown in later parts of this study, the properties of these two populations also differed somewhat in their association with different geomagnetic conditions.

Consistent with the distribution of occurrences shown in Table 2 and Figure 2, Figure 4a shows that the MPEs that occurred within 30 minutes of the most recent substorm onset (shown with a plus sign) were the dominant category in nearly all MLT bins at each station. The local time trends for MPEs shown with squares and triangles were similar to those for MPEs shown with plus signs for the four most poleward stations, with a broad distribution gradually rising from ~17-18 h MLT to a broad pre-midnight peak before gradually falling to ~1-2 h MLT, and with very few events occurring at later MLT. At KJPK, the pre-midnight distribution of events shown with plus signs was somewhat narrower in time and shifted toward slightly later MLT, and a second post-midnight peak (with similar peak occurrences) appeared between 2-3 and 6 h MLT. In contrast, the distributions for events shown with squares and triangles were flat across the entire MLT range shown (but with fewer occurrences).

Figure 4b shows that the largest-amplitude MPEs occurred at all 5 stations between 1800 and 2300 h MLT, but derivatives with amplitude at or above 15 nT/s also appeared after 0300 h MLT at both SALU and KJPK. Table 3 shows an analysis of the distribution of these events as a function of time delay when separated into pre- and post-midnight occurrences. In order to clearly separate these categories, pre-midnight events were chosen to include those observed between 1700 and 0100 MLT, and post-midnight event those between 0200 and 0700 MLT. The time delay distributions were similar for pre- and post-midnight events at all 5 stations, but on average over all 5 stations, post-midnight events were slightly more likely to occur within 30 min after substorm onsets than pre-midnight events (70% vs. 66%), and less likely to occur more than 60 minutes after onset (12% vs. 17%). These differences, however, were not statistically significant.

Figure 5 shows plots similar to those in Figure 4 as a function of the SYM/H index, which ranged from ~-150 to +30 nT during these events. At all five stations the occurrence distributions (Figure 5a) peaked near SYM/H ~ -20 nT, and at all but the lowest latitude station nearly all events occurred when SYM/H was between -60 and +10 nT. The tail of the distribution at more negative SYM/H values increased at the lowest latitude station, KJPK. This most likely reflects the equatorward expansion of the auroral oval during geomagnetic storms. The occurrence distributions for the 3 time delay categories were roughly similar to each other at each station. In contrast to Figure 4, where the distribution of local times during which observations were available was essentially uniform, it is important to note that in Figures 5 and 6 the overall occurrences of SYM/H and SME values were strongly biased toward quiet conditions. The occurrences shown in Figures 5 and 6 are thus not normalized.

Figure 5b shows that the SYM/H range corresponding to the largest derivative amplitudes occurred for values between -40 and -20 nT at RBY and expanded toward lower SYM/H values at CDR and IQA. There was essentially no correlation between largest derivative amplitudes and SYM/H values at either SALU or KJPK; storm-time MPEs were no more likely to have extreme derivative values than MPEs during non-storm conditions, even near 65° MLAT.

At all five stations > 6 nT/s perturbation events occurred over a wide range of SME values, as shown in Figure 6a, but very few events occurred at any station for SME < 200 nT. At the four highest latitude stations a large majority of events in each of the 3 time delay categories occurred for SME values between 200 and 900 nT. This SME range also held at the lowest latitude station (KJPK) for the $\Delta t > 60$ min category, but most of the events in the $\Delta t \leq 30$ min category were associated with SME values > 800 nT. However, fewer events occurred for high SME at KJPK (64.7° MLAT) than at SALU (70.7° MLAT) – note the differing vertical scales.

Figure 6b shows that there was a modest correlation between the amplitude of the largest derivatives and the SME index only over the SME range between 200 and 600 nT at all 5 stations; the distribution of amplitudes was nearly flat for SME > 600 nT at all stations. Most events at all SME values and all 3 time ranges were below 12 nT/s. Only 7 of the 842 total events occurred when SME exceeded 2000 nT.

6. Event Occurrence in Relation to Substorms and Magnetotail Dipolarizations

In this section we address three questions: 1) What percentages of substorms are associated with a large nighttime MPE?, 2) How important are multiple-onset substorms for large-amplitude MPEs?, and 3) to what extent are nighttime MPEs associated or not with dipolarizations observed at geosynchronous orbit?

6.1 Percentages of substorms associated with large nighttime MPEs

Figure 2 and Table 2 have shown the numbers and percentages of MPEs that are associated with substorm onsets within given ranges of time delays. We now address the reverse association: in what percentage of substorm onsets does an MPE occur within one hour?

In order to address this question, we compared the number of observed MPEs to the number of substorm onsets listed in the SuperMAG onset data base for 2015 and 2017. Roughly 80% of the MPE events at the four northernmost stations occurred between 1900 and 0100 MLT (Figure 4), and most (~60%) of the MPEs observed at all five stations occurred from 0 to 30 minutes after the most recent substorm onset (Figure 2). We thus wish to determine the number of substorm onsets that might correspond to MPE events between 1830 and 0100 MLT. Figure 7 shows the distribution of substorm onsets in the MLT range from 17 to 07 h, the same MLT range as shown in Figure 4, for both 2015 and 2017. Although both substorm distributions peaked near or shortly before midnight, the peak of the onset distribution is clearly shifted ~1-2 hours later in MLT than the peak of the MPE distribution at all stations other than KJPK. The later rise and longer tail of the substorm onset distribution may reflect the occurrence of post-midnight onsets at lower MLATs, as suggested by the MLT distribution at KJPK. The percentage of onsets in the MLT range from 1830 to 0100 h was 50% for 2015, and 55% for 2017. Although this offset makes it clear that there was only an approximate correspondence between the peaks of the MLT distributions of MPEs and substorm onsets, a comparison may still provide helpful information.

At the CDR and SALU stations, located in magnetic longitude near the center of the 5 stations, the 1830 to 0100 MLT range corresponds to a time window from 2325 to 0555 UT. The SuperMAG substorm onset data base indicated that during 2015 and 2017 combined, 932 of a total of 4031 onsets occurred during this UT time window.

Columns 2-4 of Table 4 show the number of MPE events at each station that occurred within this UT time window as a function of their time delays (0-30, 30-60, and 0-60 min) after the most recent substorm onset. Columns 5-7 show the estimated percentage of events following a documented substorm onset within these time delays, calculated by dividing the number of events in columns 2-4 by 932. Column 7 shows that the percentage of MPEs per substorm onset that occurred within 60 min after an identified substorm varied from 8.0 to 25.1%. Column 8 shows the reverse occurrence: the estimated percentage of substorm onsets after which no MPE occurred within 60 minutes after onset. The percentages in this column ranged from 75 to 92%, indicating that most substorms were not associated with large amplitude MPEs. The percentages at CDR, IQA, and SALU were near the lower end of this range, and those at RBY and KJPK at the higher end. We note the roughly inverse correlation between these percentages and the number of MPE events observed at each station (Table 2). This suggests that the modest differences in magnetic longitude between the five stations were a smaller factor in determining the dependence of MPEs on substorm onsets than the magnetic latitude. This dependence on MLAT may reflect the limited spatial extent of large MPEs, such that a station farther away from the statistical auroral oval is more likely to detect an MPE with lower amplitude, and thus in many cases one below our selection threshold of 6 nT/s.

6.2 The importance of multiple prior substorm onsets for large nighttime MPEs

We also considered the effect of multiple prior substorm onsets separately for MPEs in the two populations shown in Figure 4a: the "pre-midnight" population observed between 1700 and 0100 MLT, and the "post-midnight" population observed between 0200 and 0700 MLT. Table 5 shows the number of > 6 nT/s MPEs observed during 2015 and 2017 at the three lowest latitude stations as a function of the number of substorm onsets that occurred within 2 hours prior to the MPE, and Figure 8 shows this same information in percentage form. Both Table 5 and

Figure 8 show that in the 1700-0100 MLT sector the distribution at each station peaked within 2 hours after 1 substorm onset and fell off rapidly after 2 substorm onsets. The much smaller number of MPEs that occurred at each station in the 0200-0700 MLT sector exhibited a broad maximum following 2-h intervals of between 1 and 4 onsets.

Comparison of the median |dB/dt| amplitude of MPEs as a function of prior substorm onsets (not shown) indicated a relatively flat distribution near 8 nT/s from 0 through 4 prior onsets in the pre-midnight sector, but a ~50% increase in median amplitude (~7 to ~11 nT/s) from 1 to 4 onsets in the post-midnight sector. These distributions were again very similar at all 3 stations.

Table 6 shows the results of applying Pearson's Chi-squared test to the data in Table 5, after reducing the number of prior substorm categories to 3: after 0, 1, and ≥ 2 onsets within 2 hours, respectively. The p values of $<< 0.05$ confirm that the difference between pre-midnight and post-midnight events is statistically significant at all 3 stations. Taken together, these differences indicate a much stronger relation between multiple substorms and subsequent MPEs in the post-midnight sector than in the pre-midnight sector.

Table 7 provides additional information on the relation between MPE onset and the level of magnetic disturbance (as represented by the SME index) following multiple substorms. This table shows for both pre-midnight and post-midnight time sectors and for IQA, SALU, and KJPK a) the total number of MPEs observed as a function of the number of substorm onsets during the 2 hours prior to the MPE, b) the number of MPEs simultaneous with very intense magnetic disturbances (SME ≥ 1000 nT), and c) the percentage of these MPEs compared to the total number of MPEs observed in each onset bin. At all 3 stations and for both pre-midnight and post-midnight events, 1) no MPEs occurred in the first bin (following a 2-h period after 0 substorms) and very few in the second bin (following 1 substorm), 2) most MPEs simultaneous with SME values ≥ 1000 nT occurred after two-hour intervals containing from 2 to 4 substorm onsets, and 3) because of the large difference in total MPE occurrence in each bin between pre-midnight and post-midnight MPEs, the percentage distribution of pre-midnight MPEs simultaneous with SME values ≥ 1000 nT increased greatly as the number of prior substorm onsets increased from 1 to 4, but was more nearly flat for post-midnight events. The overall fractions of pre-midnight MPEs associated with SME values ≥ 1000 nT were 9.2% at IQA, 8.5

% at SALU, and 19.4% at KJPK. The corresponding post-midnight fractions were much larger: 70%, 44%, and 52%, respectively.

The SME index is well correlated with auroral power (Newell and Gjerloev, 2011a). In general, the relationship among discrete precipitation, ionospheric conductance, and upward FAC density is instantaneous. In contrast, diffuse precipitation has a certain time lag; particles are injected and then later forced to precipitate into the ionosphere. The associated enhancement of ionospheric conductance lasts longer, which is favorable for more tail current to short-circuit through the ionosphere at subsequent substorms. As a result, SME may increase following multiple particle injections closely spaced in time more than it would without continuing activity, independently of the intensity of any individual substorm.

These differing patterns again indicate that intervals of large SME (or AE) index values are poorly correlated with intense pre-midnight dB/dt values but are better correlated for post-midnight events.

6.3 Relation of large nighttime MPEs to dipolarizations at synchronous orbit

In each of the three case studies of MPEs presented by Engebretson et al. (2019b), which occurred within 30 min of a substorm onset, rapid increases of from 15 to 30 nT in the Bz component of the magnetic field (dipolarizations) at GOES 13 coincided with an MPE to within a few minutes. Figure 9 presents a comparison of the Bz perturbations observed at GOES 13 within 45 minutes prior to each of the MPEs observed at RBY and KJPK during 2015 and 2017, grouped in two categories: MPEs with time delays $\geq$ 60 min and $\leq$ 30 min after the most recent substorm onset. GOES data were available for 13 (all) and 52 (all but one) of the MPEs at RBY and for 25 (all) and 79 (all) of the MPEs at KJPK, respectively. At RBY 2 of 13 and 4 of 52 GOES 13 perturbations, respectively, were negative and are not shown in Figure 9; the corresponding numbers at KJPK were 0 of 25 and 3 of 79, respectively. Figure 9 shows that at both stations the amplitude distribution of the perturbations did not extend to as large values for the $\Delta t \geq$ 60 min MPE population as for the $\leq$ 30 min MPE population.
Some of the smaller GOES 13 Bz perturbations, and especially those in the $\Delta t \geq$ 60 min category, were associated with brief (few min) transient pulses rather than step functions (dipolarizations). It is difficult to discern whether such pulses arise from spatial or temporal

effects. If spatial, GOES 13 may have been rather distant in MLT from the center of a more large-scale dipolarization. If temporal, the perturbation may have been associated with a bursty bulk flow, dipolarization front, and/or pseudobreakup (e.g., Palin et al., 2015). Further analysis of the features of the GOES 13 dataset during these MPE events is certainly warranted, but is beyond the scope of this paper.

7. Summary of Observations

This study has described the distributions of nighttime MPEs as functions of several physical parameters and geomagnetic indices, and has identified two different populations on the basis of differences in both MLT and dependence on magnetic activity levels. The first two of the MPE characteristics below confirm and extend the observations in previous reports, but others appear to provide new information.

1: Distributions of MPEs as functions of the time delay after a substorm onset were presented by Viljanen et al. (2006), using data from Longyearbyen, Sodankylä, and Nurmijarvi and by Engebretson et al. (2019a), using data from Repulse Bay. Both studies found that these distributions had long tails. This study confirms and quantifies the occurrence of these long tails: Although many of the most intense MPEs at each station occurred within 30 min of a substorm onset, from 13 to 20 % of the MPEs at each station occurred later than 1 hour after the most recent substorm onset, and from 6 to 12 % later than 2 h. The strongest MPEs at all 5 stations most often occurred within 60 min of a substorm onset, but the amplitudes of most events were below 12 nT/s at all delay times.

2. A broad distribution of nighttime MPEs appeared at all 5 stations between 1700 and 0100 MLT, and a narrower distribution appeared at the lower latitude stations between 0200 and 0700 MLT. This is consistent with earlier studies by Viljanen et al. (2001), Viljanen and Tanskanen (2011), Juusola et al. (2015), and most recently by Vorobev et al. (2019) that showed both pre-midnight and post-midnight occurrence peaks. Our study has shown that 1) MPEs occurring within 30 min of a substorm onset dominated in nearly all MLT bins at each station.

3. The number of MPEs decreased roughly linearly with amplitude at all 5 stations and in all 3 time delay categories, with no clear latitudinal trend.

4. MPE occurrences at all 5 stations peaked during quiet conditions (near SYM/H ~ -20 nT), and at all but the lowest latitude station nearly all MPEs occurred for SYM/H values

between -60 and +10 nT. The tail of the SYM/H distribution at more negative values increased at the lowest magnetic latitude station, reflecting the equatorward expansion of the auroral oval during geomagnetic storms. We would thus expect that stations at subauroral latitudes would observe even more MPEs at times corresponding to more negative SYM/H values.

The SYM/H range corresponding to the largest MPE amplitudes was between -40 and -20 nT at RBY and expanded toward lower SYM/H values with lower latitudes, but there was little or no correlation between the largest MPE amplitudes and SYM/H values at the two lowest latitude stations (SALU and KJPK). Storm-time MPEs were no more likely to have extreme derivative values than MPEs during non-storm conditions, even near 65° MLAT (KJPK).

5. MPE occurrences at all 5 stations were spread over a wide range of SME values above ~200 nT. At the 4 highest latitude stations a large majority of MPEs in each of the 3 time delay categories occurred for SME values between 200 and 900 nT. Only at KJPK was the distribution dominated by events with SME > 800 nT, and that only for events within 30 min of substorm onset. There was a modest correlation between the amplitude of the largest MPEs and the SME index over the SME range from ~200 to ~600 nT at all 5 stations, but the distribution of amplitudes was nearly flat for SME > 600 nT. The amplitude of most MPEs at all SME values and in all 3 time categories was below 12 nT/s.

6. We compared the peak range of the distributions of substorm onsets and MPE onsets during 2015 and 2017 in order to estimate the percentages of substorm onsets after which no MPE occurred within 60 minutes. These ranged from 75 to 92% at the 5 stations, indicating that most substorms were not associated with ≥ 6 nT/s MPEs.

7. The importance of multiple prior substorm onsets (within 2 h) for MPE occurrence was different for pre- and post-midnight MPEs. In the 1700-0100 MLT sector the distribution of MPEs peaked in the 1 prior substorm onset bin and fell off rapidly above 2; in the 0200-0700 MLT sector the distribution of MPEs exhibited a broad maximum between 1 and 4 prior onset bins. Pre-midnight MPEs exhibited a relatively flat distribution of median MPE amplitudes across all prior onset bins, while post-midnight MPEs exhibited a ~50 % increase in median amplitudes from 1 to 4 prior onsets. The percentage of pre-midnight MPEs associated with highly disturbed geomagnetic conditions (SME ≥ 1000 nT) varied inversely with the number of MPEs in each bin, whereas the percentage of post-midnight MPEs associated with SME ≥ 1000 nT was largest in the same bins as the number of MPEs. The overall fractions of MPEs

associated with SME ≥ 1000 nT conditions ranged from 9.2 to 19.4% pre-midnight and 44 to 70% post-midnight.

8. At both RBY and KJPK the amplitude of dipolarizations of the magnetic field at geosynchronous orbit observed by GOES 13 did not extend to as large values for the Δt ≥ 60 min MPE events as for the ≤ 30 min events. Many of the smaller dipolarizations at GOES 13 were associated with short-lived pulses rather than step functions.

8. Discussion and Conclusions

Much of the literature on GICs has focused on magnetic storms. This is reasonable because many of the regions most threatened by GICs are located at magnetic latitudes equatorward of the nominal auroral oval, and only during major magnetic storms does the auroral oval expand significantly toward the equator. However, the extreme magnetic perturbations that cause nighttime GICs occur much more often at high latitudes, so that a study of MPEs at these latitudes provides a larger data base to characterize their occurrence and amplitude distributions, as well as to provide more information on their location in latitude and local time relative to auroral features, their temporal relation to substorms and nightside dipolarizations, and their occurrence and amplitude relative to indices of magnetic storm and substorm activity.

This study has shown that at the stations studied here, MPEs most often occurred during magnetically quiet periods, with SYM/H > - 40 nT, and that there was little or no correlation between the occurrence of the largest MPEs and disturbed conditions (as parameterized by more negative SYM/H values) at any of these stations. This result confirms that large MPEs are not restricted to times when SYM/H is large and negative; it simply means that they occur at higher latitudes at these times.

We have also found that only 60 - 67% of the ≥ 6 nT/s MPEs we observed occurred within 30 minutes of the most recent substorm onset. A recent study by Freeman et al. (2019) found a similar result. They noted that in data from 3 stations in the UK over two solar cycles (only) 54–56% of all extreme rate of change values occurred during substorm expansion or recovery phases.

The separation of nighttime MPEs into two populations in MLT, a pre-midnight one that appeared at all 5 stations and a post-midnight one that was prominent only at the two lowest latitude stations, has been noted by other recent observers. This study has shown that the post-midnight MPE population occurred more often in conjunction with large SME values and after multiple substorm onsets than the pre-midnight MPEs.

Engebretson et al. (2019b) presented 3 cases of multi-station magnetometer observations of MPEs that occurred within the 17-01 h MLT range as well as simultaneous auroral images and satellite observations, and reviewed several studies linking these phenomena to westward traveling surges, polar boundary intensifications, auroral streamers, and small-scale nighttime magnetospheric phenomena such as BBFs (Angelopoulos et al., 1992) and their associated dipolarization fronts (Runov et al., 2009, 2011; Palin et al., 2015) and dipolarizing flux bundles (Gabrielse et al., 2014; Liu et al., 2015).

The local time range of the 02 – 07 h MLT distribution matches that of omega bands (Syrjäsuo and Donovan, 2004), which were identified along with other auroral phenomena by Akasofu and Kimball (1964) and Akasofu (1974). Omega bands have been associated with substorms, and especially their recovery phase (e.g., Opgenoorth et al., 1983; 1994), but they can also occur during extended intervals of steady magnetospheric convection (SMC) when no substorm signatures are present (Solovyev et al., 1999). They have also been closely associated with long period irregular Pi3 or Ps6 magnetic pulsations with periods of 5 – 15 min (e.g., Kawasaki and Rostoker, 1979; Andre and Baumjohann, 1982; Solovyev et al., 1999; Henderson et al., 2002, Connors et al., 2003; and Wild et al., 2011).

Several of the above studies and many others, including those of Lühr and Schlegel (1994), Henderson et al. (2002), Sergeev et al. (2003), Amm et al. (2005), Henderson et al. (2012), Weygand et al. (2015), Henderson (2016), and Partamies et al. (2017), have also looked at ionospheric and magnetospheric phenomena associated with these bands and pulsations. Opgenoorth et al. (1983) used magnetometer, radar, riometer, and all-sky imager data to develop a model current system for omega bands consisting of a meandering ionospheric Hall current composed of a westward background electrojet and circular Hall current vortices around the locations of eastward-moving localized field-aligned currents. Lühr and Schlegel (1994) similarly proposed that omega bands are driven by a pair of counterrotating source-free ionospheric current vortices driven by field-aligned currents, an upward current centered in the luminous part of the Ω band and a downward current in the dark part with its center about 400 km west of the upward current. Opgenoorth et al. (1994) also characterized these events as incorporating both large scale and small scale instabilities, leading to omega bands and pulsations, respectively.

Weygand et al. (2015), using both ground- and space-based data sets, concluded that the most probable mechanism driving omega bands involved azimuthally localized high speed flows in the magnetotail that distorted magnetic shells when they reach the inner magnetosphere. Similarly, Henderson (2016) provided evidence that magnetotail flow bursts penetrated close to the Earth and produced omega bands between substorm onsets, and Partamies et al. (2017) found that the occurrence distribution of omega bands in their large statistical study was in very good agreement with the distribution of fast earthward flows in the plasma sheet during expansion and recovery phases reported by Juusola et al. (2011).

Most recently, Apatenkov et al. (2020) provided detailed observations in northern Scandinavia and northwest Russia of a very large GIC that was associated with an interval of omega bands. As a result of pointing out that the magnetic field created by ionospheric and magnetospheric currents may vary due to both temporal changes of current amplitudes and to motion of the current structures, they modeled this event using the sum of two basic current systems: a 1D linear current (mimicking the auroral electrojet) and a 2D vortex that passed eastward over the field of view of the ground magnetometers. Based on this model, they suggested that propagating nonexplosive and relatively long-lived structures might be responsible for large rapid magnetic field variations if their propagation speeds were sufficiently large.

The main implications of this study are 1) that neither a magnetic storm nor a fully developed substorm is a necessary or sufficient condition for the occurrence of the extreme nighttime magnetic perturbation events that can cause GICs, and 2) that the pre-midnight and post-midnight populations of ≥ 6 nT/s MPEs and their consequent GICs differ not only in their occurrence in local time and latitude but also in their dependence on prior substorm activity and magnetospheric disturbance level. Both this study and the several studies cited above thus point to localized processes in the nightside magnetosphere, several of which often occur during substorms but can also occur at other times and may take different configurations before and after midnight, as being responsible for generating these events. This underlines the importance of further studies of the associations between MPEs and these processes in order to fully understand their role in generating MPEs and the resulting GICs.

Acknowledgments

This work was supported by NSF grants AGS-1651263 to Augsburg University, AGS-1654044 to the University of Michigan, and AGS-1502700 to JHU/APL, and at UCLA by the MMS project. MC thanks NSERC for research support and the Canadian Space Agency for support of AUTUMNX. HO and AS thank the National Swedish Space Agency (SNSA) for support. We thank Laura Simms for contributing statistical analyses.

MACCS magnetometer data are available at http://space.augsburg.edu/maccs/requestdatafile.jsp, AUTUMNX magnetometer data are available in IAGA 2002 ASCII format at http://autumn.athabascau.ca/autumnxquery.php?year=2015&mon=01&day=01, and CANMOS magnetometer data, provided by the Geological Survey of Canada, are available in IAGA 2002 ASCII format at http://geomag.nrcan.gc.ca/data-donnee/sd-en.php. GOES 13 magnetometer data are available at https://satdat.ngdc.noaa.gov/sem/goes/data/new_full/. SYM/H index data are available at the Goddard Space Flight Center Space Physics Data Facility at https://cdaweb.sci.gsfc.nasa.gov/index.html/. SME index data are available from SuperMAG (http://supermag.jhuapl.edu/indices/), Principal Investigator Jesper Gjerloev, derived from magnetometer data from INTERMAGNET, Alan Thomson; USGS, Jeffrey J. Love; CARISMA, PI Ian Mann; CANMOS, Geomagnetism Unit of the Geological Survey of Canada; The S-RAMP Database, PI K. Yumoto and Dr. K. Shiokawa; The SPIDR database; AARI, PI Oleg Troshichev; The MACCS program, PI M. Engebretson; GIMA; MEASURE, UCLA IGPP and Florida Institute of Technology; SAMBA, PI Eftyhia Zesta; 210 Chain, PI K. Yumoto; SAMNET, PI Farideh Honary; IMAGE, PI Liisa Juusola; Finnish Meteorological Institute, PI Liisa Juusola; Sodankylä Geophysical Observatory, PI Tero Raita; UiT the Arctic University of Norway, Tromsø Geophysical Observatory, PI Magnar G. Johnsen; GFZ German Research Centre For Geosciences, PI Jürgen Matzka; Institute of Geophysics, Polish Academy of Sciences, PI Anne Neska and Jan Reda; Polar Geophysical Institute, PI Alexander Yahnin and Yarolav Sakharov; Geological Survey of Sweden, PI Gerhard Schwarz; Swedish Institute of Space Physics, PI Masatoshi Yamauchi; AUTUMN, PI Martin Connors; DTU Space, PI Dr. Thom R. Edwards and Anna Willer; PENGUIn; South Pole and McMurdo Magnetometer, PIs Louis J. Lanzerotti and Allan T. Weatherwax; ICESTAR; RAPIDMAG; British Antarctic

Survey; McMAC, PI Dr. Peter Chi; BGS, PI Dr. Susan Macmillan; Pushkov Institute of Terrestrial Magnetism, Ionosphere and Radio Wave Propagation (IZMIRAN);; MFGI, PI B. Heilig; Institute of Geophysics, Polish Academy of Sciences, PI Anne Neska and Jan Reda; and University of L'Aquila, PI M. Vellante; BCMT, V. Lesur and A. Chambodut; Data obtained in cooperation with Geoscience Australia, PI Marina Costelloe; AALPIP, co-PIs Bob Clauer and Michael Hartinger; SuperMAG, Data obtained in cooperation with the Australian Bureau of Meteorology, PI Richard Marshall.

References

Akasofu, S.-I, and D. S. Kimball (1964), The dynamics of the aurora, 1, Instabilities of the aurora, *Journal of Atmospheric and Terrestrial Physics, 26,* 205-211, doi:10.1016/0021-9169(64)90147-3

Akasofu, S.-I. (1974), A study of auroral displays photographed from the DMSP-2 satellite and from the Alaska meridian chain of stations, *Space Science Reviews, 16,* 617-725, ISSN: 0038-6308

Amm, O., Aksnes, A., Stadsnes, J., Østgaard, N., Vondrak, R. R., Germany, G. A., et al. (2005), Mesoscale ionospheric electrodynamics of omega bands determined from ground-based electromagnetic and satellite optical observations, *Annales Geophysicae*, *23*, 325–342, doi:10.5194/angeo-23-325-2005

André, D., and W. Baumjohann (1982), Joint two-dimensional observations of ground magnetic and ionospheric electric fields associated with auroral currents. 5. Current system associated with eastward drifting omega bands, *Journal of Geophysics*, *50,* 194–201, https://journal.geophysicsjournal.com/JofG/article/view/201.

Angelopoulos, V., W. Baumjohann, C. F. Kennel, F. V. Coroniti, M. G. Kivelson, R. Pellat, R. J. Walker, H. Lühr, and G. Paschmann (1992), Bursty Bulk Flows in the inner central plasma sheet, *Journal of Geophysical Research*, *97*, 4027-4039, doi:10.1029/91JA02701

Apatenkov, S. V., Pilipenko, V. A., Gordeev, E. I., Viljanen, A., Juusola, L., Belakhovsky, V. B.,Sakharov, Ya. A., and Selivanov, V. N. (2020). Auroral omega bands are a significant cause of large geomagnetically induced currents, *Geophysical Research Letters*, *47*, e2019GL086677, doi:10.1029/2019GL086677

Belakhovsky, V. B. et al. (2018), Characteristics of the variability of a geomagnetic field for studying the impact of the magnetic storms and substorms on electrical energy systems, Izvestiya, *Physics of the Solid Earth*, *54*, 52–65, doi:10.1134/S1069351318010032

Belakhovsky, V., V. Pilipenko, M. Engebretson, Ya. Sakharov, and V. Selivanov (2019), Impulsive disturbances of the geomagnetic field as a cause of induced currents of electric power lines, *Journal of Space Weather and Space Climate*, *9*, A18, doi:10.1051/swsc/2019015

Connors, M., G. Rostoker, G. Sofko, R. L. McPherron, and M. Henderson (2003), Ps 6 disturbances: Relation to substorms and the auroral oval, *Annales Geophysicae, 21,* 493-508, doi:10.5194/angeo-21-493-2003

Connors, M., Schofield, I., Reiter, K., Chi, P. J., Rowe, K. M., & Russell, C. T. (2016), The AUTUMNX magnetometer meridian chain in Québec, Canada, *Earth, Planets and Space*, *68*, doi:10.1186/s40623-015-0354-4

Dimmock, A. P. et al. (2019), The GIC and geomagnetic response over Fennoscandia to the 7-8 September 2017 geomagnetic storm, *Space Weather, 17,* 989 –1010, doi:10.1029/ 2018SW002132.

Engebretson, M. J., W. J. Hughes, J. L. Alford, E. Zesta, L. J. Cahill, Jr., R. L. Arnoldy, and G. D. Reeves (1995), Magnetometer array for cusp and cleft studies observations of the spatial extent of broadband ULF magnetic pulsations at cusp/cleft latitudes, *Journal of Geophysical Research, 100,* 19371-19386, doi:10.1029/95JA00768

Engebretson, M. J., Pilipenko, V. A., Ahmed, L. Y., Posch, J. L., Steinmetz, E. S., Moldwin, M. B., Connors, M. G., Weygand, J. M., Mann, I. R., Boteler, D. H., Russell, C. T., and Vorobev, A. V. (2019a), Nighttime magnetic perturbation events observed in Arctic Canada: 1. Survey and statistical analysis, *Journal of Geophysical Research: Space Physics, 124,* 7442–7458, doi: 10.1029/2019JA026794.

Engebretson, M. J., E. S. Steinmetz, J. L. Posch, V. A. Pilipenko, M. B. Moldwin, M. G. Connors, D. H. Boteler, I. R. Mann, M. D. Hartinger, J. M. Weygand, L. R. Lyons, Y. Nishimura , H. J. Singer, S. Ohtani, C. T. Russell, A. Fazakerley, and L. M. Kistler (2019b), Nighttime magnetic perturbation events observed in Arctic Canada: 2. Multiple-instrument observations, *Journal of Geophysical Research: Space Physics, 124,* 7459-7476, doi:10.1029/2019JA026797.

Freeman, M. P., C. Forsyth, and I. J. Rae (2019), The influence of substorms on extreme rates of change of the surface horizontal magnetic field in the United Kingdom, *Space Weather, 17,* 827 –844, doi:10.1029/2018SW002148.

Gabrielse, C., V. Angelopoulos, A. Runov, and D. L. Turner (2014), Statistical characteristics of particle injections throughout the equatorial magnetotail, *Journal of Geophysical Research: Space Physics, 119,* 2512–2535, doi:10.1002/2013JA019638

Henderson, M. G., Kepko, L., Spence, H. E., Connors, M., Sigwarth, J. B., Frank, L. A., Singer, H.,J., and Yumoto, K. (2002), The evolution of north-south aligned auroral forms into auroral torch structures: The generation of omega bands and Ps6 pulsations via flow bursts, in the *Proceedings of the Sixth International Conference on Substorms*, edited by R. M. Winglee, University of Washington, Seattle, WA, ISBN:0971174032 9780971174030

Henderson, M. G. (2012). Auroral substorms, poleward boundary activations, auroral streamers, omega bands, and onset precursor activity, In A. Keiling et al. (Eds.), *Auroral phenomenology and magnetospheric processes: Earth and other planets* (Vol. 197, pp. 39–54), Washington, DC: American Geophysical Union.

Henderson, M. G. (2016), Recurrent embedded substorms during the 19 October 1998 GEM storm, *Journal of Geophysical Research: Space Physics*, *121*, 7847–7859, doi:10.1002/2015JA022014

Juusola, L., Østgaard, N., Tanskanen, E., Partamies, N., and Snekvik, K. (2011), Earthward plasma sheet flows during substorm phases, *Journal of Geophysical Research*, *116*, A10228, https://doi.org/10.1029/2011JA016852

Juusola, L., A. Viljanen, M. van de Kamp, E. I. Tanskanen, H. Vanhamäki, N. Partamies, and K. Kauristie (2015), High-latitude ionospheric equivalent currents during strong space storms: Regional perspective, *Space Weather*, *13*, 49–60, doi:10.1002/2014SW001139

Kawasaki, K., and Rostoker, G. (1979), Perturbation magnetic fields and current systems associated with eastward drifting auroral structures, *Journal of Geophysical Research*, *84*, 1464–1480, doi:10.1029/JA084iA04p01464

Liu, J., V. Angelopoulos, X. Chu, X.-Z. Zhou, and C. Yue (2015), Substorm Current Wedge Composition by Wedgelets, *Geophysical Research Letters*, *42*, 1669–1676, doi:10.1002/2015GL063289.

Lühr, H., and K. Schlegel (1994), Combined measurements of EISCAT and the EISCAT magnetometer cross to study Ω bands, *Journal of Geophysical Research*, *99*, 8951-8959, doi:10.1029/94JA00487

Newell, P. T., and Gjerloev, J. W. (2011a), Evaluation of SuperMAG auroral electrojet indices as indicators of substorms and auroral power, *Journal of Geophysical Research*, *116*, A12211, doi:10.1029/2011JA016779.

Newell, P. T., and Gjerloev, J. W. (2011b), Substorm and magnetosphere characteristic scales inferred from the SuperMAG auroral electrojet indices, *Journal of Geophysical Research*,

116, A12232, doi:10.1029/2011JA016936

Nikitina, L., Trichtchenko, L., and Boteler, D. H. (2016), Assessment of extreme values in geomagnetic and geoelectric field variations for Canada. *Space Weather, 14,* 481–494, doi:10.1002/2016SW001386

Opgenoorth, H., Oksman, J., Kaila, K., Nielsen, E., & Baumjohann, W. (1983), Characteristics of eastward drifting omega bands in the morning sector of the auroral oval, *Journal of Geophysical Research*, *88*, 9171–9185, doi:10.1029/JA088iA11p09171

Opgenoorth, H. J., M. A. L. Persson, T. I. Pulkkinen, and R. J. Pellinen (1994), Recovery phase of magnetospheric substorms and its association with morning-sector aurora, *Journal of Geophysical Research*, *99*, 4115-4129, doi:10.1029/93JA01502

Palin, L., C. Jacquey, H. Opgenoorth, M. Connors, V. Sergeev, J.-A. Sauvaud, R. Nakamura, G. D. Reeves, H. J. Singer, V. Angelopoulos, and L. Turc (2015), Three-dimensional current systems and ionospheric effects associated with small dipolarization fronts, *Journal of Geophysical Research - Space Physics*, *120*, 3739–3757, doi:10.1002/2015JA021040

Partamies, N., Weygand, J. M., and Juusola, L. (2017), Statistical study of auroral omega bands, *Annales Geophysicae,* 35, 1069–1083, doi:10.5194/angeo-35-1069-2017

Runov, A., Angelopoulos, V., Sitnov, M. I., Sergeev, V. A., Bonnell, J., McFadden, J. P., et al. (2009), THEMIS observations of an earthward propagating dipolarization front, *Geophysical Research Letters*, *36*, L14106, doi:10.1029/2009GL038980

Runov, A., Angelopoulos, V., Zhou, X.-Z., Zhang, X.-J., Li, S., Plaschke, F., & Bonnell, J. (2011), A THEMIS multicase study of dipolarization fronts in the magnetotail plasma sheet, *Journal of Geophysical Research*, *116*, A05216, doi:10.1029/2010JA016316

Sergeev, V. A., Yahnin, D. A., Liou, K., Thomsen, M. F., and Reeves, G. D, (2003), Narrow plasma streams as a candidate to populate the inner magnetosphere, in *The Inner Magnetosphere*, edited by T. I. Pulkkinen, N. A. Tsyganenko, and R. H. W. Friedel, Geophysical Monograph Series, 55–60, Washington, D.C., American Geophysical Union, doi:10.1029/155GM07

Singer, H. J., Matheson, L., Grubb, R., Newman, A., & Bouwer, S. D. (1996). Monitoring space weather with the GOES magnetometers, in *SPIE Conference Proceedings, vol. 2812*, edited by E. R. Washwell, pp. 299–308, GOES-8 and Beyond, SPIE, Bellingham, Wash.

Solovyev, S. I., Baishev, D. G., Barkova, E. S., Engebretson, M. J., Posch, J. L., Hughes, W. J., Yumoto, K., and Pilipenko, V. A. (1999), Structure of disturbances in the dayside and nightside ionosphere during periods of negative interplanetary magnetic field Bz, *Journal of Geophysical Research*, *104*, 28,019–28,039, doi:10.1029/1999JA900286

Syrjäsuo, M. T., and Donovan, E. F. (2004), Diurnal auroral occurrence statistics obtained via machine vision, *Annales Geophysicae*, *22*, 1103–1113, doi:10.5194/angeo-22-1103-2004

Viljanen, A., Nevanlinna, H., Pajunpää, K., & Pulkkinen, A. (2001), Time derivative of the horizontal geomagnetic field as an activity indicator, *Annales Geophysicae*, *19*(9), 1107–1118, doi:10.5194/angeo-19-1107-2001

Viljanen, A., E. I. Tanskanen, and A. Pulkkinen (2006), Relation between substorm characteristics and rapid temporal variations of the ground magnetic field, *Annales Geophysicae*, *24*, 725-733, doi:10.5194/angeo-24-725-2006.

Viljanen, A., and Tanskanen, E. (2011), Climatology of rapid geomagnetic variations at high latitudes over two solar cycles. *Annales Geophysicae*, *29*, 1783–1792, doi:10.5194/angeo-29-1783-2011

Viljanen, A., (1997), The relation between geomagnetic variations and their time derivatives and implications for estimation of induction risks, *Geophysical Research Letters*, *2*4, 631–634, doi:10.1029/97GL00538

Vorobev, A., Pilipenko, V., Sakharov, Y.,and Selivanov, V. (2019), Statistical relationships between variations of the geomagnetic field, auroral electrojet, and geomagnetically induced currents, *Solar-Terrestrial Physics*, *5*, 35–42, doi:10.12737/stp-51201905

Weygand, J. M., Kivelson, M. G., Frey, H. U., Rodriguez, J. V., Angelopoulos, V., Redmon, R., Barker-Ream, J., Grocott, A., and Amm, O. (2015), An interpretation of spacecraft and ground based observations of multiple omega band events, *Journal of Atmospheric and Solar-Terrestrial Physics, 133*, 185–204, doi:10.1016/j.jastp.2015.08.014

Wild, J. A., Woodfield, E. E., Donovan, E., Fear, R. C., Grocott, A., Lester, M., Fazakerley, A. N., Lucek, E., Khotyaintsev, Y., Andre, M., Kadokura, A., Hosokawa, K., Carlson, C., McFadden, J. P., Glassmeier, K. H., Angelopoulos, V., and Björnsson, G. (2011), Midnight sector observations of auroral omega bands, *Journal of Geophysical Research,*

116, A00130, doi:10.1029/2010JA015874

Table 1. Locations of the magnetometer stations used in this study. Geographic and corrected geomagnetic (CGM) latitude and longitude are shown, as well as the universal time (UT) of local magnetic noon.

Array	Station	Code	Geog. lat.	Geog. lon.	CGM lat.	CGM lon.	UT of Mag Noon	Cadence, s
MACCS	Repulse Bay	RBY	66.5°	273.8°	75.2°	-12.8°	17:47	0.5
	Cape Dorset	CDR	64.2°	283.4°	72.7°	3.0°	16:58	0.5
CANMOS	Iqaluit	IQA	63.8°	291.5°	71.4°	15.1°	16:19	1.0
AUTUMNX	Salluit	SALU	62.2°	284.3°	70.7°	4.1°	16:54	0.5
	Kuujuarapik	KJPK	55.3°	282.2°	64.4°	0.2°	17.06	0.5

Note: CGM coordinates were calculated for epoch 2015, using http://sdnet.thayer.dartmouth.edu/aacgm/aacgm_calc.php#AACGM .

Table 2. Numbers of MPEs observed at each station with derivative amplitude $|dB/dt| \geq 6$ nT/s in any component, as a function of Δt.

Station	MLAT	$\Delta t \leq 30$ min		$30 < \Delta t < 60$ min		$\Delta t \geq 60$ min		All
		#	%	#	%	#	%	#
RBY	75.2°	53	60	22	25	13	15	88
CDR	72.7°	112	67	32	19	22	13	166
IQA	71.4°	119	66	29	16	32	18	180
SALU	70.7°	187	66	47	17	48	17	282
KJPK	64.4°	79	64	20	16	25	20	124

Table 3. Distribution of pre- and post-midnight ≥ 6 nT/s MPEs at each station as a function of time between the most recent substorm onset and event occurrence. Pre-midnight MPEs include those observed between 1700 and 0100 MLT, and post-midnight events those between 0200 and 0700 MLT.

Pre-midnight

Station	RBY		CDR		IQA		SALU		KJPK	
	#	%	#	%	#	%	#	%	#	%
t ≤ 30 min	50	60	105	69	107	65	168	69	46	59
30-60 min	20	24	28	18	24	15	37	15	15	19
t ≥ 60 min	13	16	20	13	34	21	39	16	17	22
Sum	83		153		165		244		78	

Combined: t ≤ 30 min: 66%, 30-60 min: 17%, t ≥ 60 min: 17%

Post-midnight

Station	RBY		CDR		IQA		SALU		KJPK	
	#	%	#	%	#	%	#	%	#	%
t ≤ 30 min	3	75	5	71	7	70	17	61	30	75
30-60 min	1	25	1	14	3	30	5	18	6	15
t ≥ 60 min	0	0	1	14	0	0	6	21	4	10
Sum	4		7		10		28		40	

Combined: t ≤ 30 min: 70%, 30-60 min: 18%, t ≥ 60 min: 12%

Table 4. The numbers of ≥ 6 nT/s MPEs observed at 5 stations during 2015 and 2017 between 2325 and 0555 UT as a function of their time delays (0-30, 30-60, and 0-60 min) after the most recent substorm onset (columns 2-4), these numbers as percentages of the estimated number of substorm onsets (columns 5-7), and the estimated percentages of substorm onsets after which no MPE occurred within 60 minutes after onset (column 8).

Station	Number of Events			% following a substorm onset			SS onset % not
	0- 30 min	30 - 60 min	0-60 min	0- 30 min	30 - 60 min	0-60 min	related to MPEs
RBY	53	22	75	5.7	2.4	8.0	92.0
CDR	112	32	144	12.0	3.4	15.5	84.5
IQA	119	29	148	12.8	3.1	15.9	84.1
SALU	187	47	234	20.1	5.0	25.1	74.9
KJPK	79	20	99	8.5	2.1	10.6	89.4

Table 5. The number of ≥ 6 nT/s MPEs observed during 2015 and 2017 at the three lowest latitude stations as a function of the number of substorm onsets that occurred within 2 hours prior to the MPE. Events are separated into two local time ranges: from 1700 to 0100 MLT and 0200-0700 MLT.

	Number of Onsets							
Station	0	1	2	3	4	5	6	Total
IQA								
1700-0100 MLT	20	102	43	15	4	0	0	184
0200-0700 MLT	0	2	2	4	2	0	0	10
SALU								
1700-0100 MLT	21	118	71	21	5	1	0	237
0200-0700 MLT	3	4	7	7	6	0	0	27
KJPK								
1700-0100 MLT	12	28	23	11	2	1	0	77
0200-0700 MLT	1	5	16	10	8	0	2	42

Table 6. Application of Pearson's Chi-squared test with 2 degrees of freedom to the number of pre-midnight and post-midnight MPE occurrences as a function of the number of prior substorm onsets with 2 hours.

MLT Range	17 - 1	2 - 7	17 - 1	2 - 7	17 - 1	2 – 7
Station	IQA		SALU		KJPK	
0 onsets	20	0	21	3	12	1
1 onset	102	2	118	4	28	5
≥ 2 onsets	62	8	98	20	37	36
X^2	8.94		12.36		16.48	
p-value	0.011		0.0021		0.00026	

Table 7. The normalized percentage of pre- and post-midnight ≥ 6 nT/s MPEs events with SME ≥ 1000 nT observed at IQA, SALU, and KJPK during 2015 and 2017, as a function of the number of substorm onsets that occurred within 2 hours prior to the MPE.

	Number of Onsets							
Station	0	1	2	3	4	5	6	7
1700-0100 MLT								
IQA								
Total MPEs	20	102	43	15	4	0	0	0
# SME ≥ 1000 nT	0	2	6	5	4			
% SME ≥ 1000 nT	0	2	14	33	100			
SALU								
Total MPEs	21	118	71	21	5	1	0	0
# SME ≥ 1000 nT	0	6	6	5	3	1		
% SME ≥ 1000 nT	0	5	8	24	60	100		
KJPK								
Total MPEs	12	28	23	11	2	1	0	0
# SME ≥ 1000 nT	0	2	6	5	2	0		
% SME ≥ 1000 nT	0	7	26	45	100	0		
0200-0700 MLT								
IQA								
Total MPEs	0	2	2	4	2	0	0	0
# SME ≥ 1000 nT	0	0	2	3	2			
% SME ≥ 1000 nT	0	0	100	75	100			
SALU								
Total MPEs	3	4	7	7	6	0	0	0
# SME ≥ 1000 nT	0	1	2	5	4			
% SME ≥ 1000 nT	0	25	29	71	67			
KJPK								
Total MPEs	1	5	16	10	8	0	1	1
# SME ≥ 1000 nT	0	1	9	6	4		1	1
% SME ≥ 1000 nT	0	20	56	60	50		100	100

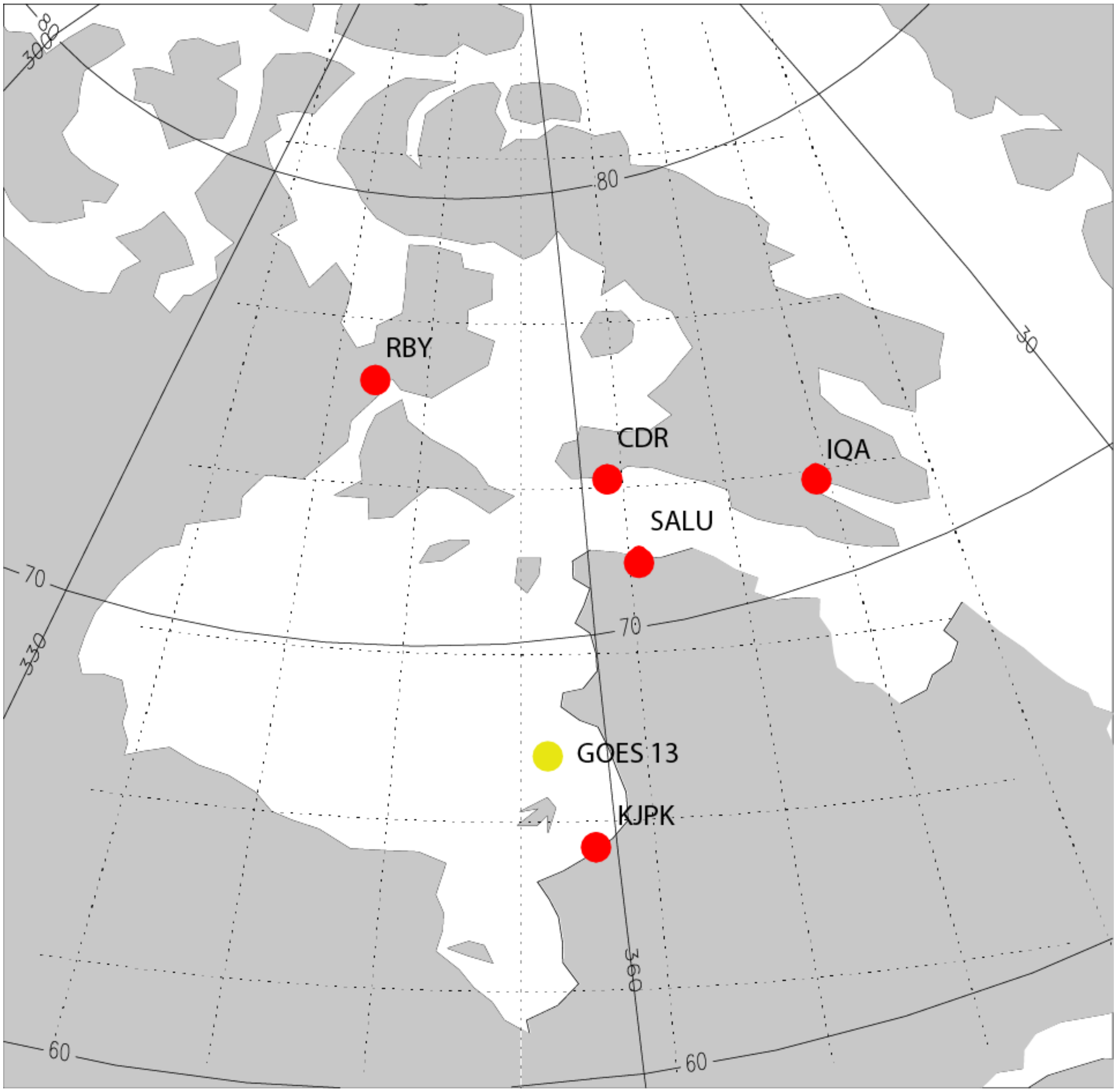

Figure 1. Map of Eastern Arctic Canada showing the location of the five ground magnetometers that provided data for this study. Also shown by the yellow circle is the approximate northern magnetic footpoint of the geosynchronous GOES-13 spacecraft. Solid lines show corrected geomagnetic coordinates.

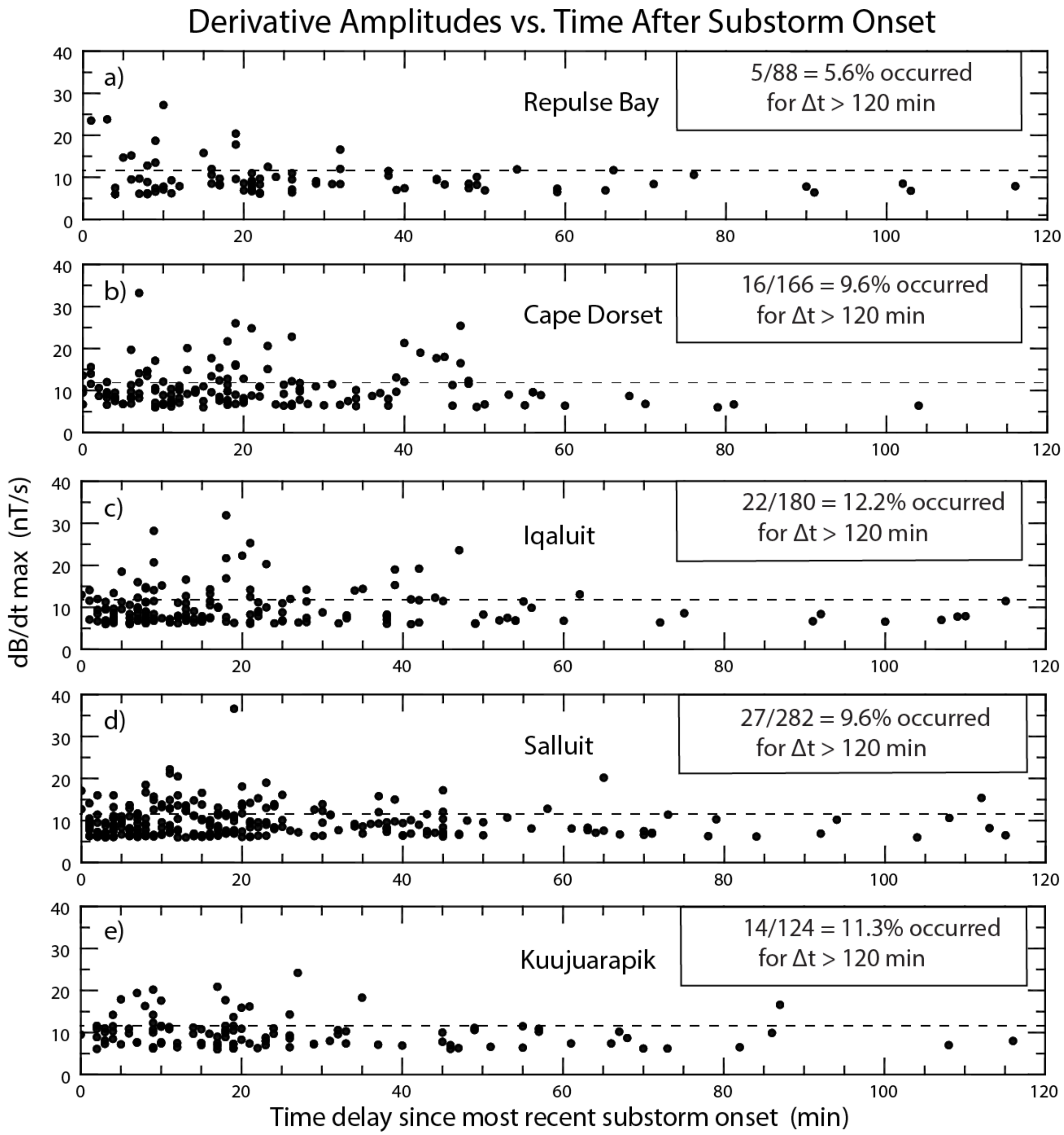

Figure 2. Plot of the amplitude of the maximum |dB/dt| value in any nighttime MPE component observed at each station as a function of its delay after the most recent substorm onset: a) Repulse Bay, b) Cape Dorset, c) Iqaluit, d) Salluit, and e) Kuujuarapik. Only events with maximum derivative amplitude ≥ 6 nT/s are shown. The horizontal dotted line indicates an amplitude of 12 nT/s.

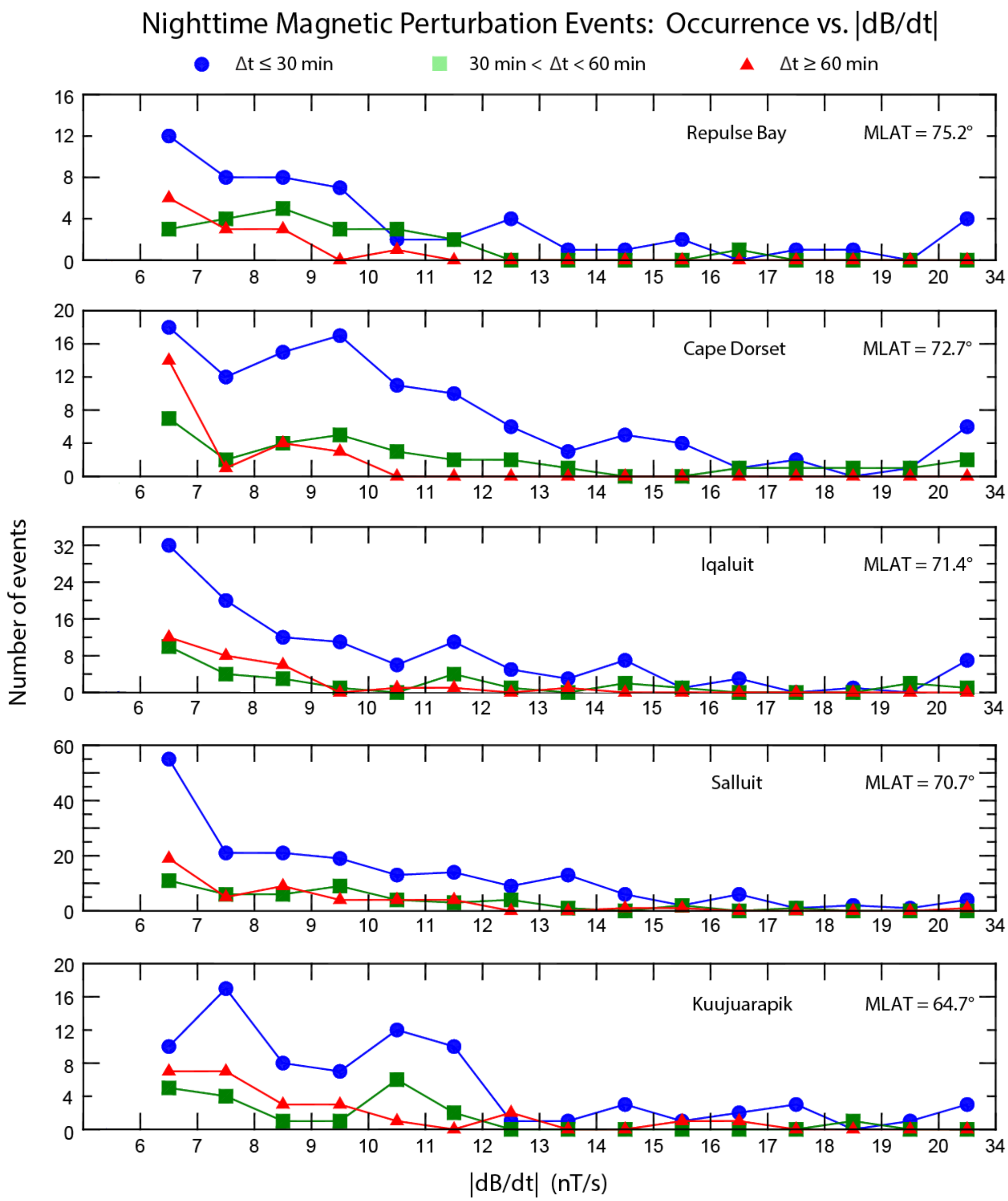

Figure 3. Plots of the number of occurrences of ≥ 6 nT/s nighttime MPEs observed at Repulse Bay, Cape Dorset, Iqaluit, Salluit, and Kuujuarapik as a function of the maximum derivative amplitude, sorted by each station's magnetic latitude. Events are color-coded based on time of occurrence after the closest prior substorm onset: Δt ≤ 30 min (blue circles), 30 < Δt < 60 min (green squares), and Δt ≥ 60 min (red triangles). The last interval at the right includes all events with amplitude > 20 nT/s. Note that the vertical scales are different in each panel.

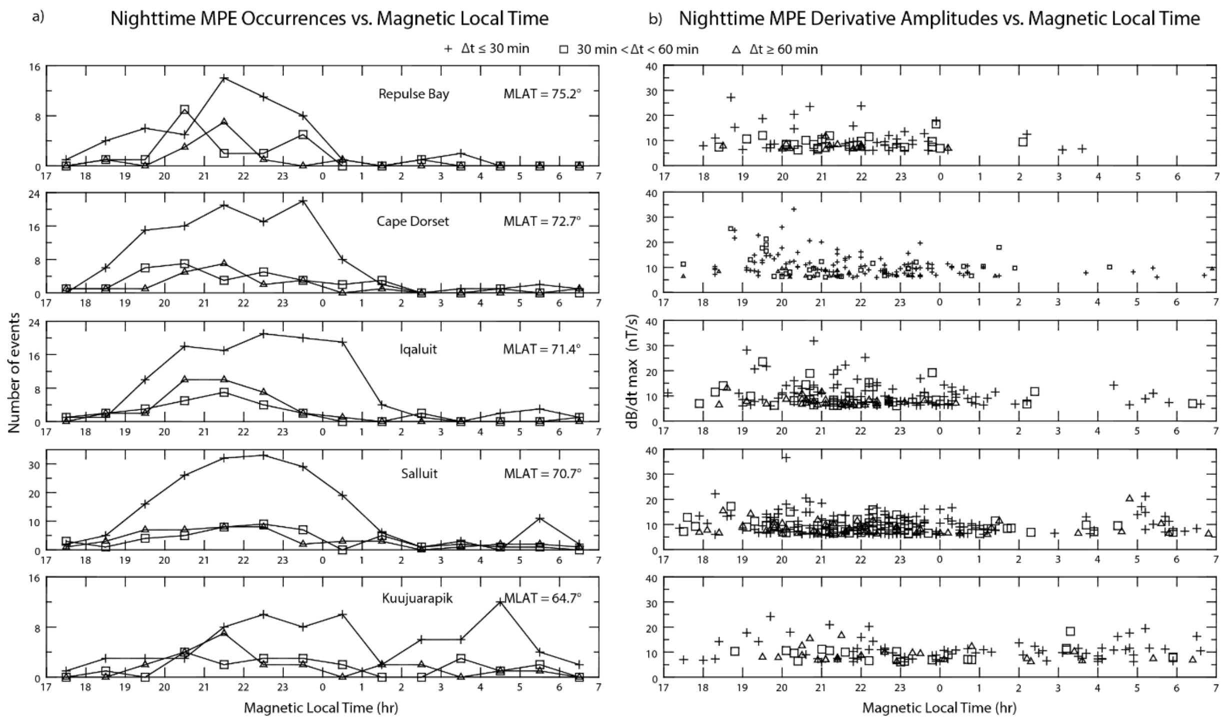

Figure 4. Panel a shows the number of occurrences of ≥ 6 nT/s nighttime MPEs observed at Repulse Bay, Cape Dorset, Iqaluit, Salluit, and Kuujjuarapik in 1-hour bins of magnetic local time (MLT) from 17 h to 07 h, sorted by each station's magnetic latitude. Panel b shows the distribution of MPE derivative amplitude at these same stations. Different symbols are used to designate events based on the time of MPE occurrence after the closest prior substorm onset: plus signs for $\Delta t \leq 30$ min, open squares for Δt between 30 and 60 min, and open triangles for $\Delta t \geq 60$ min.

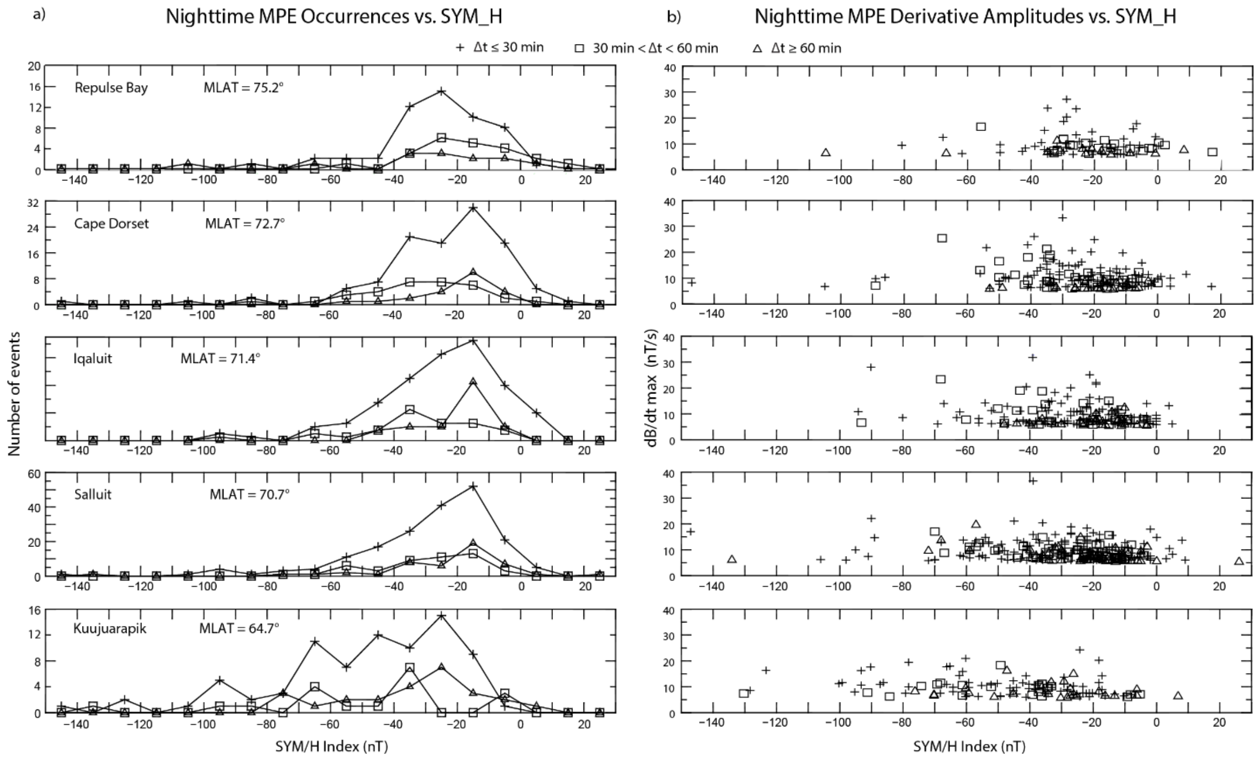

Figure 5. Plot of ≥ 6 nT/s nighttime MPE occurrences and amplitudes as in Figure 4, but as a function of the SYM/H index.

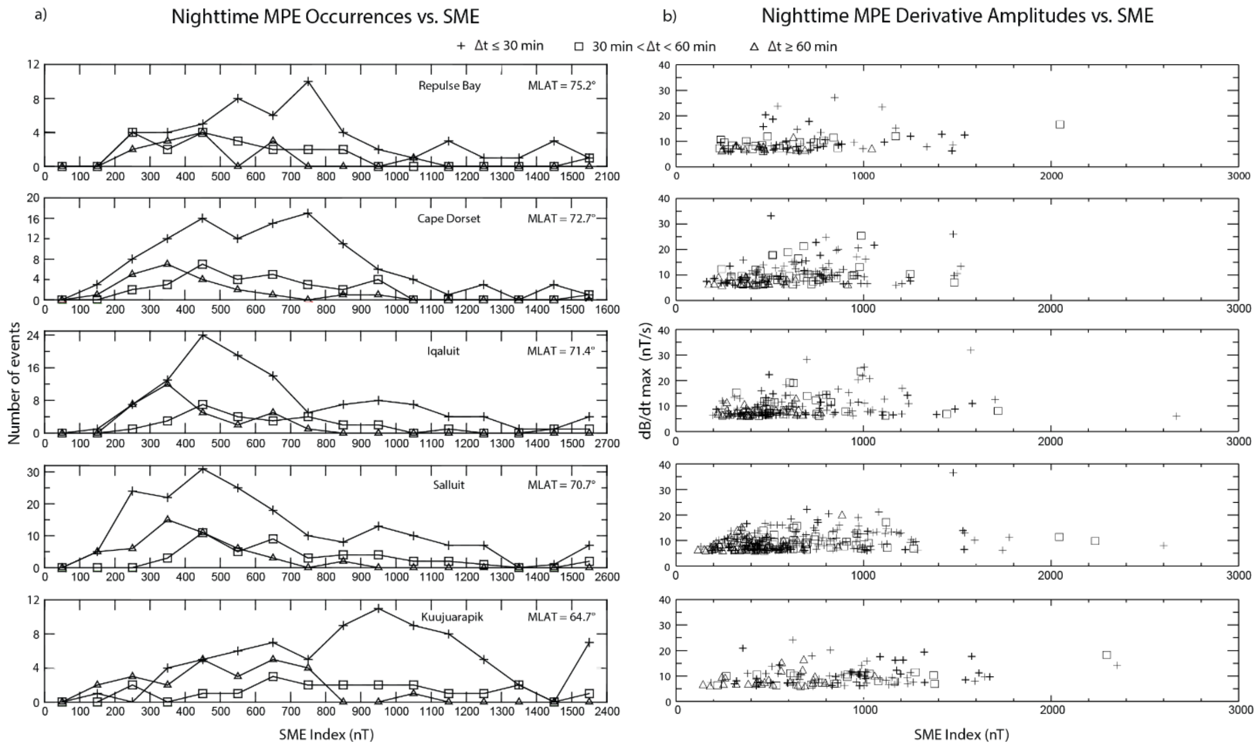

Figure 6. Plot of ≥ 6 nT/s nighttime MPE occurrences and amplitudes as in Figure 4, but as a function of the SME index. In panel a) the events at each station are binned in steps of 100 nT, except for the rightmost bin, which includes all events with SME between 1500 and the maximum value shown in the horizontal legend for each station.

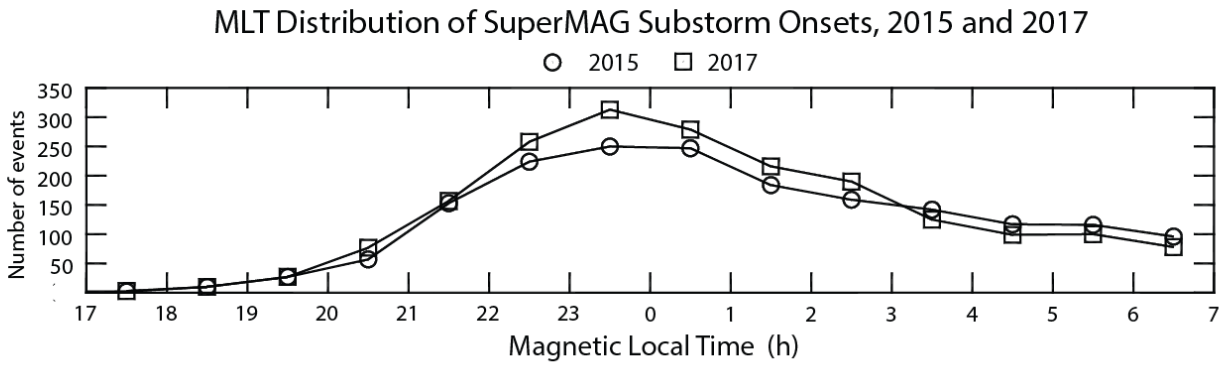

Figure 7. Plot of the number of substorm onsets during 2015 (circles) and 2017 (squares) in 1-h bins between 17 and 07 MLT, based on the SuperMAG substorm onset data base.

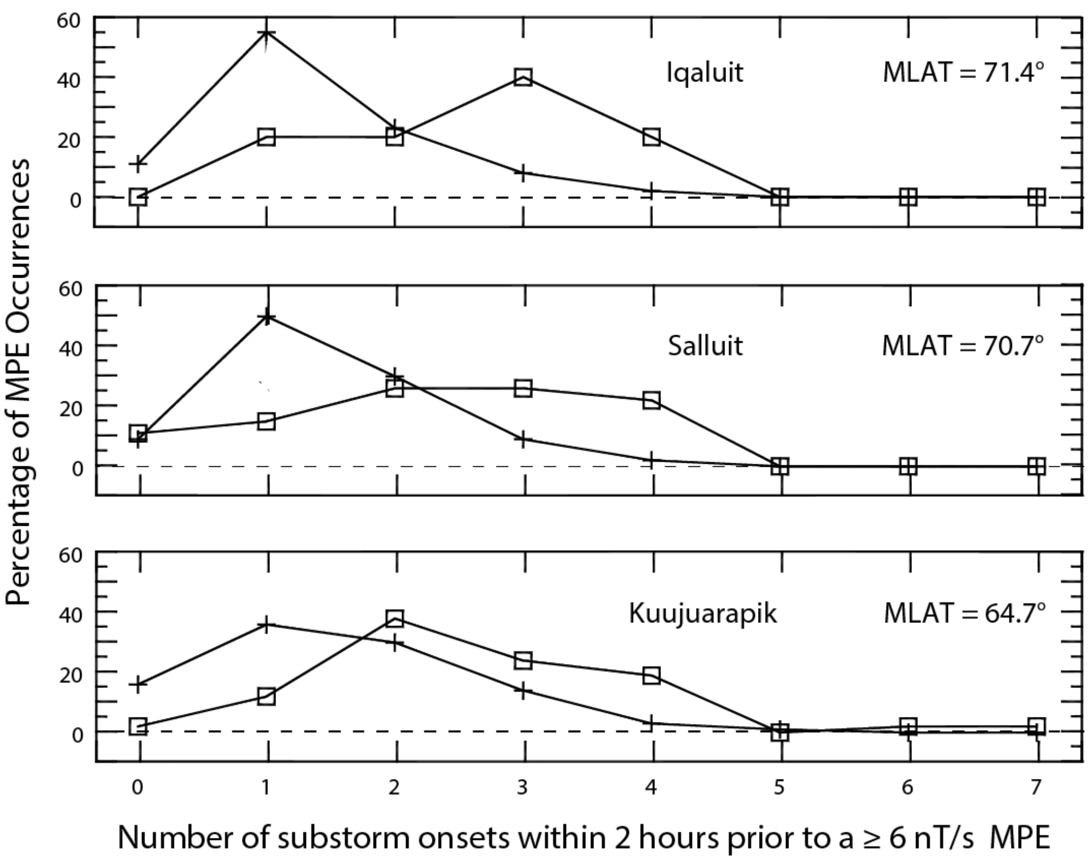

Figure 8. Plot of the percentage of MPEs observed during 2015 and 2017 as a function of the number of substorm onsets that occurred within 2 hours prior to the MPE, at IQA, SALU, and KJPK. Plus signs and open squares indicate pre-midnight and post-midnight events, respectively.

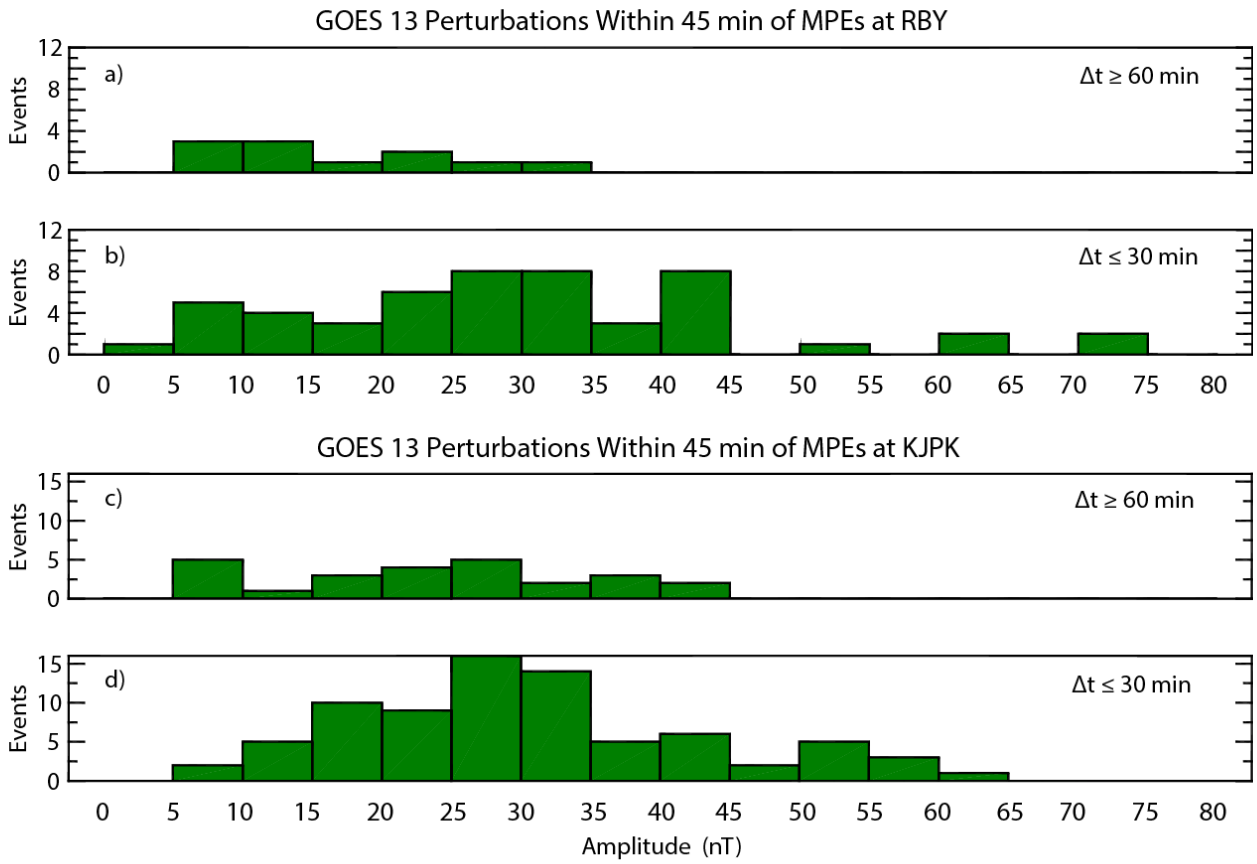

Figure 9. Plots of the number of GOES 13 perturbations occurring within 45 minutes prior to MPEs observed at RBY and KJPK, as a function of amplitude. Panels a) and c) show the distribution of amplitudes for MPEs occurring ≥ 60 min after the most recent substorm onset, and panels b) and d) show the distribution for MPEs occurring ≤ 30 min after the most recent substorm onset.